AIAA

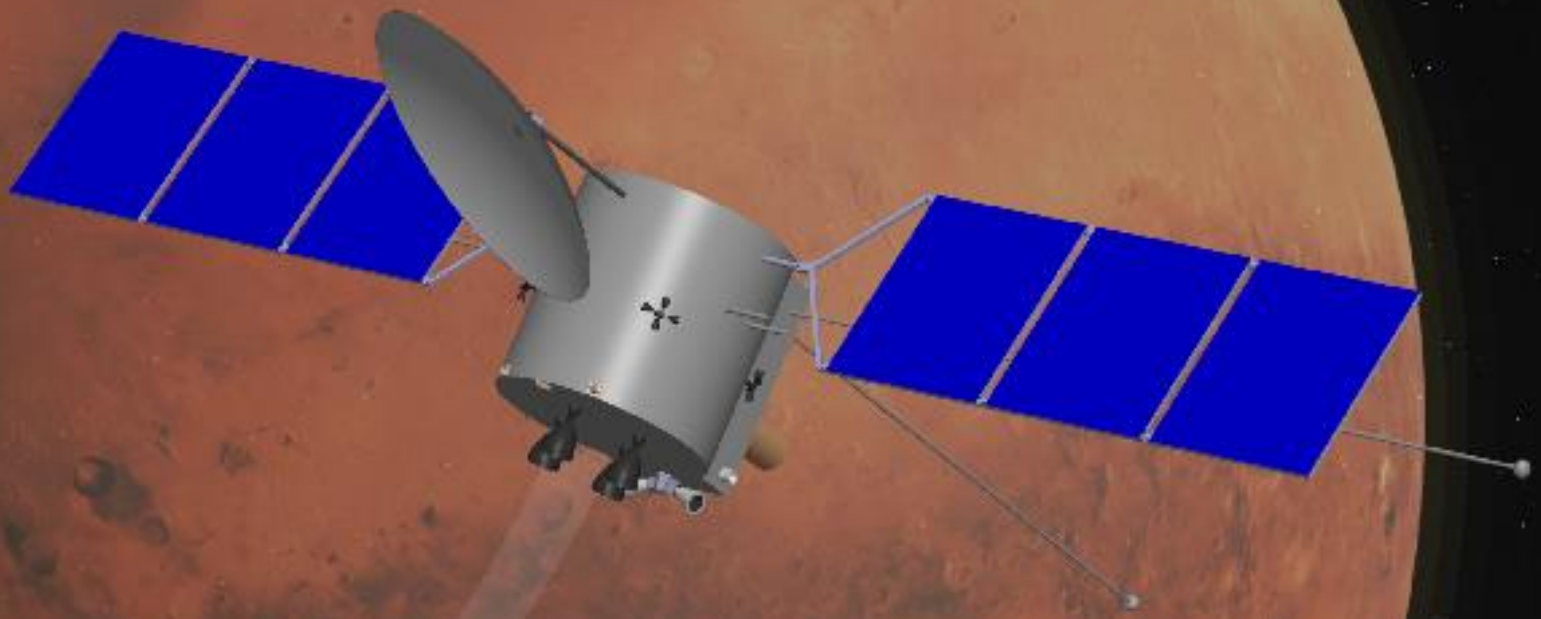

ARES

ARES II

Ernesto Socorro Perez AIAA ID: 1809960 Team Lead, Structures and Mechanisms, Propulsion  	Ricard Solà González AIAA ID: 1809962 Team Lead, Attitude Determination and Control  
Justis LaPier AIAA ID: 1810955 Structures and Mechanisms Justis LaPier 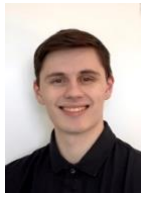	Kian Ojo AIAA ID: 1811301 Orbital Mechanics and Flight Control  
Aadhith Ravi AIAA ID: 1811319 Electrical Power  	Rui Fernandes AIAA ID: 1714048 Propulsion  
Ethan Sequeira AIAA ID: 1811347 Thermal Control  	Katerina Beros AIAA ID: 1809961 Thermal Control  
Ali Ahmadi AIAA ID: 1811323 Communications and Data Handling Ali Ahmadi 	Maia Elizabeth Gorham AIAA ID: 1811343 Mission Planning and Systems Engineering  
Dr. John Enright AIAA ID: 156067 Faculty Advisor  	

Executive Summary

The ARES II mission is designed to address critical knowledge gaps that currently constrain the feasibility and safety of future human missions to Mars. Previous missions, including Mars Global Surveyor, Mars Reconnaissance Orbiter, and various rovers, have greatly enhanced our understanding of Mars' topography and resources. However, existing datasets still lack sufficient resolution, coverage, and sensor redundancy to accurately characterize meter-scale surface features, quantify subsurface resources like water ice, and thoroughly map surface hazards. These shortcomings significantly impact landing site selection, in-situ resource utilization (ISRU), and habitat placement—key factors for human exploration.

The ARES II mission aims to put a satellite to orbit Mars to bridge these gaps through high-resolution global mapping of the Martian surface and subsurface, using advanced instrumentation specifically optimized for detailed terrain and resource analysis. By systematically addressing these scientific and engineering challenges, ARES II will significantly enhance Mars exploration readiness and reduce risks for subsequent crewed missions.

The mission shall be capable of identifying slopes, elevation, and small-scale hazards, and characterize surface and subsurface resources, including hydrated minerals, water ice, caves, and lava tubes. It will complete primary data collection activities by covering at least 75% of Mars' surface by December 31, 2033, and will continue payload operations for extended scientific data collection through at least 2039. To ensure mission viability, the project will adhere to a total program cost of $1 Billion (FY24), encompassing all phases from design, manufacturing, testing, integration, launch, to primary operations, including a contingency reserve of at least 15%. Additionally, the spacecraft design will robustly address reliability in the deep-space environment, accounting for radiation exposure, thermal extremes, and loads experienced during launch vehicle integration and aerobraking maneuvers at Mars.

The mission requirements set clear operational goals to enhance data collection capabilities beyond existing Mars missions. This is achieved through a payload consisting of a laser altimeter (MAS) for high-resolution topography, a high-resolution and context-imaging camera (MID) for surface hazard identification, a dual-frequency sounding radar (DFRS) for subsurface exploration, and a hyperspectral spectrometer (MSIS) for surface mineralogy and hydration mapping.

ARES II will execute a detailed geographic survey to locate regions suitable for safe landings and efficient rover mobility, meeting NASA's stringent criteria for minimal slopes, low elevation variance, and the absence of significant obstacles like large rocks, rugged outcrops, or extensive sand dune fields. The mission employs a sophisticated combination of laser altimetry and high-resolution optical imaging technologies, significantly improving upon the capabilities of past instruments such as the Mars Orbiter Laser Altimeter (MOLA). Specifically developed for ARES II, MAS will provide highly accurate topographic measurements with vertical accuracy better than 2.5 meters and horizontal resolution of approximately 165 meters. This represents a marked advancement over previous Mars topographic surveys.

Complementing the altimeter, MID is designed to capture high-resolution imagery at a spatial resolution of up to 1 meter per pixel. MID will effectively identify small-scale hazards, such as rocks and dunes, and monitor sand ripple movements and dust accumulations, critical for assessing mobility risks and infrastructure planning. MID's dual-mode capability to capture both detailed and contextual imagery ensures robust terrain characterization, enabling precise hazard avoidance and route optimization strategies for future human explorers.

The second core scientific objective targets the detection and analysis of Martian resources, specifically water ice, hydrated minerals, caves, and lava tubes, essential for human survival and operational sustainability. To achieve detailed subsurface mapping, ARES II incorporates a DFRS, derived from heritage instruments like SHARAD and MARSIS. DFRS will map the subsurface to depths ranging from tens of meters to several kilometers, revealing buried water ice deposits and potential habitable voids, including lava tubes and cave systems, substantially advancing current understanding of Mars' accessible subsurface resources.

Additionally, the MSIS will carry out hyperspectral imaging in the wavelength range of 310-5100 nm, providing detailed mineralogical mapping of the Martian surface. MSIS's enhanced spectral resolution surpasses previous spectrometers, allowing precise identification and quantification of hydrated minerals critical for future water extraction efforts. The detailed distribution data generated by MSIS will enable mission planners to select optimal resource extraction sites and devise effective strategies for long-term human missions to Mars.

By systematically combining detailed topographic, optical, radar, and hyperspectral data, ARES II will substantially enhance Mars exploration readiness, significantly reducing risks for future crewed missions and paving the way for sustained human presence on Mars.

The ARES II spacecraft's mission design includes multiple operational phases that ensure a smooth transition from Earth departure to Mars orbital insertion and subsequent scientific operations. Initially, the spacecraft will launch aboard SpaceX's Falcon 9 into a temporary 200 km Earth parking orbit. Following a comprehensive systems check, the spacecraft will perform a Trans-Martian Injection (TMI) maneuver, initiating a Hohmann transfer trajectory designed for optimal fuel efficiency and alignment with Mars arrival conditions.

Upon Mars approach, a Mars Orbit Insertion (MOI) burn will place ARES II into a highly elliptical capture orbit. The spacecraft will then conduct an extensive aerobraking campaign over approximately two months, using Mars' thin atmosphere to gradually reduce orbital eccentricity and altitude. This campaign ensures minimal fuel usage, significantly reducing mission mass and cost.

The scientific orbit selection is a critical component of the mission design, chosen to optimize scientific return. The final orbit will be a circular, sun-synchronous orbit at a 350 km altitude and 92.79° inclination. This orbit provides consistent lighting conditions, optimal power generation, and ideal observational conditions for payload instruments, ensuring continuous and stable data collection.

The science operations overview is structured into distinct phases designed to efficiently achieve mission goals. Initially, all instruments except the high-resolution camera are activated, due to its high data rate. Instruments with large fields of view, like the DFRS radar and MSIS spectrometer, quickly achieve 75% coverage—completed in 15 and 335 days, respectively—by leveraging their extensive swath widths. After 761 days, with initial mapping completed and additional validation data collected by the spectrometer and radar, the high-resolution camera is activated for targeted investigations. Concurrently, the spectrometer is deactivated to manage data volume effectively. The high-resolution imagery captured during this phase provides crucial details for hazard characterization and mobility assessments. By the conclusion of primary data collection around day 1460, the altimeter completes its required 75% surface mapping, while the high-resolution camera has generated detailed imagery covering approximately 20% of the Martian surface. This would have marked the conclusion of primary gathering activities, and the scientific objectives would have been completed

The spacecraft's primary structure consists of a primary structure made from lightweight yet strong aluminum 6061-T6 alloy, configured as a semi-monocoque truss design optimized for launch vehicle compatibility. Secondary

structures precisely position payload instruments, while deployable mechanisms for solar arrays and antennas are implemented to maximize space efficiency within launch constraints and enable proper spacecraft operations.

The Command and Data Handling (C&DH) subsystem enables autonomous control, science data processing, and communication for ARES II. It is centered around dual-redundant, radiation-hardened RAD750 processors responsible for system management, task scheduling, telemetry, and FDIR. Data is stored on 2 TB radiation-tolerant solid-state drives (SSDs). Communications are handled via a gimbaled 4.5-meter dual-band High-Gain Antenna (HGA) with Ka-band downlink and X-band uplink, using a diplexer and two-axis articulation for precise Earth-pointing. A Medium-Gain Antenna (MGA) in X-band supports safe-mode operations, while omnidirectional Low-Gain Antennas (LGAs) ensure backup telemetry and command. A UHF relay transceiver enables emergency communications via Mars orbiters. The RF front-end includes diplexers, LNAs, and a Ka-band Traveling Wave Tube Amplifier (TWTA) for high-power signal transmission. A dedicated Modem handles modulation, demodulation, and error correction. The TT&C system manages real-time command and telemetry, ensuring connectivity across mission phases. Together, these elements support high-rate data return and robust spacecraft control in Mars orbit.

The Electrical Power subsystem ensures continuous energy supply throughout the mission, primarily utilizing advanced triple-junction gallium arsenide solar cells selected for their high efficiency and proven reliability in deep-space conditions. Solar panels are deployed to maximize exposure to sunlight and are coupled with lithium-ion batteries, providing consistent power during eclipses. A dedicated power regulation and control system manages energy distribution across spacecraft subsystems, ensuring optimal functionality and robust power margins to support scientific instrument operation and communication with Earth.

Thermal Control is critical for maintaining payload and spacecraft system performance. It incorporates multi-layer insulation blankets, AZ-93 white thermal paint, polished aluminum, strategically placed radiators, and active heaters. These thermal control components regulate spacecraft and instrument temperatures within narrow operational limits (0 to 15 °C), ensuring data integrity and hardware longevity.

Propulsion is delivered via a bipropellant chemical system utilizing Monomethylhydrazine (MMH) and MON-25. Arianne group's engines S400-15 and S10-18 have been selected due to their exceptional performance and ease of integration. There are 4 main engines in a diamond shape configuration, 3 of these would be sufficient to perform the most critical maneuvers of the mission. The attitude thrusters are located 90 degrees apart along the lateral

phase of the structure, providing precise orbit insertion, station-keeping, and attitude control. Propellant and pressurant are stored in titanium-alloy tanks, designed for structural robustness. The total fuel budget for the mission is 1077 kg, considering 20 % reserves for operation flexibility.

The Attitude Determination and Control subsystem combines star trackers, inertial measurement units (IMUs), reaction wheels, and attitude control thrusters to maintain precise orientation. This suit of sensors and actuators will guarantee scientific accuracy, data collection consistency, and effective communications.

The ARES II mission design comprehensively fulfills all top-level requirements laid out at the start of the project. The primary science phase has been proven to be completed by December 2033. Simulations conducted in STK confirm that 75% of the Martian surface will be observed by DFRS and MSIS within 335 days. MAS completes its mapping objective within the four-year primary science window, and MID collects detailed imaging over key regions. Furthermore, as required the mission was designed complete an extended data collection phase until at least 2039.

Cost requirements are satisfied through efficient subsystem integration and the selection of commercial-off-the-shelf components where feasible. The estimated total mission cost is $771 million, staying well below the $1 Billion FY24 cap, with contingency reserves exceeding 15%. The mission timeline, detailed in the project's Gantt chart, ensures alignment with key milestones and guarantees timely execution of all critical phases.

Reliability under Martian environmental stressors is addressed through structural and component-level design. The semi-monocoque structure supports both launch and aerobraking stresses. The thermal subsystem maintains internal temperatures between 0°C and 15°C ensuring all components remain undamaged throughout the mission.

ARES II's design is supported by a comprehensive risk analysis covering potential failures across all mission phases, including launch, orbital insertion, and extended science operations. The mission risk matrix outlines scenarios ranging from attitude control failures to thermal regulation issues with mitigation strategies such as subsystem redundancy, onboard autonomy, and structural margins integrated throughout the spacecraft.

With all science objectives achievable, budgets met, and risks systematically addressed, ARES II stands as a mission-ready platform to enable the next generation of Mars exploration.

Table of Contents

List of Figures

List of Tables

1 Introduction

The ARES II mission is proposed in response to the critical data gaps that limit safe and suitable human exploration of Mars. Current and past, robotic missions such as the Mars Global Surveyor, Mars Reconnaissance Orbiter, and various surface rovers have contributed significantly to the understating of Mars' Martian geology, climate, and potential water sources. However, important knowledge gaps remain – particularly in high-resolution surface mapping, subsurface resource detection, and the fine-scale characterization of terrain hazards. These gaps directly affect the feasibility of future crewed missions, where decision around landing site selection, in-situ resource utilization (ISRU), and habitat deployment demand accurate, localized data.

Previous missions have utilized instruments such as radars and altimeters to expand understanding for Martian topography and shallow subsurface exploration. It is clear this technology is not resolution, coverage, and sensor redundancy to characterize meter-scale terrain features, detecting and quantifying near surface water ice, and mapping subsurface voids such as caves and lava tubes.

ARES II aims to bridge these gaps with an integrated orbital platform equipped with a comprehensive scientific payload. By combining high-resolution laser altimetry, dual frequency radar sounders, hyperspectral imaging and advanced thermal control, ARES II will generate detailed maps of Mar's elevation, slope gradients, subsurface composition and resource distributions. The spacecraft will operate in a low-altitude Mars orbit, enabling systemic data acquisition with at least 75% global coverage during the primary science phase.

This report outlines the product of the critical design phase for the ARES II mission. It details the mission's scientific objectives and design rationale, payload configuration, orbital mechanics and mission timeline, propulsion and power system, thermal system architecture, communications strategy, attitude control, structural design, and system-level integration. Additionally, it presents supporting trade studies, mass and power budgets, cost analysis and schedule assessments in compliance with the Request for Proposal. The report comprehensively outlines the current design status of ARES II and supports its development as a mission to enable future human exploration of Mars.

2 Mission Overview

This section outlines the overall mission profile and key scientific objectives. It provides a high-level summary of how ARES II will achieve its science goals through a phased operations plan, detailing the sequence of mission events, payload utilization strategy, and system-level coordination required to meet all performance and coverage requirements in Mars orbit.

The ARES II mission consists of a satellite equipped with various scientific instruments to accomplish the science objectives explained in Section 2.1. The satellite will depart from Earth on board SpaceX's Falcon 9 on November 29, 2028, and will arrive to Mars on September 13, 2029. The following figure shows the mission's Concept of Operations (ConOps), which outlines the ARES II mission timeline, key phases, and spacecraft operations from launch to end-of-life disposal.

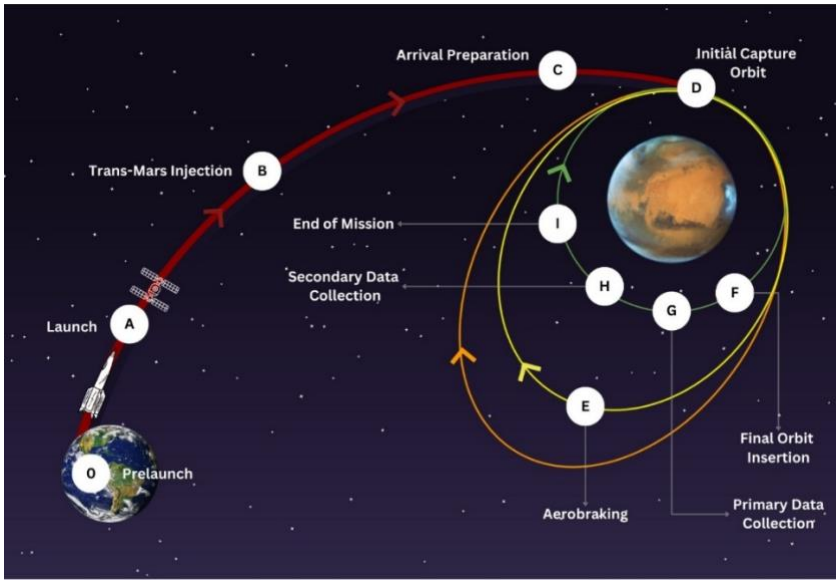

Figure 2.1 ARES II Mission ConOps

ARES II will collect critical data to allow scientists to uncover safe landing sites, traverse paths, and valuable resources that could help future manned missions. The satellite (shown in **Figure 2.2**) will primarily consist of a cylindrical structure containing four instruments: a Dual-Frequency Radar System (DFRS), the MSIS (Metropolitan Spectroscopy Imaging System), MID (Metropolitan Imaging Device), and MAS (Metropolitan Altitude Sensor). Moreover, a suit of sensors, antennas, actuators, and solar panels will be integrated into the satellite.

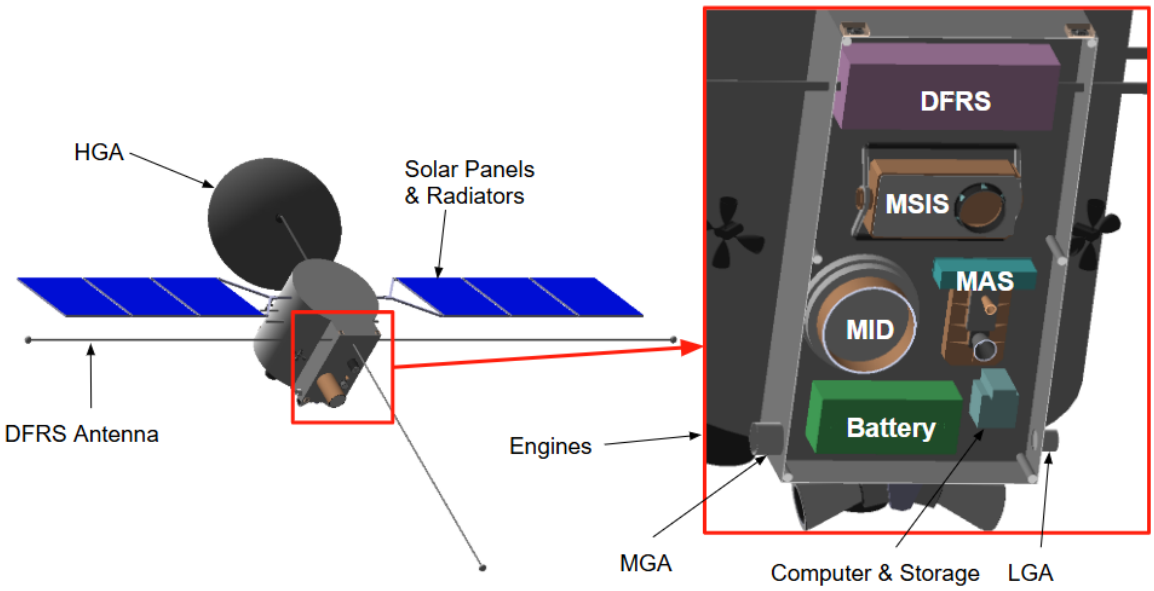

Figure 2.2 Complete Assembly of ARES II Satellite with Payload

As for the payload utilization strategy, all the instruments in the payload will not be used at the same time, but rather a schedule has been designed based on the data production and transmission data rate and power available to turn on and off each one, as further explained in Section 3.10.

2.1 Science objectives

This section outlines the two science objectives that will bridge the critical data gaps necessary for safe and effective human exploration of Mars: (1) obtaining a detailed geographic survey of Mars and (2) investigating its surface and subsurface resources.

2.1.1 Objective 1: Detailed Geographic Survey of Mars

This objective calls for a detailed geographic survey of Mars to identify safe landing sites and viable traverse paths for future human exploration. NASA's criteria for landing site selection emphasize that a safe landing zone must feature low, flat terrain to allow sufficient deceleration time during descent [1]. Equally as important is the absence of large obstacles, such as boulders or rugged outcrops, and the avoidance of extensive sand dune fields, which can compromise landing stability and hinder rover mobility.

Over the next sections, these features will be explored, and a proposed detection method will be elaborated.

2.1.1.1 Elevation Mapping

Scientific Rationale and Measurement Requirements

The elevation of the terrain is fundamental for identifying low-lying, flat areas that can serve as safe landing zones. Accurate elevation data also supports the planning of traverse paths by highlighting variations that could impact rover and human mobility. Up to this day, the Mars Orbiter Laser Altimeter (MOLA) on board NASA's Mars Global Surveyor has captured the Martian terrain elevation of almost all the surface with a vertical accuracy of less than 5 m, and a spatial resolution of 15 km at the equator [2]. Other planetary bodies, such as the Moon, have also been mapped with a vertical accuracy of 1 m, and a horizontal resolution of 10 m [3]. This level of detail makes it the benchmark for high-resolution elevation mapping beyond Earth, facilitating safe landing operations and geological exploration. For Mars, a vertical accuracy of 2.5 meters and a horizontal accuracy of 165 meters would represent a step up from the accuracy obtained by MOLA, doubling the accuracy of the previous model.

Proposed Detection Methods

Accurate elevation mapping is achieved through a combination of optical imaging and active remote sensing techniques. In our approach, a high-resolution camera will capture detailed visual images of the Martian surface to provide contextual information and assist in interpreting terrain features, while a laser altimeter will deliver precise, direct measurements of surface elevation by emitting laser pulses and analyzing the reflected signals. This dual-method strategy, successfully employed in previous missions, offers robust coverage and high vertical accuracy, ensuring that even subtle variations in terrain are reliably detected and accurately quantified.

2.1.1.2 Slope Detection

Scientific Rationale and Measurement Requirements

Measuring the slope of Mars' terrain is critical for selecting safe landing sites and designing optimal traverse paths for surface operations [4]. Detecting slopes greater than 5° is crucial, as steeper inclines greatly increase the likelihood of lander instability, tipping, or sliding. To mitigate these hazards, a minimum detection capability of 5° is essential, a requirement supported by the Autonomous Precision Landing and Hazard Avoidance Technology (ALHAT) project, which was developed to facilitate precision landings on both the Moon and Mars [5]. There are science gaps in slope detection that current orbiter instruments, specifically MOLA, have been unable to fully address.

One primary gap is that MOLA's resolution, with its 300-meter along-track spacing, limits the direct measurement of slopes at finer scales (such as meter- to decameter-scale slopes) that are critically relevant for landing system performance. The Mars Exploration Rovers (MER) landing studies revealed that the descent and landing systems are particularly sensitive to slopes on the order of 3 m and 100 m scales. However, MOLA's data are primarily effective for characterizing slopes at hectometer to kilometer scales, leaving an uncertainty in quantifying the small-scale roughness that directly impacts landing stability [6].

Detection Methods

Slope detection can be achieved using a combination of imaging and active altimetry techniques that have demonstrated strong heritage in previous planetary missions. For instance, laser altimeters have been successfully employed in missions such as Mars Global Surveyor with its MOLA instrument to acquire precise topographic data that can then be processed to derive slope gradients. Similarly, high-resolution cameras, already proven on several planetary missions, provide essential visual context that supports the derivation of digital elevation models, from which slope measurements are extracted. In our approach, the integration of these established methods will allow for reliable mapping of terrain slopes across the Martian surface without delving into overly detailed instrument specifications, leveraging the proven heritage of these instruments for effective slope detection.

2.1.1.3 Small-Scale Terrain Features

Scientific Rationale and Measurement Requirements

Accurate characterization of meter-scale surface roughness is critical for selecting safe landing sites and designing traverse pathways. While instruments like MOLA have provided valuable baseline measurements at the ~75-m scale, there is strong evidence that the roughness of the Martian surface exhibits important variations on finer, meter-to-decameter scales [7], [8]. Recent work using radar sounding techniques has demonstrated that by examining the spreading and decay of radar echoes, one can estimate a roughness parameter that is sensitive to horizontal variations on scales of roughly 10 m to 100 m [9]. In addition, by comparing these radar-derived roughness estimates with high-resolution digital elevation models, one can both validate and refine the measurements, leading to improved assessments of potential hazards.

Detection Methods

For our satellite, we intend to combine optical imaging and radar sounding techniques to measure meter-scale roughness. A high-resolution camera will capture detailed images of the Martian surface that enable the creation of digital elevation models (DEMs) with meter-scale horizontal resolution.

Complementing the imaging system, we propose to incorporate a radar sounder inspired by the Mars Shallow Radar (SHARAD) sounder. This radar will operate over a frequency band that yields vertical resolution on the order of a few meters. By processing the returned radar echoes through synthetic aperture techniques, we can extract key parameters serving as a quantitative roughness parameter, as demonstrated by Campbell et al. [9]. This method is particularly effective at revealing subtle variations in surface texture that are not resolved by conventional DEM analysis alone.

2.1.1.4 Sand Dunes and Dust Accumulation

Scientific Rationale and Measurement Requirements

The detection and monitoring of sand dunes and dust accumulation is essential for identifying stable regions for landers, rovers, and long-term surface operations. Sand dunes indicate areas of active sediment movement and granular instability and are therefore considered potential mobility hazards. Mapping these features supports the avoidance of difficult terrain, the selection of safe landing zones, and the placement of infrastructure in stable areas. Dust accumulation poses a risk by degrading solar power performance, obscuring optical sensors, and potentially interfering with thermal regulation. Observations from the InSight lander showed a loss of up to 2% solar power generation per sol due to dust buildup [10].

For mapping sand dunes, a minimum spatial resolution of 6.8 meters per pixel is required. This specification is consistent with the imaging performance of the Mars Orbital Camera (MOC) onboard the Global Surveyor probe (MGS), which has successfully resolved dune forms [11]. Nonetheless, to detect ripple motion the spatial resolution would have to increase to levels like the High-Resolution Imaging Science Experiment (HiRISE) camera on NASA's Mars Reconnaissance Orbiter, which is about 0.3 m/pixel [12]. Even so, a spatial resolution of approximately 1 m/pixel is likely sufficient to detect prominent dune structures and observe significant ripple or dune migration over seasonal timescales. For detecting dust accumulation, a spatial resolution of 6 m/pixel, as demonstrated by the Context Camera (CTX) on Mars Reconnaissance Orbiter, is sufficient to observe localized changes [13].

Detection Methods

Detection will rely on two imaging modes. The high-resolution imaging mode will capture detailed views of dune morphology, allowing for the observation of ripple structures and migration patterns over seasonal timescales. The context imaging mode will enable broad regional mapping to identify the extent of dune fields and monitor large-scale dust redistribution. Together, these modes will support both localized surface change detection and global characterization of aeolian activity.

2.1.2 Objective 2: Identification and Quantification of Surface and Subsurface Resources

This objective is dedicated to exploring and quantifying the natural resources available on Mars that are essential for supporting long-term human exploration. Key resources include water ice, various minerals, and other elements that can contribute to life support, fuel production, and other critical mission operations. In addition to these surface resources, significant value lies in identifying subsurface features such as caves and lava tubes. These formations not only have the potential to house valuable materials but may also provide natural shelter and serve as protected environments for future exploration activities. By creating a comprehensive resource inventory, this objective aims to establish a robust understanding of Mars' capability to support sustained human presence.

2.1.2.1 Water

Scientific Rationale and Measurement Requirements

Water is among the most critical resources for enabling sustained human presence on Mars. Access to water would directly support multiple aspects of a crewed mission, including radiation shielding, human consumption, oxygen extraction, plant cultivation for food, and the production of rocket propellant through the electrolysis of water into hydrogen and oxygen [14]. Given its immense utility, the detection and characterization of near-surface and subsurface water ice is central to achieving Objective 2 of this mission.

Current orbital missions have left several critical gaps in our understanding of the true extent, depth, and nature of subsurface ice on Mars. Although there is widespread indirect evidence for buried ice across the midlatitudes these datasets remain limited in their ability to resolve water content, vertical structure, and local-scale variability [15]. Existing data products typically rely on isolated measurements or regionally focused studies and cannot deliver globally consistent, high-resolution maps of subsurface ice distribution.

As highlighted in recent work [15], there is a particular need to better constrain the equatorward extent of buried ice deposits, especially within 0–10 m of the surface. These depths are most relevant for human access and in-situ resource utilization. Furthermore, uncertainties persist regarding the small-scale distribution of ice (below approximately 3 km resolution), the character of the overburden that may protect or obscure ice deposits, and the volumetric abundance of water ice within identified units.

Detection Methods

For our satellite, we intend to use a suite of radar-based instruments to detect and map water ice, addressing key knowledge gaps in both horizontal and vertical resolution. In particular, the synthetic aperture radar (SAR) imager operating in the L-band (around 930 MHz with a wavelength of approximately 32 cm) capable of compare different orientations of the radar waves to better distinguish between ice and rock or dust [15]. Additionally, we plan to include a C-band SAR imager, with adequate bandwidth to achieve resolutions on the order of tens of meters, which would allow for the detailed mapping of near-surface ice deposits. To better constrain the vertical structure of the Martian subsurface, we also intend to integrate a very high-frequency radar sounder designed to penetrate the overburden and characterize the depth, distribution, and nature of buried ice.

2.1.2.2 Minerals

Scientific Rationale and Measurement Requirements

For supporting human exploration of Mars, detailed mapping of the mineral composition is essential, as minerals play a critical role in resource extraction and construction. Engineers and scientists are particularly interested in several key categories of minerals:

1. Hydrated Minerals:

Hydrated clays, sulfates (such as gypsum), and perchlorates are of high priority because these minerals contain chemically bound water. Extracting this water is crucial for human consumption, oxygen production via electrolysis, and manufacturing rocket propellant. Their diagnostic absorption features typically occur in the near-infrared (around 1.4, 1.9, and between 2.2 and 2.4 μm) which sets a requirement for a spectrometer to cover at least the 0.4 to 4 μm range [16].

2. Mafic Silicates:

Basalt-derived minerals like olivine and pyroxene dominate the Martian regolith. Their characteristic absorption near 1 µm is valuable not only for understanding the regolith's chemical and mechanical properties but also for assessing its suitability for construction applications, such as sintered regolith concrete that can yield high strength building materials [17]. Additionally, their relative abundance is tied to the feasibility of producing oxygen and other extraction products from the Martian surface.

3. Metallic and Semi-Metallic Elements:

Mineral deposits containing elements such as iron, copper, nickel, and the platinum-group elements (PGEs) are of interest for future industrial applications. Even though current data on these resources is limited, identifying such minerals can inform long-term resource strategies for Mars settlement, even if they are not targeted in early missions.

Detection Methods

Our satellite's mineral detection strategy builds on the heritage of previous instruments—such as the Compact Reconnaissance Imaging Spectrometer for Mars (CRISM)—by using an advanced hyperspectral imaging spectrometer to acquire reflectance data. We intend to use a spectrometer that covers a wavelength range of roughly 0.31 to 5 µm, which is critical for detecting the diagnostic absorption features of the minerals of interest. Specifically, hydrated minerals (e.g., clays, gypsum, and perchlorates) exhibit absorptions near 1.4, 1.9, and between 2.2 and 2.4 µm. By capturing spectral signatures in these wavelengths, we can accurately estimate the water content and assess the potential for water extraction. Simultaneously, mafic silicates such as olivine and pyroxene display absorption bands near 1 µm, and our instrument's spectral resolution will be designed to distinguish these features even if they overlap with those of other minerals.

Heritage instruments have demonstrated the effectiveness of this approach, but our improved design will benefit from enhanced detector sensitivity and finer spectral resolution. This will allow us to more precisely quantify the abundance of each mineral phase and to map the spatial distribution of these resources at a scale that supports both construction material development and water processing strategies for in-situ resource utilization.

2.1.2.3 Caves and Lava Tubes

Scientific Rationale and Measurement Requirements

Caves and lava tubes on Mars have gained significant interest as natural shelters that could support long-term human habitation. These subsurface voids offer inherent protection against cosmic radiation, meteoroid impacts, and

extreme temperature fluctuations. In addition, they can serve as stable environments for resource extraction and habitat construction [18]. Past missions to Mars have largely relied on indirect evidence to infer the presence of subsurface caves. Instruments such as high-resolution optical cameras (like the HiRISE) and orbital altimeters (such as the MOLA) have been used to identify skylights and collapse features on the surface, which suggest the existence of underlying cave systems. However, these methods do not directly capture the internal structure of the caves, as they simply record surface expressions of potential caves. Additionally, early ground-penetrating radar systems operating in the MHz range provided limited spatial resolution (on the order of 100 m or more) and suffered from high levels of clutter, making it challenging to resolve the finer features associated with cave interiors.

Detection Methods

Our detection methods aim to overcome these limitations by integrating advanced very-high-resolution (VHR) SAR imaging with high-resolution optical data. Our approach builds on the heritage of recent work using VHR SAR systems that have demonstrated the potential to extract cave characteristics by analyzing radar backscatter anomalies associated with skylight regions [18]. By utilizing a radar system with improved range and azimuth resolution, and by implementing enhanced synthetic aperture processing algorithms, we plan to capture not only the surface collapse features but also to directly map the subsurface void geometry. This method enables us to isolate signals from a cave interior (which typically exhibit higher, more coherent backscatter due to rock-strewn floors) from the surrounding surface clutter. This direct approach should allow us to more reliably determine cave dimensions, such as roof height, cave width, and internal structure, rather than merely inferring their existence from indirect surface indicators [19].

2.2 Science Objectives and Requirements Summary

The following table is the science traceability matrix (STM) where a summary of this section can be found, providing a clear flow down from science objective to mission and payload requirements.

Table 2.1 Science Traceability Matrix

Science Objectives	Measurement Objective	Measurement Requirements	Instrument	Instrument Requirements	Data Products
A. Detailed geographic survey of Mars for human exploration for landing site location and traverse paths purposes.	I. Obtain high-resolution global topographic data	Cover ≥75% of the surface Mars at a horizontal resolution of less than ± 165 m and a vertical accuracy of less than ±2.5 m. The altimeter must have a spatial resolution of <16 m.	Laser Altimeter	The altimeter shall provide a measurement spot size, pulse frequency, and vertical accuracy sufficient to meet the stated measurement requirements.	1. Digital Elevation Map (DEM) 2. Identification of steep crates, canyons, and large dunes 3. Derived slopes and roughness estimates
		Photograph selected areas of high interest - covering at least 10% of the Martian surface - with a ground sampling ≤1 m/pixel, using stereo imaging to support DEM generation. Must cover the visible spectrum (400-700 nm wavelength)	Camera	The camera shall provide sufficient spatial resolution and operational capability to acquire imagery meeting the stated standards for all identified areas of interest by the end of the mission.	1. Stereo image mosaics for 3D mapping. 2. Photogrammetric DEM (if altimeter is unavailable). 3. Visual context for geologic units and landing site selection.
	II. Identify hazards (slopes, rocks, dunes, etc.)	Cover ≥75% of the Mars' surface detecting slopes ≥5 with ±2° accuracy.	Laser Altimeter	The altimeter shall provide a measurement spot size, pulse frequency, and vertical accuracy sufficient to meet the stated measurement requirements.	1. Hazard and slope maps for prospective landing zones. 2. Identification of steep crates, canyons, large dunes, and caves. 3. Exclusion zones for safe landings.
		The imaging system shall identify rocks ≥60 cm and dune ripple movement at ≤1 m/pixel over 10% of Mars' surface, focusing on selected areas of high interest. It shall be able to detect dust accumulation at ≤6 m/pixel over 10% of Mars' surface.	Camera	The camera shall provide sufficient spatial resolution and operational capability to meet the stated measurement requirements.	1. Hazard imaging sets. 2. Rock-size distribution maps for each candidate zone. 3. Combined slope and rock density overlays.
B. Investigate, identify, and quantify surface and subsurface resources.	I. Map surface water and minerals	Cover ≥75% of Mars with a spatial resolution ~150 m/pixel, a spectral range of 400-5000 nm with a spectral resolution ≤10 nm. The mission should also measure water ice or hydrogen content to within ±5% by mass.	Spectrometer	The spectrometer shall meet the required spatial resolution, spectral range, spectral resolution and operational capabilities to detect water ice and minerals.	1. Global maps of minerals outlined in Section 2 and water ice distribution.
	II. Characterize deeper subsurface layering	Map ≥75% of Martian surface at a depth penetration ≥3 km, with a minimum vertical resolution of 300 m.	Ground Penetrating Radar	The radar shall meet the required penetration depth, minimum vertical resolution, and operational capabilities to characterize subsurface layering.	1. Subsurface radargrams showing layering (ice, rock, possible caves). 2. 3D models or maps of subsurface reflectors. 3. Resource distribution correlated with topographic features.

3 Mission Operations

The ARES II mission design translates broad scientific objectives into a feasible and robust interplanetary architecture, constrained by technical, operational, and cost requirements. This section outlines the system-level requirements, mission profile, operational phases, and trajectory strategy that enable the spacecraft to achieve its primary goal: conducting a detailed geographic and resource survey of Mars. The mission leverages a proven Earth-Mars transfer, employs aerobraking for fuel-efficient orbit insertion, and maintains a science-optimized polar orbit throughout operations. Design decisions are supported by trade studies and simulations to ensure compatibility with the spacecraft's payload, environmental conditions, and mission timeline.

3.1 Mission Requirements

The following mission requirements have been derived from the mission and scientific objectives, as well as the payload requirements and constraints.

Table 3.1 Mission Requirements

Req. ID	Description
MLR-001	The mission shall be able to identify slopes, elevation and small-scale hazards.
MLR-002	The mission shall characterize surface and subsurface resources, including hydrated minerals, water ice, and caves and lava tubes.
MLR-003	The mission shall complete the primary data collection activities, covering 75% of Mars surface by December 31, 2033.
MLR-004	The mission shall support extended operations, with the payload continuing to gather data until at least 2039.
MLR-005	The project shall remain within a total program cost of $1 Billion (FY24), including design, manufacturing, testing, integration, launch, and primary operations, and incorporating a contingency reserve of ≥15%.
MLR-006	The spacecraft shall be designed to operate reliably in the deep-space environment, including exposure to radiation, thermal extremes, launch vehicle and aerobraking loads.

The requirements above ensure that the mission design will provide the necessary scientific data to support safe human exploration of Mars while operating within the defined technical, environmental, and budgetary

constraints. The detailed performance targets for sensors and the spacecraft's operational parameters will be the foundation for subsequent design decisions and trade studies.

3.2 Mission Architecture

To determine the best mission architecture to achieve the scientific objectives while satisfying the mission requirements, three potential strategies were evaluated: deploying landers, utilizing a satellite constellation, and employing a single orbiter. Each option was assessed against the mission's core requirements: ≥75% global coverage of Mars, completion of the primary science phase by December 31, 2033, and adherence to a $1 billion FY24 budget cap.

Landers were ruled out due to their highly localized data collection capabilities, environmental limitations, and prohibitive cost. Even with optimistic estimates, a lander's field of view rarely exceeds 100 km, and covering 75% of Mars (≈109 million km²) would require thousands of units. This is operationally infeasible and financially prohibitive, e.g., the Perseverance rover cost $2.2 billion in 2020 [20]. Additionally, landers face reliability issues in extreme Martian conditions, such as dust storms and seasonal frost, and cannot access key regions like cliffs and polar ice caps. A satellite constellation provides certain advantages, like increased temporal resolution and real-time monitoring, but introduces redundancy and exceeds mission needs. For planetary mapping, the benefits do not justify the added cost and complexity. Mars Reconnaissance Orbiter (MRO) demonstrated that a single, well-designed spacecraft can map nearly the entire Martian surface [21]. Given the mission's timeline and objectives, a constellation offers little added value for significantly higher cost [22]. A single orbiter emerged as the optimal mission architecture. A near-polar, sun-synchronous orbit enables systematic, long-duration mapping of Mars with consistent lighting conditions. This approach has been validated by multiple past missions. Mars Global Surveyor produced the first global topographic map of Mars [23], while MRO identified subsurface resources and terrain hazards [24]. ExoMars Trace Gas Orbiter further demonstrated the potential for subsurface hydrogen detection and global spectral analysis [25]. The single-orbiter approach enables full science return, minimizes redundancy, and stays well within mass and cost constraints.

3.3 Concept of Operations

This section expands on some of the phases (named A through I) previously shown in the mission's ConOps in Figure 2.1

Phase 0 includes details before launching and is not considered part of the mission phases. Phase A includes launching from Earth, orbiting in a parking orbit 200 km above the Earth's surface, and launch vehicle separation. While in the parking orbit, the spacecraft will do initial system checks to ensure all systems are functioning correctly and is ready to travel to Mars. A detailed diagram of Phase A can be seen in **Figure 3.1**.

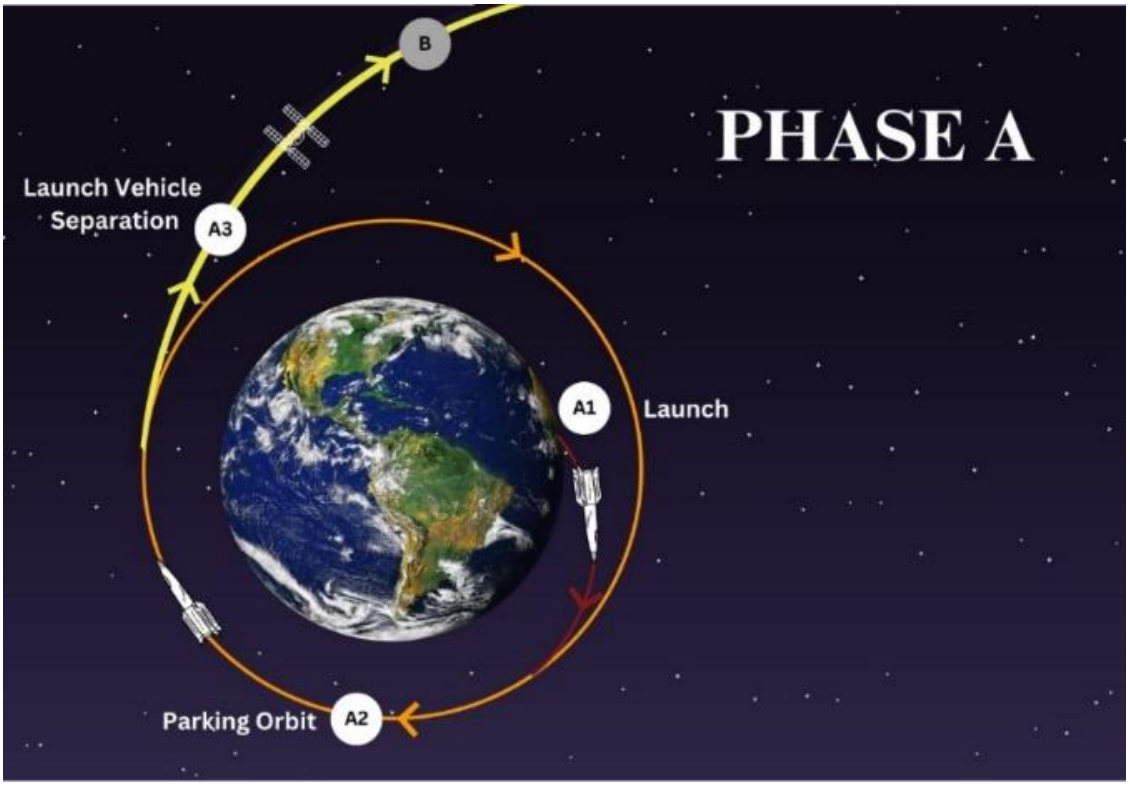

Figure 3.1 Phase A Details

Phase B is initiated once Phase A is completed. This includes necessary course corrections and maneuvers for the spacecraft to arrive at Mars. Phase C includes running system checks to ensure the spacecraft is set for initial orbit capture and aerobraking maneuvers, Phases D and E, respectively. These phases are thoroughly described in Subsection 4.4. Phase F includes entering the final scientific orbit where data collection will take place. Details of this orbit are given in Subsection 4.7. After final orbit insertion, science operations commence in Phase G which is pictured in **Figure 3.2**.

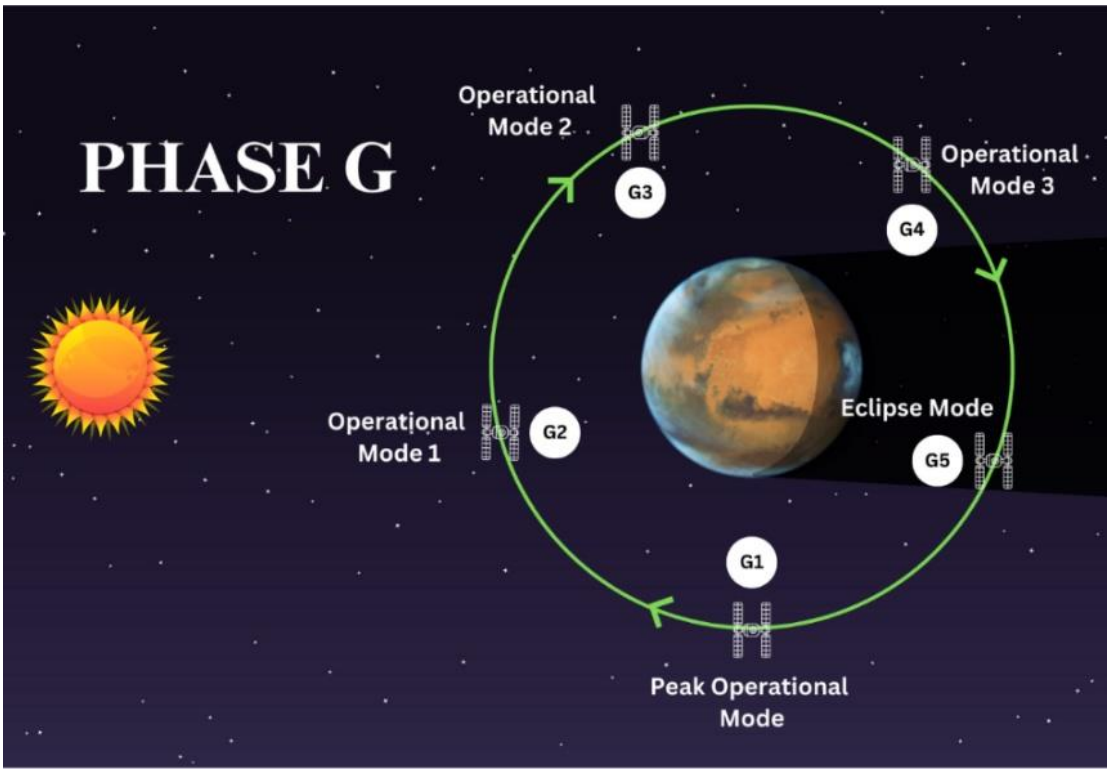

Figure 3.2 Phase G Details

During the data collection phases, the spacecraft will be operating in different modes. These operational modes describe which sensors and instrumentation will be active and are detailed in Section 5. The only operational mode based on a specific orbital position is the eclipse mode (G5), which is active when the spacecraft is in eclipse. Modes G1-G4 are not necessarily in the order or orbital locations depicted in **Figure 3.2**, they merely reflect that the spacecraft will have different active sensors at different times. Once the primary data has been collected by December 2033, the mission will move on to Phase H. The spacecraft will continue to collect Martian data in the same scientific orbit as in Phase G. The secondary data is collected to supplement the primary data with more accuracy and to monitor Mars' changing conditions. The ARES II spacecraft will continue collecting data until December 2039, then Phase I will be initiated, and the spacecraft will deorbit.

3.4 Project Timeline

The mission timeline outlines ARES II's major mission phases from pre-launch to end-of-life. It is designed to meet the AIAA Request for Proposal (RFP) deadline stating primary data gathering activities shall be completed no later than December 31, 2033. The timeline is in the form of a Gantt Chart which can be seen in **Figure 3.3** and **Figure 3.4**.

TASK TITLE	START DATE	END DATE	DURATION (DAYS)
PHASE 0: PRELAUNCH			
Define mission objectives and requirements	01/13/25	01/31/25	1
Conduct trade studies and technology selection	01/13/25	02/07/25	26
Mission conception finalization	01/13/25	02/23/25	42
Prliminary design review	02/23/25	02/23/25	1
Subsystem design and trade studies	02/23/25	04/10/25	47
Critical design review	04/10/25	04/10/25	1
Prototype development and testing	04/10/25	04/10/27	730
Final system integration and testing	04/10/27	10/31/28	571
PHASE A: LAUNCH AND EARTH DEPARTURE			
Launch from Earth	11/28/28	11/28/28	1
Parking orbit	11/28/28	11/28/28	1
Trans-Martian injection	11/29/28	11/29/28	1
PHASE B: CRUISE			
Interplanetary cruise	11/29/28	09/13/29	290
PHASE C: MARS APPROACH AND ORBIT INSERTION PREPARATION			
Adjust approach trajectory for optimal Mars arrival	8/29/29	09/13/29	16
Finalize aerobraking entry conditions	09/12/29	09/13/29	2

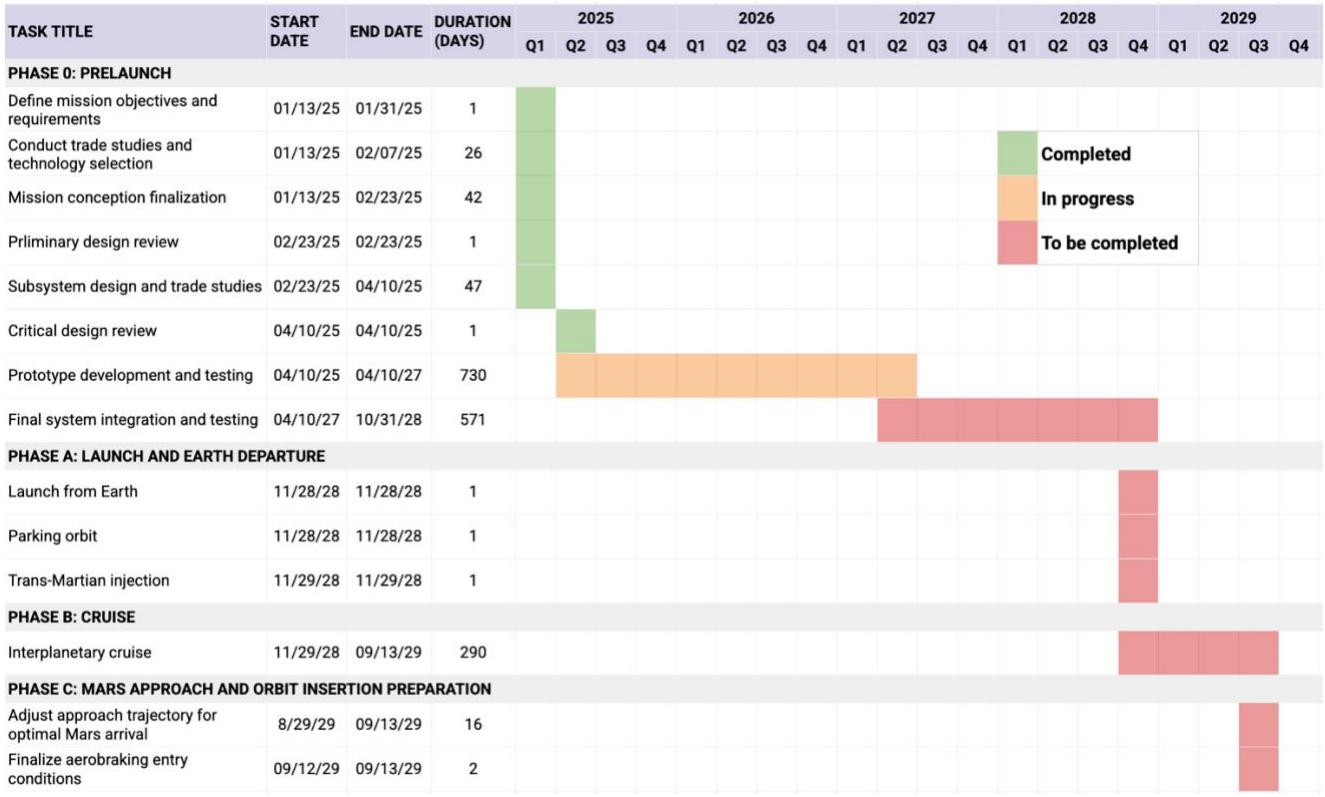

Figure 3.3 Project Gant Chart (A)

TASK TITLE	START DATE	END DATE	DURATION (DAYS)	2029				2030				2031				2032				2033				2034				2039			
				Q1	Q2	Q3	Q4	Q1	Q2	Q3	Q4	Q1	Q2	Q3	Q4	Q1	Q2	Q3	Q4	Q1	Q2	Q3	Q4	Q1	Q2	Q3	Q4	Q1	Q2	Q3	Q4
PHASE D: MARS ORBIT INSERTION																															
Initial capture orbit insertion	09/13/29	09/13/29	1																												
PHASE E: AEROBRAKING CAMPAIGN																															
Controlled aerobraking maneuvers	09/14/29	10/31/29	47																												
PHASE F: TRANSITION TO FINAL ORBIT																															
Scientific orbit insertion	10/31/29	10/31/29	1																												
Instrument deployment	10/31/29	10/31/29	1																												
PHASE G: PRIMARY SCIENCE OPERATIONS																															
Payload activation and calibration	10/31/29	10/31/29	1																												
Primary science data collection	11/1/29	12/31/33	1521																												
PHASE H: EXTENDED SCIENCE OPERATIONS																															
Extended science data collection	12/31/33	12/31/39	2192																												
PHASE I: END-OF-MISSION																															
Deorbit planning and execution	12/31/39	12/31/39	1																												
Spacecraft disposal	12/31/39	12/31/39	1																												

Figure 3.4 Project Gantt Chat (B)

Following the schedule outlined in the Gantt Chart ensures that the mission will be completed according to the deadlines set in the RFP. The ARES II spacecraft will also be able to gather plenty of secondary data to supplement the primary data until deorbit in late 2039. Phases A-I are the same phases represented in the ConOps.

3.5 Orbital Mechanics and Flight Control Requirements

This section provides the key parameters and constraints that govern the mission's orbital mechanics, including trajectory design, aerobraking maneuvers, station-keeping strategies, and decommissioning. Table 4.2 outlines all the requirements for Orbital Mechanics and Flight Control Subsystem.

Table 3.2 Orbital Mechanics and Flight Control Requirements.

Requirement ID	Description
SYS-ORB-001	The ΔV requirements across all mission phases shall be minimized.
SYS-ORB-002	The spacecraft shall be placed in a 200 km circular parking orbit around Earth in preparation for trans-Martian injection.
SYS-ORB-003	The spacecraft shall be inserted into a Hohmann transfer to arrive at Mars with an inclination angle range of 92.79° ± 4°.
SYS-ORB-004	The total mission duration of the interplanetary transfer shall be within 290 ± 10 Earth days.
SYS-ORB-005	The spacecraft shall be inserted into a highly elliptical capture orbit upon arrival at Mars with a periapsis altitude of 150 km and an eccentricity of 0.725.
SYS-ORB-006	The spacecraft shall perform single impulsive ΔV maneuvers at the aerobraking apoapsis, whenever necessary, to raise the aerobraking periapsis to 150 ± 3 km, maintaining the specified density corridor.
SYS-ORB-007	The spacecraft shall perform necessary reboosts for station-keeping purposes to maintain scientific orbit altitude of 350 ± 5 km, and eccentricity of 0-0.05 throughout the entire mission.
SYS-ORB-008	The spacecraft shall safely deorbit from its scientific orbit upon the conclusion of the extended mission phase.

3.6 Trajectory

SYS-ORB-001 places a stringent requirement for TMI ΔV from the parking orbit to be minimized. To satisfy this requirement, the spacecraft will be inserted in a Hohmann transfer orbit as this type of orbital maneuver is well-known for being the most energy efficient. The *Earth-Mars Ballistic Transfer Trajectories 2028* porkchop plots published by NASA served as guides to determine the departure and arrival dates for the ARES II mission, as presented in **Figure 3.5** [26]. Only transfer opportunities with lower departure energy and lower Mars arrival excess speed requirements were considered in the interplanetary mission selection process.

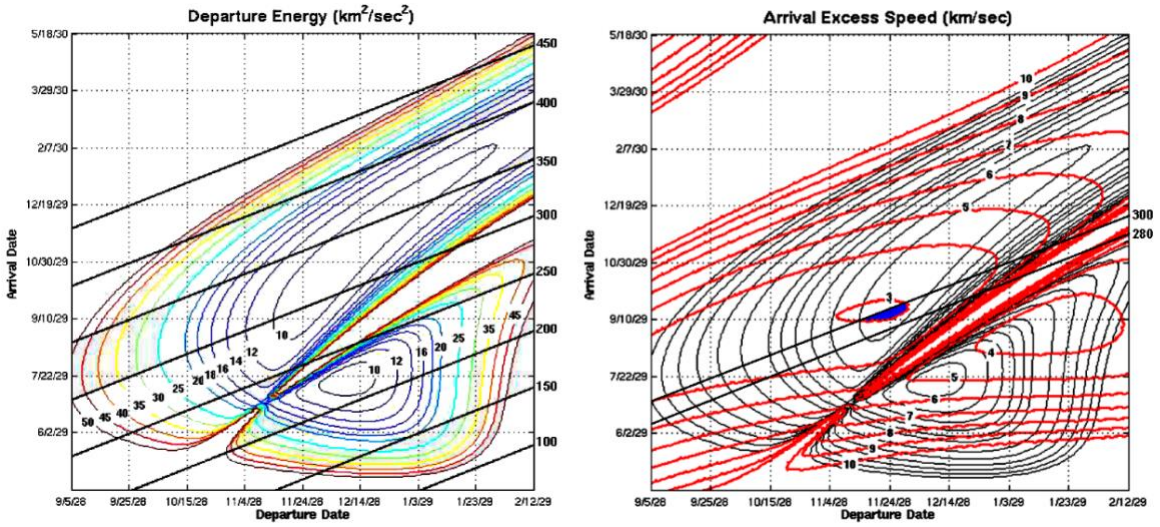

Figure 3.5 Earth-to-Mars 2028 to 2029 Mission Opportunities Porkchop Plots. [26]

Whilst there were two minimum departure energy areas, the departure window with the lower Mars arrival excess speed lay above the 180° transfer ridge, indicating a Type II trajectory. Since SYS-ORB-002 requires the mission trip time to be within 290 ± 10 Earth days, this gave the ARES II mission a departure period from approximately 13 Nov. 2028 to 1 Dec. 2028, as depicted by the blue region in **Figure 3.5**. Several factors, such as weather conditions, procedure slippage, launch vehicle readiness status, may cause the departure date to be delayed and not necessarily centered on the date with the minimum departure energy. Therefore, it is important for this window to be as wide as possible to account for these uncertainties. The speed of the spacecraft at 200 km parking orbit, V_c, and hyperbolic excess speed at departure, $V_{\infty,D}$, were calculated using the method of patched conics to determine the required ΔV to insert ARES II into a heliocentric trajectory to rendezvous with Mars.

$$\Delta V = V_c\left(\sqrt{2+\left(\frac{V_{\infty,D}}{V_c}\right)^2}-1\right) \tag{4.1}$$

Using the equations above, the required TMI ΔV for ARES II will be 3.60 km/s and the transfer will take about 290 Earth days when departing on 29 Nov. 2028. ARES II will embark on a Type II trajectory, meaning that it will travel more than 180° but less than 360° true anomaly around the Sun, as illustrated in **Figure 3.6**.

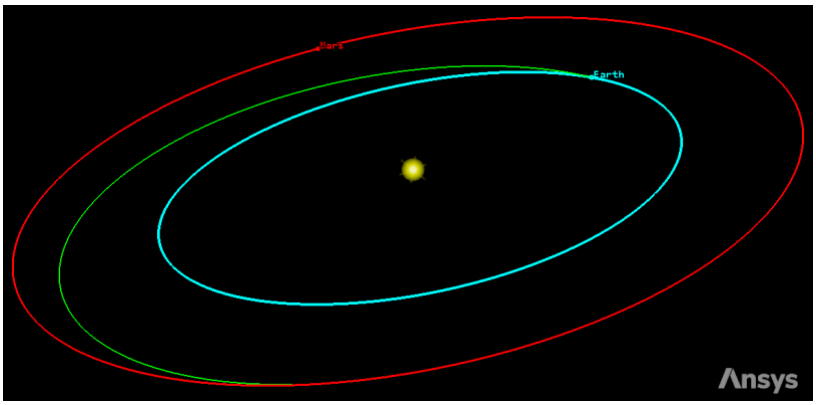

Figure 3.6 STK Simulation of ARES II Heliocentric Trajectory.

Upon arrival at Mars' sphere of influence, ARES II will have an excess speed of 2.648 km/s relative to Mars' heliocentric velocity. A required ΔV burn of 1.02 km/s opposite the velocity vector will be imparted to insert ARES II into a highly elliptical capture orbit, as illustrated in **Figure 3.7**, with a periapsis altitude of 150 km and an eccentricity of 0.725. This orbit will serve as the initial state for the next mission phase.

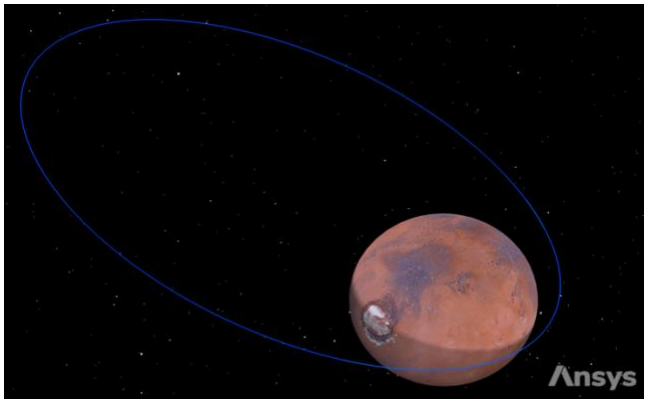

Figure 3.7 STK Simulation of ARES II Initial Capture Orbit.

ARES II will perform aerobraking technique to efficiently put itself into the intended scientific orbit around Mars, as shown in **Figure 3.8**. The team selected to do this approach instead of imparting a significantly large impulsive burn, in compliance to the requirements specified in SYS-ORB-001. The aerobraking campaign will take approximately 2 months to complete, with a total of 320 passes, gradually lowering the apoapsis to 350 km. Upon completion of the aerobraking campaign, ARES II will impart a required ΔV of 0.1 km/s at the apoapsis to circularize the orbit for the primary data gathering mission. In the case where a plane change of up to 4° is needed, this would be the ideal time, as performing both speed and plane changes at the same time at the apoapsis is more fuel-efficient. Should a plane change maneuver be necessary, the required ΔV may increase to 0.239 km/s.

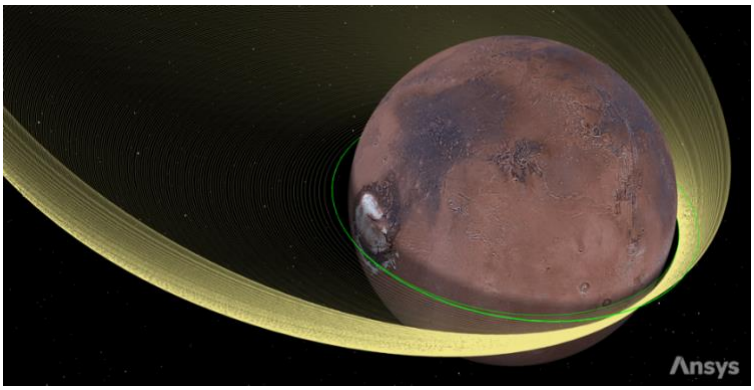

Figure 3.8 STK Simulation of ARES II Aerobraking Campaign.

3.7 Launch Vehicle Trade Study

The launch vehicle is one of the primary design drivers of the mission, making it crucial to select the best one that maximizes the overall spacecraft design to meet mission objectives and requirements. The team prioritized a launch vehicle capable of delivering a payload fairing mass to direct-to-Earth escape trajectories at low launch costs. Other criteria such as reliability and payload fairing volume were also considered. Four heavy-lift rockets were explored in the trade study, namely the Falcon 9 and Falcon Heavy of SpaceX, Ariane 64 configuration of Arianespace SA, and Vulcan Centaur 6S configuration of ULA. A trade study was conducted for all the aforementioned launch vehicles, with the key findings summarized in **Table 3.3**.

Table 3.3 ARES II Launch Vehicle Trade Study [27] [28] [29]

Category	Falcon 9	Falcon Heavy	Ariane 64	Vulcan Centaur 6S
Payload Capacity for Earth-Escape Trajectory [kg, (lb)]	4,020 (8,860)	16,800 (37,040)	6,900 (15,215)	7,600 (16,800)
Launch Cost ($M)[1]	73	105	120	110
Reliability	99.3 (435 missions)	100 (11 missions)	75 (1 mission partial failure)	100 (2 missions)
Payload Fairing Volume (m^3)	278	278	458	390

[1] Adjusted for inflation.

Reliability played a factor in the selection process. The team sought a launch vehicle with a proven track record of successful missions. SpaceX's Falcon family of launch vehicles boasts excellent track records with 436 successful launch services out of 437 missions combined, making them particularly appealing to the team. With all factors carefully considered, the Falcon 9 was selected as the launch vehicle for ARES II mission, capping the maximum payload mass at 4,020 kg. However, the team is also aware that newer and more advanced heavy-lift rockets, such as SpaceX's Starship and Blue Origin's New Glenn, are currently under development and may provide better performance than Falcon 9. If they become available for launch services within the mission's timeframe, the team may reassess and opt to replace the current launch vehicle of choice.

3.8 ΔV Budget

Presented in **Table 3.4** is the ΔV budget for various critical mission phases of ARES II from its parking orbit around Earth to EOL disposal, once the extended mission phase has ended. Few of the numbers were already discussed in Section 4.5.

Table 3.4 ARES II ΔV Budget.

ARES II Mission Phase	Nominal Required ΔV (km/s)	Nominal Burn Time (s)
Parking Orbit to TMI	3.60	-
Attitude Corrections Post-Payload Separation	0.005	55
Mid-Course Corrections	-	-
Mars Orbit Insertion	1.02	1,810
Corridor Control Aerobraking Maneuver (Periapsis Targeting)	0.005	465
Insertion Burn to Final Orbit *Without Plane Change* *With Plane Change (±4°), if necessary*	 0.100 0.239	 - 280
Station-keeping Throughout the Mission	0.012	125
EOL Disposal	0.075	90
TOTAL	3.60 + 1.456	47.1 min

After the TMI maneuver, the team allocated ΔV provisions of 0.005 km/s for spacecraft attitude corrections post-payload separation. Following the *Earth-Mars Ballistic Transfer Trajectories 2028* porkchop plots again, ARES II is not expected to execute mid-course corrections, indicating that the transfer is entirely ballistic. Furthermore,

during the aerobraking campaign, ARES II may perform single impulsive ΔV maneuvers at the aerobraking apoapsis to raise the periapsis to within 150 ± 5 km. The team apportioned a total ΔV of 0.005 km/s for these maneuvers, maintaining the spacecraft within the desired density corridor. During the primary data gathering mission, natural space environments such as, solar radiation pressure, gravity-gradient torque and atmospheric drag, may cause deviations in the ARES II scientific orbit. Therefore, a ΔV of 0.012 km/s will be reserved to counteract these effects on the spacecraft, ensuring regular reboots for station-keeping and spacecraft-pointing purposes. Lastly, ARES II will impart a ΔV of 0.075 km/s for EOL disposal, ensuring the safe and controlled deorbiting of the spacecraft from its scientific orbit upon completion of extended mission phase.

3.9 Scientific Orbit

ARES II will be placed in a near-polar, circular, sun-synchronous orbit around Mars, ensuring consistent lighting conditions crucial for the power-intensive spacecraft and some on-board instruments (i.e. cameras and spectrometer). The team performed an orbit altitude trade study for ARES II. While the main goal was to provide scientific data coverage of at least 75% of Mars' surface, gathering high quality data was secondary to the team. Most scientific instruments on board must operate at low altitudes to yield high quality and accurate data given their respective intrinsic features, therefore, restricting the orbit altitude trade to low Martian orbits. The team used STK's built-in *Simple Coverage* tool from the *Figure of Merit* object to determine the Percent Satisfied and Area Satisfied metrics.

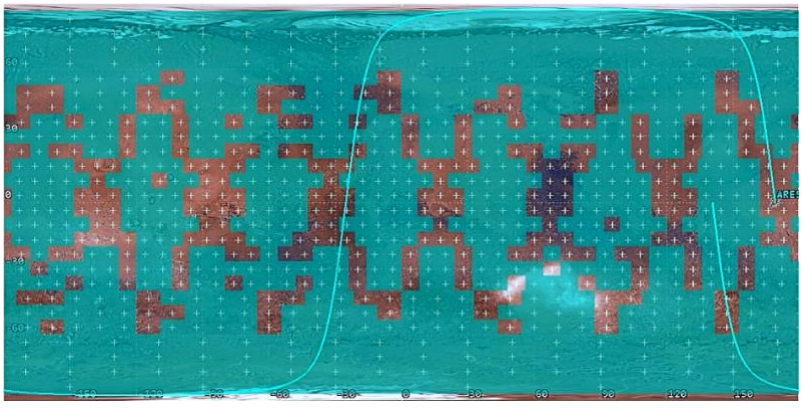

Figure 3.9 STK Simulation of Area Satisfied of ARES II with Altimeter FOV – 2D Map.

Given the 350 km orbit altitude, an inclination angle of 92.79° and a limiting sensor FOV of 0.116° from the altimeter, the team simulated the scenario over a 4 year-period, following the primary data gathering period scheduled

to end on 31 Dec. 2033, as stated in the RFP. The simulation indicated that the considered parameters could achieve 76% coverage of the Martian surface, thereby satisfying MRL-003 requirements. The simulation results are provided in **Table 3.5**.

Table 3.5 ARES II Coverage Simulation Results.

Metric	Value
Percent Satisfied *(%)*	76.12
Martian Surface Area Satisfied *(km^2)*	109.9e8

3.10 Scientific Operations Overview

The science operations timeline for the ARES II mission is organized into five distinct phases, each designed to align instrument activity with mission objectives, operational constraints, and data return capabilities. These phases reflect a progressive strategy to maximize scientific return.

To inform the design of these phases, careful consideration was given to the mapping performance of each instrument. The table below summarizes the estimated time required for each science payload to achieve 75% global coverage of the Martian surface. These estimates assume continuous operation whenever observational conditions are suitable—such as daytime-only activity for certain instruments (see more in Section 0)—and these constraints were accounted for in the simulations. The simulations were performed in STK using the Simple Coverage tool, consistent with the orbit trade study described in the previous section. The context camera is excluded from this table, as it is primarily operated in support of other instruments, not as a standalone mapping tool.

Table 3.6 Time to 75% Surface Coverage by Instrument

Sensor	FOV (°)	Operational Constraint	75% Coverage Duration (Earth Days)
Altimeter	0.116	None	1460
Camera (High Resolution Mode)	2	Daytime Only	104
Radar (High Frequency Mode) Radar (Low Frequency Mode)	0.343 2.292	None	335 90
Spectrometer	8	Daytime Only	14

The following figure provides an overview of the mission's scientific operations, showing the activity timeline of each instrument throughout the mission.

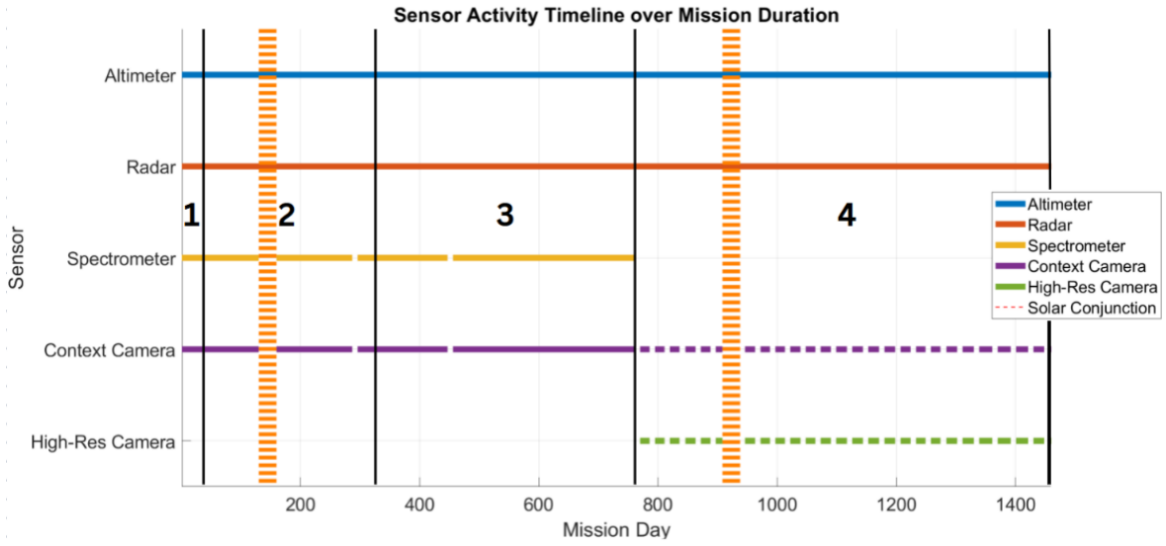

Figure 3.10 ARES II Sensor Activity During Scientific Operations Phases

Day 0 marks the start of nominal science operations in Mars orbit. Prior to this, a theoretical Phase 0—though not a primary mission deliverable—offers valuable science return: during 320 aerobraking passes at 150 km periapsis, the IMU collects drag data to derive vertical density profiles of the Martian upper atmosphere, helping refine current models. From Day 0, Phases 1 through 4 define the main science operations. Instruments with wide fields of view, such as the spectrometer and radar, quickly achieve their primary mapping goals and are then used primarily for measurement redundancy and validation. During Phases 1 to 3, the high-resolution mode of the camera remains inactive due to its high data rate, which makes unscheduled imaging inefficient. Instead, the camera operates in context mode to support spectrometer observations. By the end of Phase 3, accumulated data and team analysis yield a prioritized list of candidate sites for targeted imaging. Phase 4 begins with the deactivation of the spectrometer to reduce data volume. The radar and altimeter remain active, the former due to low data demands and the latter to complete its mapping goal. With a targeted imaging plan in place, the high-resolution mode of the camera is activated - context mode is still operational to provide wider context for the images - to capture selected regions of interest. This final phase lasts ~700 days and is expected to complete the altimeter's coverage and return high-resolution imagery for over 30,000,000 km² of the Martian surface.

4 ARES II Payload

The ARES II mission will deploy a carefully chosen suite of scientific instruments to meet the mission's key science objectives and satisfy the measurement requirements. Acting as a reference design, this payload confirms that the mission's goals are achievable with existing technologies while also defining critical performance drivers and operational constraints that shape the spacecraft's design envelope. All performance values presented herein correspond to a near-polar, sun-synchronous circular orbit at 350 km altitude, chosen to optimize mapping coverage and resolution.

We began by reviewing instruments used in successful space missions, ensuring their relevant performance characteristics were well understood. We then assessed how each instrument would function under ARES II conditions and conducted trade studies among the primary instrument categories — lidar, radar, cameras, and spectrometers — to determine which specific models would yield the best combination of performance and mission feasibility for ARES II's objectives and requirements. Following these evaluations, we introduced modifications to instrument parameters where needed. These changes are carefully justified and simple enough that their effects remain within well-understood, acceptable limits.

Table **4.1** summarizes the key measurement requirements that guided the design and selection of the reference payload, based on the mission-level science objectives defined in Section 2.2.

Table 4.1 Payload Requirements

Req. ID	Requirement Description
SYS-PAY-001	The payload shall generate elevation data from the Martian surface with a horizontal accuracy better than ±165 meters and a vertical accuracy better than ±2.5 meter.
SYS-PAY-002	The payload shall be able to acquire stereo imagery of selected areas of high interest at a spatial resolution of ≤1 m/pixel to support altimeter readings.
SYS-PAY-003	The payload shall detect surface slopes ≥5° with an angular accuracy of ±2°.
SYS-PAY-004	The imaging system shall identify rocks ≥60 cm and dune ripple movement at ≤1 m/pixel and detect dust accumulation at ≤6 m/pixel
SYS-PAY-005	The spectrometer shall identify minerals and water ice at a spatial resolution of ~15–20 m/pixel, across a spectral range of 400–5000 nm, with a spectral resolution ≤10 nm.

Req. ID	Requirement Description
SYS-PAY-006	The subsurface radar payload shall subsurface structures with a penetration depth of ≥1 km and a vertical resolution of approximately 10% of the depth.
SYS-PAY-007	The imaging system shall include a context imaging mode operating at intermediate resolution to provide spatial context for high-resolution and spectroscopic observations, ensuring coordinated targeting and scientific interpretation.

4.1 Payload Overview

This section presents an overview of the ARES II payload, summarizing the scientific role, performance, and requirement traceability of each instrument. Table **4.2** provides the relevant performance specifications for each instrument (for more information see the subsequent sections).

Table 4.2 ARES II Payload Scient Purposes and Performance Parameters

Instrument	Scientific Purpose	Performance Parameters	Requirements Satisfied
Altimeter	Provides high-precision elevation data to generate global Digital Elevation Models (DEMs) and detect slopes.	709 m spot size 28 Hz Pulse Rate 0.59 m Vertical Accuracy 147.5 m Horizontal Accuracy	PAY-SYS-001 PAY-SYS-003
Camera (Context Mode)	Captures wide-area, lower-resolution imagery to support terrain mapping. Crucially, it provides contextual information for interpreting high-resolution camera data and spectrometer observations.	Spectral range 400-700 nm 150 m horizontal resolution	PAY-SYS-007
Camera (High Resolution Mode)	Enables fine-scale imaging of surface features such as rocks, dunes, and cracks. Supports photogrammetric DEM generation, ripple motion detection, and landing site hazard characterization at meter-scale resolution.	Spectral range 310-5100 nm <1 m horizontal resolution	PAY-SYS-002 PAY-SYS-004
Radar	<u>High Frequency Mode</u> Probes the shallow subsurface (tens to hundreds of meters) with high vertical resolution. It enables mapping of stratigraphy, shallow layering, and surface roughness. <u>Low Frequency Mode</u> Penetrates deeper into the Martian subsurface (up to several kilometers), enabling the detection of buried structures such as lava tubes, ice layers, and voids.	<u>High Frequency</u> 1 km Penetration Depth 7.5 Vertical Resolution 3 km Swath Width 0.3-1 km by 3-7 km Horizontal Resolution (Along-track by Cross-track) <u>Low Frequency</u> 5 km Penetration Depth 75 Vertical Resolution 10 km Swath Width 5-9 km by 15-30 km Horizontal Resolution (Along-track by Cross-track)	PAY-SYS-006

Instrument	Scientific Purpose	Performance Parameters	Requirements Satisfied
Spectrometer	Provides hyperspectral imaging to identify surface mineralogy and hydration features, including clays, sulfates, and ice.	Spectral range 310-5100 nm 10 nm Spectral sampling interval 15 nm Spectral resolution 150 m horizontal resolution	SYS-PAY-005

4.2 Altimeter

The performance of the altimeter was obtained by analysing and studying three altimeters from previous successful missions: the MOLA, the LOLA, and the ATLAS. All three altimeters work by transmitting pulses at continuous bursts and measuring the time that takes to bounce back from the surface of Mars back to the receiver. Table **4.3** compiles the specifications and performance of the instruments considered.

Table 4.3 Key Parameters for MOLA, LOLA, and ATLAS

Parameter	**MOLA** [30]	**LOLA** [31]	**ATLAS**
Mass (kg)	25.9	9.6	470
Power (W)	30.9	26.2	420
Cost (FY24 M$)[2]	18	37	55
Pulse Frequency (Hz)	10	28	10
Vertical Accuracy (m)	5	0.1	0.0254
Horizontal Accuracy (m)	330	25	0.7
Spot Size (m)	160	50	17

Among the three altimeters analyzed, LOLA is the most suitable heritage instrument to base the design of the ARES II altimeter on. MOLA, while proven on Mars, lacks the precision and resolution required for this mission's small-scale terrain characterization and hazard detection. ATLAS, although highly precise, presents significant drawbacks in terms of mass and power consumption, making it less compatible with the constraints of the ARES II platform. LOLA strikes the optimal balance by offering higher precision than MOLA and significantly lower mass and power demands than ATLAS, while its five-beam configuration ensures dense surface coverage and reduced

[2] Adjusted for inflation.

terrain sampling gaps. This distinct operational mode, in which the laser is split into five beams, enhances both accuracy and spot distribution. Although LOLA was originally designed for lunar conditions, its advanced technology and lightweight design make it an ideal foundation for adaptation [31] [32] [33]. To address the environmental differences, we propose integrating MOLA's Mars-proven design with LOLA's multi-beam configuration to develop the MAS [34]. This hybrid instrument will retain MOLA's reliability in Mars' atmosphere while leveraging LOLA's superior resolution and coverage capabilities to meet the specific scientific and operational needs of the ARES II mission.

The LOLA has a distinct operational mode where the laser is split into five beams, increasing the accuracy and spot size. Although the LOLA boasts a lightweight design and incorporates more advanced, accurate laser altimetry technology, it is only designed to function in lunar conditions. To overcome this issue, we intend to integrate the MOLA's Mar's proven design, with the advanced technology of the LOLA, developing the MAS specifically for this mission. The MAS will maintain MOLA's reliability in Mars' atmosphere and Martian conditions while incorporating LOLA's multi-beam system for higher resolution and accuracy.

To optimize the performance of the MAS for the conditions of this mission, the accuracy of the altimeter must be maintained given the increase in operating altitude. LOLA was originally designed to operate at an orbital altitude of 50 km, whereas the ARES II mission will place the altimeter in a 350 km orbit. This significant increase in altitude naturally reduces measurement accuracy due to signal attenuation and beam divergence. To mitigate this, design parameters for the MAS were carefully adjusted based on the findings of Bruzzi [35], which analyzed the relationship between system performance and effective range. Specifically, the pulse energy was increased to extend the effective range, which we used to derive a factor for increase in accuracy. Additionally, the MAS beam divergence was increased—doubling the conical half-angle through geometric analysis—to produce a larger spot size for faster surface coverage. Since a larger spot size typically compromises accuracy, the aperture size was also increased to reduce the drop in accuracy, again using the proportional relationships established in the Bruzzi study. These modifications ensure that MAS maintains the necessary precision and surface coverage performance. Regarding cost and mass, these are assumed to remain unchanged. However, power consumption will increase by 14 watts due to the increase in pulse energy [36]. This increase is considered justified due to the enhanced functionality and performance. **Table 4.4** outlines the modifications made to the parameters of the LOLA.

Table 4.4 Modifications to LOLA for the Development of MAS

Parameters Modified	LOLA	MAS
Operating Height (km)	50	350
Conical Half Angle (deg)	0.029	0.058
Pulse Energy (mJ)	2.7	5.6
Receiver Aperture Diameter (cm)	14	21.6

Table **4.5** presents how these modifications made to the LOLA define the new parameters of the MAS and how its performance compares to the MOLA, the most advanced altimeter system currently used on Mars.

Table 4.5 Performance Comparison of LOLA, MAS, and MOLA

Parameter	LOLA	MAS	MOLA
Mass (kg)	9.6	9.6	25.9
Power (W)	26.2	40.2	30.9
Cost (FY24 M$)	37	37	18
Pulse Frequency (Hz)	28	28	10
Vertical Accuracy (m)	0.1	0.59	5
Horizontal Accuracy (m)	25	147.5	330
Spot Size (m)	50	709	160

Orbit, operations, pointing and other mission requirements

The operation of MAS introduces several constraints and requirements, primarily related to spacecraft altitude control, surface tracking geometry, and data acquisition. These are summarized in Table **4.6**.

Table 4.6 MAS Operating Constraints

Parameter	Value / Requirement
Pointing Direction	Nadir
Daylight Requirement	None (operates in day or night)
Acquisition Mode	Continuous along ground track

Parameter	Value / Requirement
Pointing Direction	Nadir
Average Data Rate During Operation	0.03 Mbps
Required Orbit Altitude Range	250–450 km (Based on Instrument Limitations)
Time for 75% Coverage	1460 days

4.3 Camera

Three existing camera designs were considered as the baseline for the design of the camera: the Mars Orbiter Camera (MOC), the HiRISE (High Resolution Imaging Science Experiment), and the CASSIS (Colour and Stereo Surface Imaging System).

The MOC was used on NASA's Mars Global Surveyor (MGS) alongside the MOLA. It was designed to observe the Martian surface as well as the atmosphere and its various meteorological changes over time. The camera structure consists of an 0.88 m tall and 0.4 m diameter cylinder that encompasses the three optical systems in use. These are made up of a narrow angle system located within the main cylinder, and two wide angle systems mounted on the outside, one using a red filter and the other using a violet filter [27]. This allows the camera to operate at multiple different wavelengths and varying spatial resolutions, with the narrow angle camera able to produce about 1.5 m per pixel. The multiple wide angles allow for built in redundancy and the ability to lower power usage when certain wavelengths are preferred at certain times. All the narrow images are compiled into a map associated with the wide lens images in a larger contextual map [28].

The CASSIS represents ingenuity in planetary imaging, using rotational mechanisms to photograph the same location at different angles to produce 3 dimensional images in colour [32]. Used onboard ESA's Exomars Trace Gas Orbiter, the CASSIS is composed of two main structural elements: the camera rotation unit that contains the imaging system itself, rotational mechanisms and associated cables alongside the electronics unit that are used to make the camera operational. The images themselves are at a resolution of about 4.6 m per pixel at an orbit of about 400 km in altitude [33]. The images are taken at periods to strategically overlap and help create larger scale mapped images [34]. Although the technology to produce layered 3D images is extremely effective, the rotation required can be very energy intensive and is used sparingly to allocate energy efficiently across the orbiter.

To meet the mission and payload requirements, the Metropolitan Imaging Device (MID) being used for this mission will incorporate technology from the HiRISE into the simplistic design of the MOC to strengthen the narrow lens system. This involves increasing the number of CCDs, applying different filters, incorporating more precise calibration techniques and stronger signal processing. Although drawing more power, the spatial resolution can be expected to increase significantly, as estimated in the final column of Table **4.7**.

Table 4.7 Specifications of MID

Parameter	MID
# Cross-track pixels[3]	407 (CTX resolution) 12,217 (high resolution)
Spectral range (nm)	400 - 700
# Spectral bands[4]	60
FOV[5]	10° (CTX resolution) 2° (high resolution)
IFOV[6] (mrad)	0.4286 (low resolution) 0.0029 (high resolution)
Spectral sampling interval	5 nm
Power consumption (W)	80
Average Data Rate During Operation (Mbps)	4 (CTX resolution) 18,000 (high resolution)
Mass (kg)	60

Orbit, operations, pointing and other mission requirements

The camera design will impose requirements and constraints in the mission; these are listed in the following table.

Table 4.8 Spectrometer Requirements

Parameter	Value / Requirement
Pointing Direction	Nadir
Daylight Requirement	Only operates during daylight

[3] Number of cross-track pixels is calculated as 1.5×(FOV/IFOV). The 1.5 factor is added to account for the "smile distortion" on this type of sensor and to add conservatism when calculating the data size of each sample.
[4] Calculated as (upper spectral range - lower spectral range) / (spectral sampling interval).
[5] Value chosen to minimize collection time of 75% of Martian surface.
[6] IFOV is calculated as GRD÷h, using the small angle approximation.

Parameter	Value / Requirement
Pointing Direction	Nadir
Acquisition Mode	Pushbroom
Average Data Rate During Operation	4 Mbps (CTX) 19980 (High Resolution)
Required Orbit Altitude Range	350 km based on design constraints
Time for 75% Coverage	10 (CTX) 335 (High resoltion)

4.4 Radar

To fulfill mission requirement MLR-001, which mandates the acquisition of detailed information about Mars' surface topology and subsurface resources, the selection of a capable radar system was critical. For the instrument selection a trade study was conducted to identify the most suitable candidate among several proven radar systems: SHARAD (Shallow Radar), MARSIS (Mars Advanced Radar for Subsurface and Ionosphere Sounding), NISAR (NASA-ISRO Synthetic Aperture Radar), and ALOS-4 (Advanced Land Observing Satellite-4). The following table compiles the specifications and performance of these instruments which were considered during the study [37].

To fulfill mission requirement MLR-001, which mandates the acquisition of detailed information about Mars' surface topology and subsurface resources, the selection of a capable radar system was critical. For the instrument selection a trade study was conducted to identify the most suitable candidate among several proven radar systems: SHARAD (Shallow Radar), MARSIS (Mars Advanced Radar for Subsurface and Ionosphere Sounding), NISAR (NASA-ISRO Synthetic Aperture Radar), and ALOS-4 (Advanced Land Observing Satellite-4). The following table compiles the specifications and performance of these instruments which were considered during the study [37].

Table 4.9 Comparison between SHARAD, MARSIS, NISAR and ALOS-4 radars

Instrument Parameter	SHARAD	MARSIS	NISAR	ALOS-4
Mass (kg)	11	20	950[7]	700[7]

Instrument Parameter	SHARAD	MARSIS	NISAR	ALOS-4
Power	60	30	2000[7]	1750[7]
Cost (FY24 M$)[8]	30.07	23.28	200	125
Penetration Depth	0.1-1 km	0.5-5 km	0-25 cm	1-2 m
Vertical Resolution	7.5 m	75 m	N/A	N/A
Horizontal Resolution (Along-track by Cross-track)	0.3-0.45 km by 3 km [37]	5-10 km by 10-30 km	7 m by 2-8 m	1-25 m by 3-25 m
Swath Width	3 km	10 km	240 km	35-700 km

MARSIS and SHARAD are both sounding radars that operate in the low-frequency range—1.3–5.5 MHz [35] and 15–25 MHz [36], respectively. MARSIS - flown aboard ESA's Mars Express mission since 2005 - is capable of deep subsurface probing, achieving penetration depths of up to 5 km with a vertical resolution of 75 m, which exceeds the mission's required resolution threshold. This makes MARSIS fully capable of satisfying the radar performance requirements and supporting the detection of subsurface structures such as ice deposits and stratified geological layers. While SHARAD - carried by NASA's Mars Reconnaissance Orbiter since 2006 - offers a more limited penetration depth of 0.1–1 km, it delivers significantly finer vertical resolution (7.5 m), making it well-suited for resolving shallow subsurface features in greater detail [37].

In contrast, NISAR and ALOS-4 are L-band SAR designed primarily for Earth observation. Their operational frequencies (~1–2 GHz) are optimized for high-resolution surface imaging and deformation monitoring [41]. While they offer excellent horizontal resolution and wide swath imaging, their limited penetration depth makes them unsuitable for deep subsurface exploration on Mars [42][43]. Furthermore, their extremely high mass and power requirements far exceed what can be accommodated by the ARES II platform.

The team selected a hybrid Dual-Frequency Radar System (DFRS) as the baseline radar payload. This integrated system combines the low-frequency, deep-penetration capability of MARSIS with the higher-frequency, high-resolution performance of SHARAD. Although MARSIS alone could meet mission requirements, SHARAD

[7] Estimated value.
[8] Price adjusted to FY2024.

complements it to achieve better results. This hybrid approach directly supports the radar's science goals and ensures full compliance with both the mission's science traceability and system-level constraints. The following table outlines the performance characteristics of the DFRS.

Table 4.10 Comparison of DFRS Performance to SHARAD and MARSIS

Instrument Parameter	SHARAD (High Freq.)	MARSIS (Low Freq.)	DFRS
Mass (kg)	16.6	20	45
Power	60	30	140
Cost ($M)	30.07[9]	23.28	40
Penetration Depth	0.1-1 km	0.5-5 km	0.1-5 km
Vertical Resolution	7.5 m	75 m	75 m (Low Freq.) 7.5 m (High Freq.)
Horizontal Resolution (Along-track by Cross-track)	0.3-0.45 km by 3 km [37]	5-10 km by 10-30 km	5-10 km by 10-30 km (Low Freq.) 0.3-0.45 km by 3 km (High Freq.)
Swath Width	3 km	10 km	10 km (Low Freq.) 3 km (High Freq.)

Orbit, operations, pointing and other mission requirements

The operation of the DFRS introduces several constraints and requirements at the mission level, primarily related to spacecraft orientation, environmental conditions, and data handling. These are summarized in the table below:

Table 4.11 Radar Performance

Parameter	Value / Requirement
Pointing Direction	Nadir
Daylight Requirement	None (operates in day or night)
Acquisition Mode	Continuous along ground track
Average Data Rate During Operation	0.3 Mbps
Required Orbit Altitude Range	≤ 800 km [38]
Time for 75% Coverage	335 days

[9] Estimated value

4.5 Spectrometer

Four distinct spectrometers from Mars orbiter missions have been explored to compare it to the final design of the spectrometer that will be used for this mission: the Metropolitan Spectroscopy Imaging System (MSIS). Also, an estimate of what the cost and weight will be obtained. Table **4.12** shows a summary of their performance.

Table 4.12 Performance Parameters for CRISM, OMEGA, HYC, and DESIS

Instrument Parameter	**CRISM** [39]	**OMEGA** [40]	**PRISMA** [41]	**DESIS** [42]
Mass (kg)	32.92	29	90	88
Power Consumption on Normal Operation (W)	45.85	47.6	<110	<120
Cost (FY24 M$)	31.4[10]	26.4[11]	30 - 50[12]	-[13]
Spectral Range	362-3920	380-5100	400-2505	400-1000
Spectral Resolution	~6.55 nm [43]	7 nm (350-1000 nm) 13 nm (930-2650 nm) 20 nm (2510-5100 nm)	10 nm [44]	3.3 nm [45]
FOV (deg)	2.06	8.8	4.1	4.4
IFOV (deg)	0.0035	0.0683333	0.00277	0.004
f/#	4.41	4	2.95	2.8
Spectral Imaging Technique	Grating, pushbroom	Pushbroom	Prism, pushbroom	Grating, pushbroom

[10] Original cost was $17
.6 million in fiscal year 2001.
[11] Exact cost not publicly disclosed. Entire mission's cost was €150 million in 1996 prices [63]. Assuming 15% of total cost allocated to spectrometer, and applying 2024 conversion rate from euro to USD.
[12] Exact cost not publicly disclosed. Entire mission cost was €126 million in FY19 [64]. Estimate based on the whole program's cost, assuming 15% of total cost allocated to spectrometer, and applying 2024 conversion rate from euro to USD.
[13] Cost of the entire program or the instrument are not publicly disclosed.

Since MSIS' design aims to capture wavelengths from 310 nm up to ~5100 nm. Because that span encompasses UV, visible, and short- to mid-wave IR, separate optical channels or beam-splitters will be used to accommodate appropriate detectors.

Rather than employing a prism or diffraction grating, linear variable filters (LVF) are going to be used. This eliminates the bulky dispersive element at the cost of increased integration and calibration complexity, as illustrated in Figure **4.1**. The resulting mass/volume savings were deemed worthwhile for a spacecraft in low Mars orbit where payload mass is at a premium.

Figure 4.1 Hyperspectral Sensors Using Pushbroom Operating Mode [46]

As the orbit is set to ~350 km altitude around Mars, the satellite's velocity is ~3.4 km/s, giving a dwell time of about 0.044 s over each 150 m ground cell. That implies a frame rate near 23 Hz.

A 10 nm sampling interval was selected with a ~15 nm spectral resolution. Oversampling each band helps resolve mineral absorption features more robustly. Table **4.12** shows similar performance parameters in existing missions, reinforcing the feasibility of these design choices.

The mass, volume, and power of the MSIS were estimated by comparing its design to those in Table **4.12**. The following parameters, shown in Table **4.13**, are derived to satisfy the objectives and requirements stated in the matrix.

Table 4.13 MSIS key performance parameters

Parameter	MSIS
# Cross-track pixels[14]	610
Spectral range (nm)	310-5100
# Spectral bands[15]	479
FOV[16]	10°
IFOV[17] (mrad)	0.43
Spectral sampling interval	10 nm
Spectral resolution (nm)	15

[14] Number of cross-track pixels is calculated as 1.5×(FOV/IFOV). The 1.5 factor is added to account for the "smile distortion" on this type of sensor and to add conservatism when calculating the data size of each sample.
[15] Calculated as (upper spectral range - lower spectral range) / (spectral sampling interval).
[16] Value chosen to minimize collection time of 75% of Martian surface.
[17] IFOV is calculated as GRD÷h, using the small angle approximation.

Parameter	MSIS
Horizontal resolution	150 m (at 350 km)
Frame rate (Hz)	51.3
Power consumption (W)	80
Mass (kg)	60

Orbit, operations, pointing and other mission requirements

The spectrometer's design requirements and constraints in the mission are listed in the following table.

Table 4.14 Spectrometer Requirements

Parameter	Value / Requirement
Pointing Direction	Nadir
Daylight Requirement	Only operates during daylight
Acquisition Mode	Pooshbroom
Average Data Rate During Operation	9.2 Mbps
Required Orbit Altitude Range	350 km based on design constraints
Time for 75% Coverage	14 days

5 Communication and Data Handling

The Communication and Data Handling subsystem supports the high-rate data return from the ARES II spacecraft to Earth. The subsystem design is based on balancing sensor data generation, downlink capacity, and onboard storage, while meeting the mission constraint of achieving 75% Martian surface coverage within 4 years. Variability in the daily communication window due to DSN scheduling and solar conjunction outages is also accommodated.

Table **5.1** summarizes the key C & DH requirements. These requirements ensure that the downlink data rate, system reliability, redundancy, and storage capacity meet the mission's constraints and science goals.

Table 5.1 Communication & Data Handling Subsystem Requirements

Req. ID	Description
SYS-CDH-001	The subsystem shall support a minimum downlink data rate of 10 Mbps under worst-case conditions [47].
SYS-CDH-002	The subsystem shall provide a variable daily communication window between 14.9 and 17.5 hours using DSN ground stations in the U.S., Spain, and Australia [47].
SYS-CDH-003	The subsystem shall employ a dual-band transponder with Ka-band (32 GHz) for downlink and X-band (7–8 GHz) for uplink and backup, utilizing a frequency diplexer [47].
SYS-CDH-004	The subsystem shall maintain a minimum link margin of 10 dB, based on QPSK modulation and a BER of $\leq 10^{-6}$ [2].
SYS-CDH-005	The system shall provide at least 2 TB of onboard data storage with store-and-forward capability to handle downlink variability [47].
SYS-CDH-006	The C&DH architecture shall include a High-Gain Antenna (HGA), Medium-Gain Antenna (MGA), and Low-Gain Antennas (LGAs) for primary, backup, and emergency communication [47].
SYS-CDH-007	The subsystem shall utilize digital modulation and forward error correction (e.g., QPSK with LDPC or turbo codes) to achieve a BER $\leq 10^{-6}$ [2], [47].
SYS-CDH-008	The system shall regulate sensor duty cycles to ensure total data generation remains within combined downlink and onboard storage limits, enabling 75% surface coverage over 4 years [47].
SYS-CDH-009	The C&DH subsystem shall meet deep-space environmental requirements for radiation tolerance, thermal control, and structural integrity per NASA and ESA standards [2], [47].

These requirements were developed from established deep-space communication principles and tailored to the mission constraints using DSN design documents and deep-space modem specifications [2], [47].

5.1 Data Handling

Sensor data generation directly influences the design of the C&DH subsystem. The mission requires that coverage of Mars exceeds 75% in 4 years, which constrains the duty cycles of the onboard sensors. The sensor data rates, and duty cycles are detailed in Table **5.2**.

Table 5.2 Sensor Data Generation and Duty Cycles

Sensor	Data Rate (Mbps)	Duty Cycle	Rationale

Altimeter	0.03	100%	Low Field-of-View (FOV); must operate continuously to ensure 75% surface coverage over 4 years.
Radar	0.3	100%	Continuous operation supports navigation and science objectives over the full mission duration.
Spectrometer	9.2	50%	Active during daylight for planetary spectroscopy, required only in the first two years for 75% coverage.
Context Camera	4	50%	Provides visual context during daylight; duty cycle matches the spectrometer to achieve initial coverage.
High-Resolution Camera (HRC)	19980	30 seconds/day	Activated in the second mission phase to supplement the context data without exceeding storage limits.

5.2 Ground Stations and Communication Window

The DSN is employed as the primary communication network, featuring ground stations in the United States, Spain, and Australia [47]. This configuration ensures near-continuous global coverage, although practical communication windows vary between 14.9 and 17.5 hours per day due to factors such as Mars' eclipse conditions, Earth's relative geometry, and solar conjunction outages. Figure **5.1** shows the variation in the daily communication window over the 4-year period.

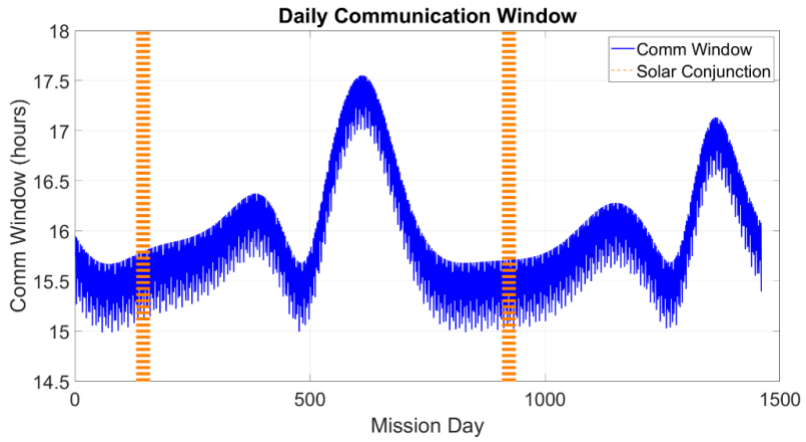

Figure 5.1 Daily Communication Window Over 4 Years

Figure **5.2** illustrates the corresponding daily transmit capacity (assuming a 10 Mbps downlink rate) alongside sensor data generation and storage behavior.

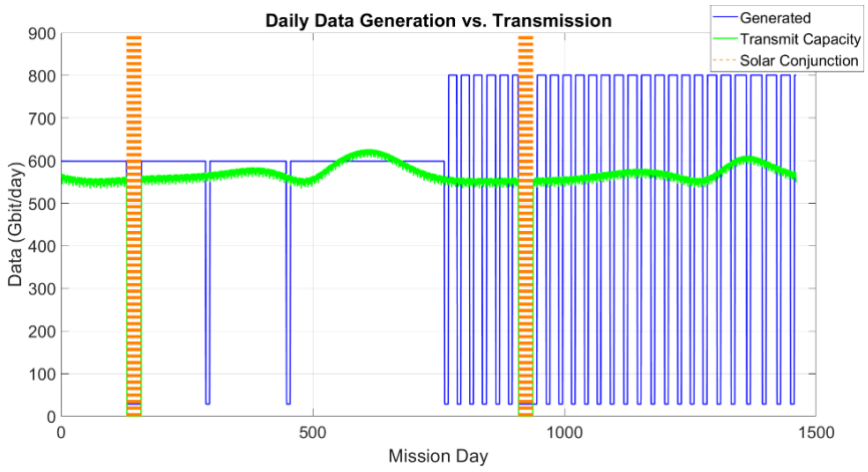

Figure 5.2 Daily Data Generation Vs. Transmission Over 4 Years

5.3 Subsystem Architecture

The subsystem architecture integrates multiple antennas and components to ensure reliable data transmission. The primary link uses a 4.5-meter dual-band High-Gain Antenna (HGA) with Ka-band downlink and X-band uplink, mounted on a two-axis gimbal and equipped with a dual-frequency feed and frequency diplexer. A Medium-Gain Antenna (MGA) provides backup X-band communication for telemetry and command in safe-mode. Low-Gain Antennas (LGAs) support emergency scenarios and initial link acquisition. A UHF Relay Transceiver enables store-and-forward communication via Mars orbiters during emergencies. Dual RAD750-based Onboard Flight and Data Handling Computers manage system control, data storage, and task scheduling, with data stored on a 2 TB radiation-hardened SSD. The RF Front-End and Signal Processing Unit handles RF signal conditioning using diplexers, filters, LNAs, and a Ka-band TWTA. The Modulator/Demodulator (Modem) performs digital modulation, error correction, and encoding. The TT&C system oversees uplink commands and downlink telemetry, maintaining spacecraft control and monitoring. The components are summarized in Table **5.3**.

Table 5.3 Communication & Data Handling Subsystem Components

Component	Frequency/Technology	Weight (kg)	Dimensions (L×W×H)	Power (W)
Dual-Band High-Gain Antenna	Ka-band (32GHz) X-band (7–8 GHz)	30	4.5 m diameter	0
Ka-band TWTA Transmitter	Ka-band TWTA	10	0.5×0.5×0.7 m	250
Medium-Gain Antenna	X-band	5	0.8×0.6×0.4 m	10

Component	Frequency/Technology	Weight (kg)	Dimensions (L×W×H)	Power (W)
Low-Gain Antennas	X-band or S/UHF	4	0.3×0.3×0.2 m (total for array)	10
UHF Relay Transceiver	UHF (390–450 MHz)	3	0.3×0.3×0.2 m	15
Flight & Data Handling Computer	RAD750	6	0.15×0.15×0.16 m	20
Onboard Data Storage	Radiation-hardened SSD	1.5	0.2×0.1×0.05 m	5
RF Front-End & Signal Processing Unit	Diplexer, waveguides, filters, LNAs, etc.	5	0.3×0.3×0.3 m	15
Modulator/Demodulator	X/Ka-band digital modulation/demodulation	2	0.2×0.2×0.1 m	10
TT&C System	X-band	3	0.3×0.3×0.3 m	15

Each component's cost estimation is based on analogous deep-space system reports and historical data from NASA and JPL [2], [47]. The Dual-Band HGA and Ka-band TWTA are the highest cost items, driven by the advanced design requirements, precision mechanisms, and space-qualified materials. Lower cost items, such as the RAD750-based computers and radiation-hardened SSD, reflect the cost premiums associated with radiation hardening and long-term reliability.

5.4 Link Budget

The link budget analysis determines the reliability of the downlink. Equation 5.1 quantifies the signal loss over distance (R) using the wavelength (λ) of the transmitted signal [2], [47].

$$FSPL(dB) = 20\log_{10}\left(\frac{4\pi R}{\lambda}\right) \tag{5.1}$$

EIRP is computed by Equation 5.2 summing the transmit power (P_t) and the antenna gain (G_t), while subtracting transmitter losses (L_{tx}). This value is critical for assessing the overall signal power available at Earth [2], [47].

$$EIRP = P_t + G_t - L_{tx} \tag{5.2}$$

Equation 5.3 calculates the ratio of carrier power to noise power density, where G_t is the gain-to-noise-temperature ratio of the receiving antenna, k is Boltzmann's constant, and L_{prop} includes atmospheric and polarization losses [2], [47].

$$\frac{C}{N_0} = EIRP + \frac{G}{T} - FSPL - 10\log_{10}(k) - L_{prop} \tag{5.3}$$

The link margin indicates the excess $\frac{C}{N_0}$ beyond the minimum required $\frac{E_b}{N_0}$. A link margin bigger than 10 dB confirms that the design is robust under worst-case conditions [2], [47].

Under current design parameters with a 4.5-m dish, 70% antenna efficiency, 250 W transmit power, and 0.01° pointing accuracy the calculated $\frac{C}{N_0}$ exceeds the required threshold, resulting in a link margin of approximately 10.6 dB. When the margin is insufficient during certain conditions, the DSN's 70-m antennas are employed to provide additional gain. Detailed link budget calculations and Parameters are provided in Table **5.4**.

Table 5.4 Key link budget parameters for link between ARES II and the DSN

Parameter	Value	Unit	Calculation/Notes
Transmitter Power, P_t	250	W	Design
P_t in dBW	24	dBW	10 log (250)
Transmission Loss, L_{tx}	1	dB	Estimated losses in transmission chain
HGA Dish Diameter, G_t	4.5	m	Design
Wavelength, λ	9.38×10^{-3}	m	$\lambda = \frac{c}{f} = \frac{3 \times 10^8}{32 \times 10^9}$
HGA Efficiency, η	0.7	(unitless)	Assumed
HGA Gain	62	dBi	$10 \log_{10}[\eta \left(\frac{\pi \times 4.5}{\lambda}\right)^2]$
EIRP	85	dBW	$P_t + +24 + 66 - 1$
Max Distance, d	3.75×10^{11}	m	Maximum distance for the maximum FSPL
FSPL	284	dB	$20 \log_{10}(\frac{4\pi d}{\lambda})$
Additional Losses	2	dB	Atmospheric and polarization losses
Total Losses	286	dB	$Loss_{total} = FSPL + Loss_{Additional}$
DSN, $\frac{G}{T}$	61	dB/K	DSN 70-m antenna specifications
Boltzmann's Constant, k	-228.6	dBW/K/Hz	Standard constant
Calculated $\frac{C}{N_0}$	88.6	dB-Hz	$\frac{C}{N_0} = EIRP + \frac{G}{T} - FSPL - Losses - k$
Data Rate, R	10	Mbps	Design
$10 \times log_{10}(R)$	70	dB-Hz	$10 \log_{10}(10 \times 10^6)$
Required $\frac{E_b}{N_0}$	8	dB	BER of 10^{-6} With QPSK Modulation
Link Margin, LM	10.6	dB	$LM = \frac{C}{N_0} - \left(\frac{E_b}{N_0} + 10 \log_{10}(R)\right)$

6 Propulsion

The propulsion subsystem, seen in Figure **6.1**, provides thrust and maneuvering capabilities for mission phases from payload separation to Mars Orbit Insertion, station keeping, and deorbiting, ensuring reliability in the vacuum of space. The design must balance propellant mass, cost, and complexity, managing thermal extremes and launch loads.

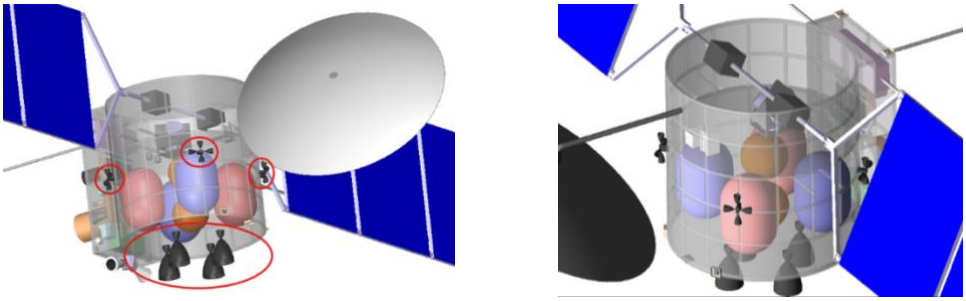

(A) **(B)**

Figure 6.1 Propulsion Subsystem Final Layout – (A) View 1 (Main Engines/Thrusters) (B) View 2 (Tanks)

Table **6.1** states the requirements for the propulsion subsystem. These requirements ensure safe and reliable spacecraft operation throughout the mission.

Table 6.1 Propulsion Subsystem Requirements

Req. ID	Description
SYS-PRP-001	The propulsion subsystem shall provide all required ΔV for all mission phases.
SYS-PRP-002	The system shall be able to achieve repeatable and controllable burns.
SYS-PRP-003	The propulsion subsystem shall be capable of autonomous operation; executing burns and trajectory adjustments based on mission requirements.
SYS-PRP-004	The propulsion subsystem shall be compatible with the ADCS to provide full 6 degrees of freedom maneuverability.
SYS-PRP-005	The propulsion subsystem shall enable precise orbital maneuvering.
SYS-PRP-006	The propulsion subsystem shall remain operational within limited environmental conditions (-50°C to +50°C).
SYS-PRP-007	The system shall implement safe-mode protocols, including emergency shutdown, pressure regulation, and fail-safe redundancy for controlled deorbiting.
SYS-PRP-008	The propulsion subsystem shall maintain sufficient propellant reserves for the entirety of the mission plus an extra 20% for emergencies cases.

6.1 Propulsion System Type

Table **6.2** [48] outlines the different criteria used in the selection process of the satellite's propulsion system type. The mission demands sufficient thrust for quick orbital insertion, station keeping, and contingency burns, with

a high specific impulse to minimize propellant mass. After evaluating the options in Table **6.2**, a chemical bipropellant system emerged as the optimal choice, offering a vast specific impulse range and a higher efficiency. In contrast, cold gas systems lack the necessary ΔV and maneuverability due to low specific impulse, and electric propulsion's power demands exceed the satellite's available resources. Monopropellant thrusters, while closer to the required thrust, do not match the specific impulse or performance efficiency of bipropellant systems. Moreover, the estimated total system weight and power requirements of the bipropellant option are well within our spacecraft's overall mass and power constraints. A chemical bipropellant system provides high thrust and specific impulse for efficient maneuvers, while reserving the extra 20% ΔV margin demanded by SYS-PRP-001. Precise throttling in attitude thrusters and main engines ensures repeatable burns per SYS-PRP-002 and accurate maneuvers per SYS-PRP-005. Overall, a bipropellant propulsion system ensures that the required performance, safety, and reliability requirements for the mission are met.

Table 6.2 Propulsion System Type Selection Criteria

Criteria	Chemical – Bipropellant	Chemical - Monopropellant	Chemical – Cold Gas	Electrical – Ion Thruster
Isp (s)	250 - 460	220 - 240	28 - 272	1500 - 4000
Efficiency (%)	90 - 95	90 - 92	20 - 40	60 - 75
Nominal Thrust (N)	10 - 26700	5 - 440	0.01 – 4	0.02 – 0.5
Estimated Total System Weight (kg)	700 - 1400	800 - 1100	750 - 1750	500 - 600
Estimated Power Requirements (kW)	0.3 – 0.5	0.2 – 0.4	0.01 – 0.1	10 - 14

6.2 Pressurant, Fuel, and Oxidizer

The propellant system trade study initially examined the pressurant that would be used. All the gases presented in Table **6.3** are inert and therefore are eligible to be used as a pressurant in the system. Helium was chosen as the pressurant as it offers a favorable combination of low molecular weight and high compressibility. Once stored at high pressure, it can be regulated to supply both the fuel and oxidizer tanks at the appropriate feed pressures without the complications of turbopumps or cryogenic systems. Taken together, the combination of helium pressurization with MMH and MON-25 ensures a reliable and straightforward propulsion architecture for long-duration missions.

Table 6.3 Pressurant Selection Criteria

Criteria	Helium	Nitrogen	Argon	Neon
Density (kg/m^3) at 0°C	0.178	1.25	1.78	0.9
Estimated Pressurant Weight (kg)	3 - 8	21 - 56	30 - 80	15 - 40

Table 6.4 Propellant Selection Criteria

Criteria	MMH/ MON-25	LH2 (Liquid Hydrogen) / LOX (Liquid Oxygen)	LCH4 (Liquid Methane) / LOX (Liquid Oxygen)	UDMH/ IRFNA
Isp (s)	336	430	350	310
Density (kg/m^3) at Optimal Temperature	Fuel - 874 Oxidizer - 1370	Fuel - 70.85 Oxidizer - 1141	Fuel - 422.6 Oxidizer - 1141	Fuel - 790 Oxidizer - 1500
Freezing Point (°C)	Fuel – (-52.4) Oxidizer – (-55)	-	-	Fuel – (-57) Oxidizer – (-47)
Boiling Point (°C)	-	Fuel – (-252.9) Oxidizer – (-182.9)	Fuel – (-161.6) Oxidizer – (-182.9)	-
Mixture Ratio (O/F)	1.65	4.83	3.8	3.4
Estimated Propellant Weight (kg)	850 - 950	550 - 650	700 - 800	950 - 1050
Hypergolic	✅	❌ - Cryogenic	❌ - Cryogenic	✅

For the propellant selection, seen in Table **6.4**, cryogenic propellants were explored for their high specific impulse but were rejected due to the complex infrastructure needed to manage their required low temperatures. Extra insulation and robust temperature control systems, required to prevent boil-off, exceeded the satellite's mass and power limits, adding complexity without sufficient performance gains. Instead, the focus shifted to easily storable hypergolic fuels, which provide a balance of reliability and efficiency. UDMH (Unsymmetrical Dimethylhydrazine) with IRFNA (Inhibited Red Fuming Nitric Acid) was compared to MMH (Monomethylhydrazine) with MON-25, which is mix of 75% N2O4 (Dinitrogen Tetroxide) and 25% HNO3 (nitric acid). MMH and MON-25's similar freezing points simplify thermal management in the propulsion system [49] [SYS-PROP-006]. While, UDMH/IRFNA has lower specific impulse and density than MMH/MON-25, requiring larger tanks, heavier structures, and a higher mixture ratio that increases propellant mass. These drawbacks with UDMH/IRFNA outweighed any benefits, making MMH/MON-25 the preferred choice for the mission's propulsion system, optimizing efficiency, tank sizing, and overall architecture.

6.3 Main Engines

In the trade study to select the main engine for the ARES II satellite, four designs were considered, as summarized in Table **6.5**. Although the R-4D-11, BT-5, and BT-4 all featured favorable thrust ranges and acceptable mass profiles, but they demanded higher power input, which conflicted with the spacecraft's overall power. By contrast, the S400-15 offers a balanced combination of thrust and specific impulse without placing excessive demands on power. This engine's inlet-pressure and flow-rate compatibility with the planned propellant feed setup helps minimize integration challenges. In addition, the S400-15 benefits from proven flight heritage in geostationary and deep-space missions, allowing for confidence in its operational stability and predictable performance. As a result, the S400-15 engine meets the propulsion objectives for thrust, Isp, and power efficiency in a way that best aligns with ARES II's mission priorities and resource constraints. Table **6.6** provides further technical specifications of the S400-15 engine. Due to the issues with the higher vapor pressure of MON-25, it can be assumed that these engines could be custom made to work with this oxidizer, as it's only certified for the following oxidizers: N2O4, MON-1, MON-3.

Table 6.5 Main Engine Selection Criteria

Criteria	S400-15	R-4D-11	BT-5	BT-4
Nominal Isp (s)	321	311	316	326
Nominal Thrust (N)	425	490	478	450
Thrust Range (N)	340 - 450	378 - 511	380 - 510	360 - 480
Weight (kg)	4.3	3.76	4	4
Power Requirements (W)	70	75	85	90

Table 6.6 Main Engine Specifications [50]

Parameter	Values
Nominal Mixture Ratio (O/F)	1.65
Inlet Pressure Range	12.5 - 18.5 bar
Nominal Chamber Pressure	10.35 bar
Flow Rate Range	110 – 142 g/s
Nozzle Area Expansion Ratio	330
Valve Type	Single Seat Solenoid
Minimum Impulse Bit	15.7 N·s

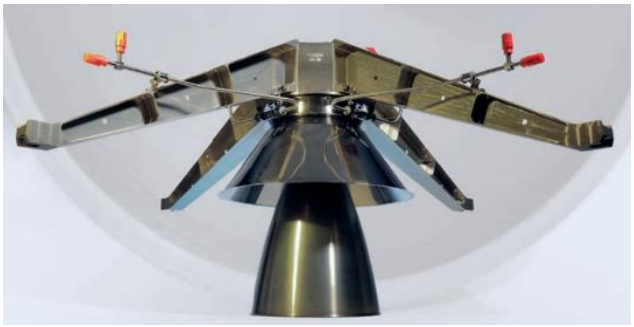

Figure 6.2 Selected Main Engine [50]

6.4 Attitude Thrusters

The attitude control thruster for the ARES II mission was chosen through a trade study evaluating candidates based on thrust output, efficiency, mass, power consumption, reliability, and cost. The S10-18 stood out for its balanced performance, delivering sufficient thrust for precise maneuvers while staying within the spacecraft's mass and power limits. Unlike the S10-21, which was too heavy and power-intensive, or the MR-103G, which lacked adequate thrust for rapid adjustments. A critical advantage of the S10-18 is its compatibility with the mission's propellants, utilizing MMH and N2O4. Like the main engines, the thrusters are to be customizable for MON-25, as they're only certified for N2O4, MON-1, and MON-3. Only the S10-18 and R-6F align with this fuel and oxidizer configuration, whereas the S10-21 and MR-103G, being monopropellant designs, require hydrazine and a catalyst for ignition. Additionally, the S10-18 surpasses the mission's durability requirement of 72,000 firing cycles, offering a robust margin for the extended orbital phase. This cycle life ensures it can handle repeated firings, from initial trajectory corrections to fine-tuned maneuvers during the science phase, without performance degradation (SYS-PROP-004).

Table 6.7 Attitude Control Thruster Selection Criteria

Criteria	Ariane Group S10-18	R-6F	MR-106L	MR-111G
Nominal Isp (s)	292	305	231.5	224
Nominal Thrust (N)	10	22	22	4
Thrust Range (N)	6 – 12.5	13.3 – 27.8	10 - 34	1.8 – 4.9
Weight (kg)	0.65	0.965	0.59	0.37
Power Requirements (W)	14	11	36.16	16.11
# of Cycles	1,100,100	20,000	120,511	420,000
Minimum Impulse Bit (N·s)	0.1	0.53	0.015	0.076

The thruster's optimized specific impulse enhances efficiency, minimizing propellant use, which is a crucial factor for sustained operations in Mars' orbit. With a proven reliability from similar missions, the S10-18 offers confidence in its performance under the harsh conditions of the vacuum of space. Table **6.8** provides further technical specifications of the S10-18 thruster. Its precision, driven by a fine minimum impulse bit, ensures steady pointing, supporting the mission's goals. Collectively, its efficiency, durability, and precise control make the S10-18 the optimal thruster for achieving ARES II's scientific objectives with reliability and accuracy.

Table 6.8 Attitude Control Thruster [50]

Parameter	Values
Nominal Mixture Ratio (O/F)	1.60 - 1.65
Inlet Pressure Range	10 - 23 bar
Nominal Chamber Pressure	9 bar
Flow Rate Range	2.3 – 4.2 g/s
Nozzle Area Expansion Ratio	150
Valve Type	Dual Seat Linear Motor
Total Burn Life	69 hours
Maximum Single Burn Time	8 hours

Figure 6.3 Selected Attitude Control Thruster [50]

6.5 Fuel Budget

The fuel budget for the ARES II mission was calculated to ensure the spacecraft has adequate propellant for all planned operations, from launch to end-of-life disposal. The total propellant requirement across all mission phases

sums to 897.73 kg, as detailed in Table **6.9**. To ensure operational flexibility, an additional 20% reserve (179.55 kg) was incorporated, resulting in a final fuel budget of 1077.28 kg (SYS-PROP-008).

Table 6.9 Fuel Budget

ARES II Mission Phase	Propellant Required (kg)	Method of Propulsion
Parking Orbit to TMI	-	Launch Vehicle
Attitude Corrections Post-Payload Separation [Hohmann]	3.0566	Attitude Thrusters
Mid-Course Corrections	-	-
Mars Orbit Insertion	672.8388	Main Engines
Corridor Control Aerobraking Maneuver (Periapsis Targeting)	62.2649	Attitude Thrusters
Insertion Burn to Final Orbit *With Plane Change (±4°)*	104.4087	Main Engines
Station-keeping Throughout the Mission	18.1134	Attitude Thrusters
EOL Disposal [Deorbiting]	37.0487	Main Engines
TOTAL PROPELLANT REQUIRED [TOTAL + 20% RESERVES]	**897.73** [1077.28]	-

6.6 Tank Design

The tank design for the ARES II mission is a critical propulsion system component, engineered to store hypergolic propellants (MMH & MON-25) alongside the pressurant gas required for propellant delivery. All the tanks are to be constructed from Ti6Al4V due to its high strength-to-weight ratio and corrosion resistance. The system consists of two tanks each for the fuel (red), oxidizer (oxidizer), and pressurant (orange). The fuel and oxidizer tanks are shaped as a cylinder with dome ends while the pressurant tanks are spherical, as seen in Figure **6.1** (B) ,with their sizing specifications set out in Table **6.10**. A 5% ullage factor was incorporated into all tanks to account for the empty volume within each tank occupied by gases or vapors. By including this 5% allowance, the design provides sufficient room for propellant expansion and prevents over-pressurization, which is critical for the safe storage and management of the hypergolic propellants and the pressurant gas [51]. Within these tanks, bladders are used, specifically Ethylene-Propylene-Diene Monomer (EPDM) for the fuel tanks and Polytetrafluoroethylene (PTFE) for the oxidizer tanks. They will serve two primary functions: isolating the propellants from the pressurant gas to prevent improper mixing and assisting in maintaining tank temperatures above the propellants' freezing points [52]. This temperature regulation is significant for both propellants to prevent solidification in their lines as MMH and MON-25 have a freezing point of -52.4°C and -55°C, respectively. The integration of all tanks within the spacecraft is optimized for mass distribution

by symmetrically positioning them along the spacecraft's central axis, which is more apparent in Figure **6.1** (B). The tanks are sized to accommodate a total propellant load of 1077.28 kg and a pressurant load of 3.14 kg, thereby supporting the mission's propulsion requirements from Mars orbit insertion through extended operations.

Table 6.10 Tank Specifications – Fuel, Oxidizer, Pressurant

Technical Specifications	Fuel	Oxidizer	Pressurant
Quantity	2	2	2
Radius (m)	0.3	0.3	0.195
Total Height (m)	1.06	1.11	0.39
Volume (m^3)	0.2442	0.2570	0.0318
Weight (kg)	17.77	18.52	8.61
Maximum Expected Operating Pressure (bar)	15	15	25
Bladder Type	EPDM	PTFE	None
Tank Material	Ti6Al4V		

6.7 System Architecture

The system architecture of the propulsion subsystem enables the seamless integration of components to fulfill mission requirements. Represented as a Piping & Instrumentation Diagram (P&ID), Figure 6.4 offers a detailed illustration of this architecture, depicting the spatial arrangement and flow paths among the fuel tanks, oxidizer tanks, pressurant tanks, main engines, and attitude thrusters. As discussed in Section 6.8, the tank layout was designed to minimize shifts in the center of mass of ARES II as propellants are expended. The main engines, located at the base (4 total), are aligned to deliver thrust along the primary axis, supporting significant maneuvers such as MOI. Additionally, attitude thrusters are distributed around the midsection in groups of 4 (16 thrusters total), providing precise control over the spacecraft's orientation, including pitch, yaw, and roll adjustments (SYS-PROP-003). Downstream of each pressurant tank, the system is equipped with pressure transducers (e.g., P1.1, P2.1) for real-time monitoring at different points in the system to enable optimal operation and early anomaly detection. While regulators reduce the high-pressure helium (25 bar) to operational levels (15 bar). Check valves are installed downstream of the regulators, prevent backflow to safeguard the system.

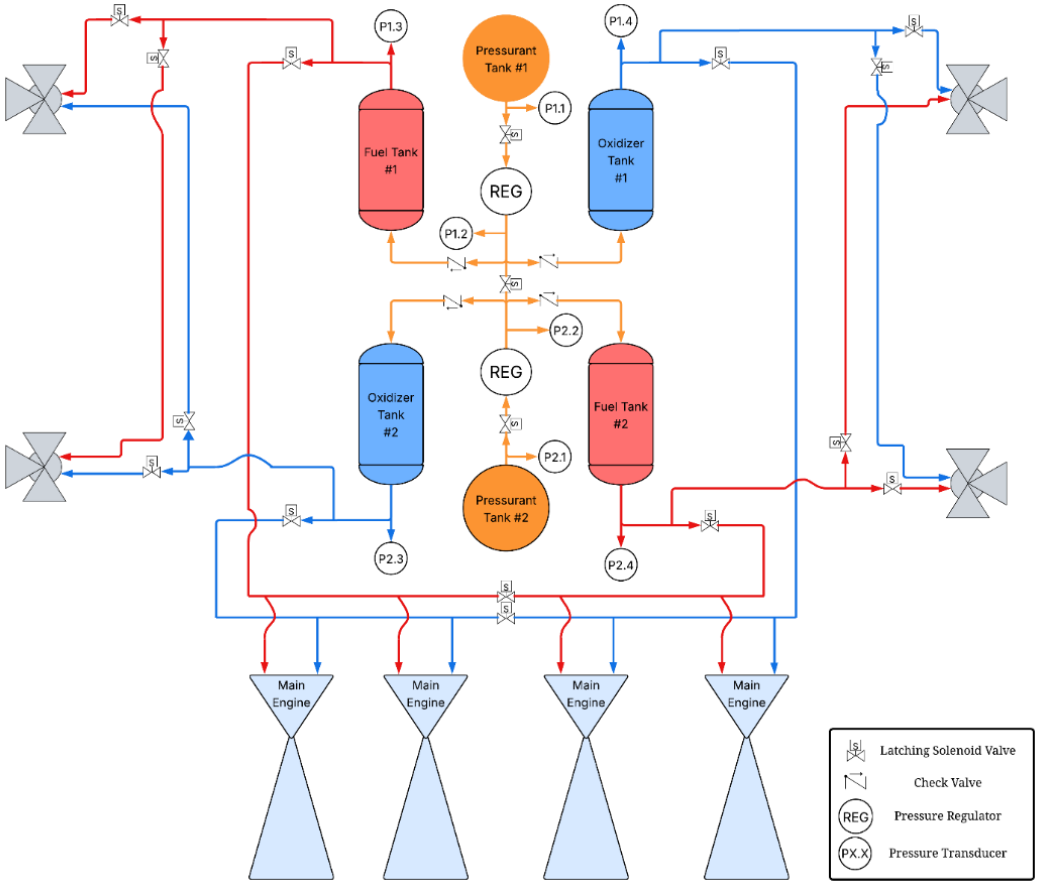

Figure 6.4 Propulsion System P&ID

Redundancy is a key feature of the subsystem's reliability, achieved through latched solenoid valves on both the pressurant and propellant sides, while saving on power via its latching mechanism. These valves act as a crossfeed, allowing for fuel & oxidizer to flow to all main engines in case of a failure of one of the tank pairs, ensuring adaptability without sacrificing performance. The inclusion of multiple valves enhances safety by being able to cut off certain portions in the system if our monitoring system detects potential issues, supporting mission success under diverse conditions [SYS-PROP-007]. The attitude thrusters' strategic placement between tank pairs reduces plumbing complexity. In summary, the propulsion subsystem's architecture, is designed to maintain a consistent and controlled propellant flow to both the engines and thrusters, ensuring the reliability and precision essential for the success of the ARES II mission.

7 Thermal Control

In developing the ARES II thermal control subsystem, thermal requirements were established based on mission objectives, environmental conditions in Mars orbit, and the operational needs of onboard systems. These requirements ensure that all components remain within their allowable temperature limits throughout the orbital cycle, including periods of full solar exposure and complete eclipse. The requirements also guide the selection of materials and insulation strategies. The following table summarizes the thermal design requirements.

Table 7.1 Thermal Subsystem Requirements

Req. ID	Description
SYS-TCS-001	The spacecraft shall utilized Multi-Layer Insulation (MLI) to provide radiation heat barriers that retars and control the flow of energy, ensuring the protection of components exposed to extreme temperature variation in Mars orbit and to withstand the extreme conditions during aerobraking.
SYS-TCS-002	The spacecraft shall apply reflective coatings (i.e.. AZ-93 or RCG) to exposed surfaces to control the absorption of solar radiation and maintain thermal balance more so when the satellite is in direct sunlight.
SYS-TCS-003	The spacecraft shall be equipped with heat pipes to dissipate excess heat from thermal components by thermally coupling them to radiators for space rejection.
SYS-TCS-004	The spacecraft shall utilize thermocouples throughout critical systems, such as, electronics, propulsion, and batteries, to monitor temperatures in real time and inform control responses.
SYS-TCS-005	The spacecraft shall model and validate thermal energy input during sunlight and eclipse phases of its Mars orbit, including solar flux, IR radiation, and internal heat generation, using a time dependent simulation tool.
SYS-TCS-006	The spacecraft shall ensure all thermal subsystem materials, coating and configurations maintain operational temperatures between 233.15K and 358.15 K

7.1 Thermal Analysis Approach

To evaluate and ensure the thermal survivability of the satellite in Mars orbit, a node-based thermal model was developed using a lumped-parameter approach. The spacecraft was discretized into seven thermal nodes: a central internal node representing the internal structure, and six face nodes corresponding to the physical surfaces of the satellite (X+, X-, Y+, Y-, Z+, Z-). Each node was given a specific thermal mass, this was calculated from the node's mass and specific heat capacity, C_p, with material properties defined per face through a Graphical User Interface (GUI). Materials such as AZ-93 white paint, polished aluminum and MLI were selected to tailor radiative behavior for each face depending on exposure conditions and mission needs.

The thermal interactions modeled include conduction, radiation, and external heating sources. Conduction was modeled both between the internal node and each face (using a standard resistance of 20 K/W) and between adjacent face nodes (with higher resistance), simulating structural thermal paths. Radiative exchanges were governed by the Stefan-Boltzmann law, with heat loss to deep space and heat gain from Mars' infrared emission and solar sources. These environmental sources and their impact on the system were approximated using view factors, dimensionless quantities used in radiative heat transfer to represent how much radiation leaving one surface reaches another. Each view factor was precomputed based on satellite altitude and orientation to Mars.

7.2 Material Selection

Developing the thermal design of the satellite, surface materials were chosen to directly influence the heat absorption, retention, and rejection. The approach centered on optimizing radiative heat exchange between the satellite and its environment while minimizing thermal fluctuations, especially upon the eclipse phases in Mars orbit. The materials were chosen to meet functional and thermal performance requirements specific to the orientation and operational role of each face. The table below summarizes the selected materials and their thermal behavior.

Table 7.2 Material Properties [53]

Face	Material	Absorptivity	Emissivity	Ratio
X+	AZ-93 (White Paint)	0.17	0.85	0.29
X-	MLI Blanket	~0.03	~0.025	1.2
Y+	AZ-93 (White Paint)	0.17	0.85	0.20
Y-	MLI Blanket	~0.03	~0.025	1.2
Z+	Polished Aluminum	0.09	0.05	1.80
Z-	MLI Blanket	~0.03	~0.025	1.2

The selection of surface materials for each of the satellite's six faces was made with consideration of the spacecraft's orbital environment, expected solar exposure, radiative balance, and thermal control requirements. The faces orientated toward the Sun or aligned with the orbital ram direction, X+ and Y+ faces, were coated with AZ-93 white thermal paint, known for its high emissivity and low solar absorptivity. Polished aluminum was selected for the Z+ as it faces open space and was expected to receive minimal direct solar radiation. Polished aluminum offers a very low emissivity and moderate reflectivity. Conversely, the X-, Y-, and Z- faces were covered with Multi-Layer

Insulations (MLI) blankets. These faces typically remained in shadow or were directed away from major heat sources. Applying MLI to these surfaces provided high thermal resistance and low radiative exchange, crucial for maintaining thermal stability and preventing deep-space cooling effects during eclipse periods. It is important to note that although this analysis was performed with six distinct external nodes implying a cube shape to the system, the material selection was applied to the cylinder by effectively dividing the surface area into regions which align with the associated vector.

The ARES II MLI configuration includes 10 layers of aluminum-coated Kapton as reflective barriers and 10 layers of Dacron mesh as spacer material. Aluminum coated Kapton was chosen for its low infrared emissivity, high reflectivity, and proven resistance to atomic oxygen and ultraviolet radiation in Martian orbital environments. Dacron mesh is a lightweight and thermally stable material that was selected to ensure vacuum integrity and layer separation during lunch and in-orbit operations. In addition, seams and panel junctions were sealed using aluminized Kapton tape, a standard solution used in previous and ongoing NASA missions.

7.3 Thermal Simulation Results

The graph below plots the incident heat flux due to direct solar radiation, infrared radiation, and albedo radiation. Referencing the solar radiation plot, the highest flux appears on the Y+ face, consistent with the satellite's nominal sun pointing attitude or orbit geometry. The other faces receive comparatively less direct sunlight. The infrared radiation plot shows the loads are consistent, but also peak when in sunlight, suggesting heating from Mar's surface at atmosphere when the satellite is in view. Finally, the albedo radiation plot reflects similar trends to solar input, with peaks corresponding to the reflected solar energy from Mars' surface. The lower values indicate that albedo is secondary to direct solar gain but must still be considered for complete modeling.

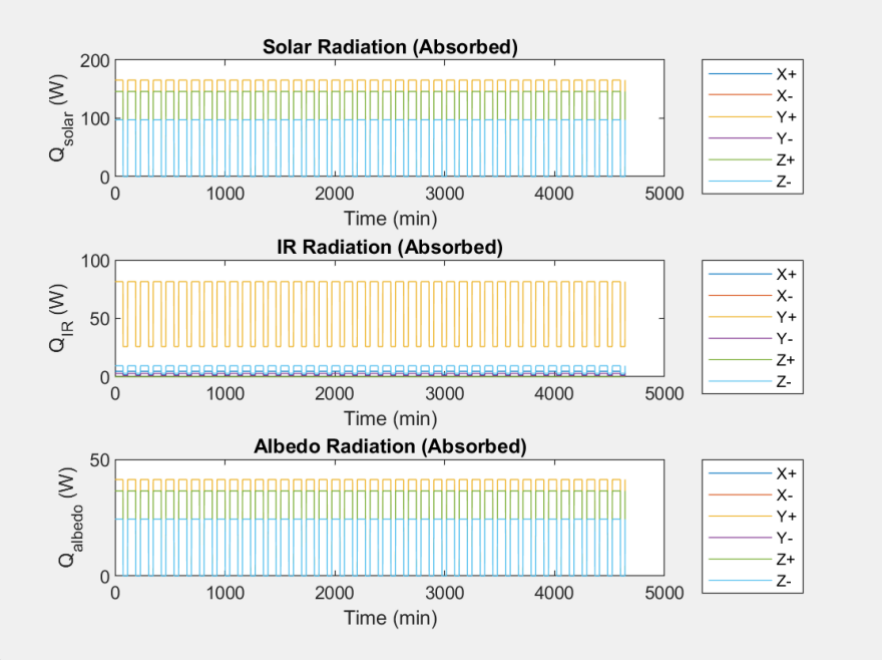

Figure 7.1 Solar, IR, and Albedo Radiation Plots

Figure **7.2** compares the total power absorbed and internally used by the spacecraft versus the power radiated back to space. The high-power input peaks correspond to periods of direct sunlight, while the sharp troughs denote eclipse.

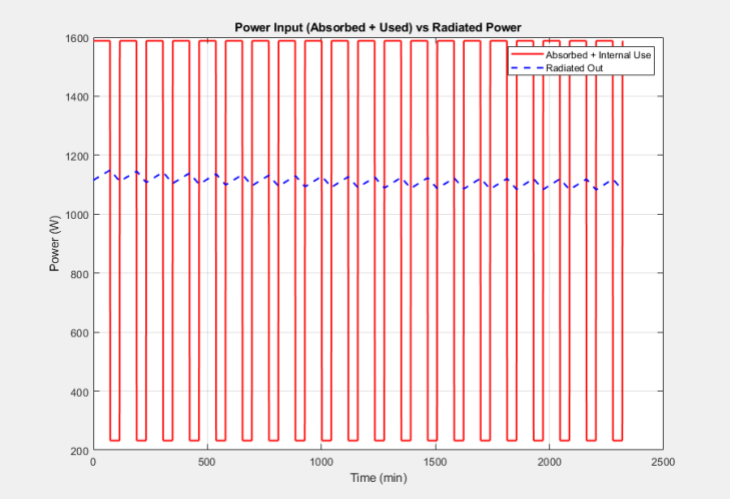

Figure 7.2 Power Input vs. Radiated Power

The power radiated in **Figure 7.2** remains relatively steady, indicating that MLI slows down the transient heat exchange, leading to a buffered response to rapid environmental changes. This thermal inertia is crucial for thermal stability, thus ensuring that thermal control does not rely heavily on active elements, saving power and mass.

This plot was simulated for a lower number of orbits for clarity of observation; however, the trend remains consistent when extended.

The internal temperature of the satellite was determined to be ~280K, with minor periodic variations corresponding to the satellite entering and exiting eclipse. The temperature limits are defined by the highest operating temperature of the instrument with the smallest thermal range, which would be the batteries. Internal temperature is calculated simultaneously with **Figure 7.2**, considering the power needed to be radiated out is a function of internal temperature. This value is subject to larger fluctuations but given that the internal temperature can be maintained while modeled solely with passive thermal control, the system is equipped for larger disparities if encountered. The radiators are located on the bottom of the solar panels – the inner most panel on each side – totalling a surface area of 6.43 m^2. All critical areas are connected to the radiators using a heat pipe system, which effectively transfers heat and reinforces the success of passive control.

7.3.1 Aerobraking Heat Loads

One major area of concern when designing the thermal control system is the aerobraking phase of the mission. Each pass can impose a significant heat load on the solar panels and structure. However, given that most of the spacecraft is properly insulated, the focus is the solar cells [54]. The cells are designed to withstand temperatures of up to 415 K for brief periods, and even with atmospheric drag the cells will not accumulate enough heat to surpass this limit. The nature of the aerobraking phase is separated into numerous passes rather than a consistent slow using drag, so the cells can withstand the temporary peaks [44]. However, during the long periods of cooling to avoid thermal shock of large fluctuations, small off the shelf polyimide heaters will be dispersed throughout the panels, and a few internally for good measure. These heaters mark the sole active component of thermal control being used and will be regulated by the measurements of the thermocouples that are also dispersed throughout the system, marking the primary source of temperature monitoring [55].

8 Attitude Determination and Control

Throughout the mission, ARES II will need to maintain different orientations to satisfy orbital, thermal, power, and payload requirements. Different stages of the mission have been considered to determine the forces and torques excreted on the satellite. Each stage imposes requirements on the Attitude Determination and Control System (ADCS) presented in Table **8.1**.

Table 8.1 ADCS Requirements per Stage

Stage	Req. ID	Description
De-tumbling	REQ-ADCS-01	The ADCS shall be able to successfully de-tumble the satellite after separation in time for TMI.
Interplanetary trajectory	REQ-ADCS-02	The ADCS shall keep the payload bay facing away from the Sun during interplanetary trajectory.
Aerobraking re-positioning	REQ-ADCS-03	The ADCS shall be capable of rotating the satellite in any axis to point the payload bay away from the airflow.
Aerobraking	REQ-ADCS-04	The ADCS shall be capable of keeping the payload pointing away from the payload during aerobraking.
Science orbit keeping	REQ-ADCS-05	The ADCS shall be capable of keeping the satellite nadir pointing with an accuracy of <0.001 deg.
	REQ-ADCS-06	The ADCS shall be able to stabilize the satellite in any axis with an accuracy less than <0.01 deg.

8.1 ADCS Design

To accomplish the ADCS requirements, ARES will contain a suit of sensors and actuators capable of stabilizing the satellite in all three axes. The sensor suit will be comprised of two star trackers, two Inertial Measurement Units (IMUs), and seven coarse sun sensors (CSS). As for the actuators, ARES II will have two types of actuators: attitude thrusters and reaction wheels. The distribution of the sensors and actuators can be seen in Figure **8.1**.

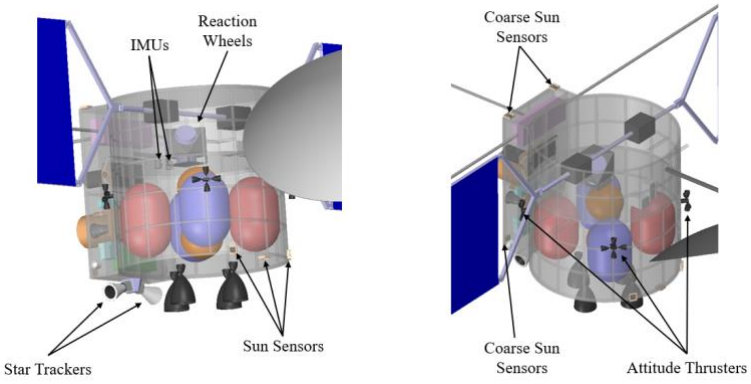

Figure 8.1 Location of ADCS sensors and actuators

8.2 Environmental Disturbances

The satellite will experience many internal and external disturbances that will directly affect the performance, as they will cause forces and torques that change the momentum of the satellite. Therefore, it is important to account for them and know how considerable their impact would be in order to propose a suitable actuator system. Some of the disturbances that affect a spacecraft include Solar Radiation Pressure (SRP), gravity gradient, gravitational potential, albedo pressure, radio frequency, leaks, thermal pressure, or thruster plumes. For the purpose of sizing the actuators, only the largest environmental disturbances have been considered: SRP, gravity gradient, and aerodynamic drag. The following table summarized the equations used to calculate the torques cause by the disturbances:

Table 8.2 Torque Disturbance Equations

Disturbance	Equation
SRP torque	$T_s = \frac{\Phi}{c} A_s (1+q)(cp_s - cm)\cos(\varphi)$ (8.1)
Gravity gradient torque	$T_{gg} = \frac{3\mu_{Mars}}{R_c^5} \underline{\boldsymbol{R_c}} \times [I] \underline{\boldsymbol{R_c}}$ (8.2)
Aerodynamic torque	$T_a = \frac{1}{2} \rho C_d A_r V^2 (cp_a - cm)$ (8.3)

The following sections will summarize the expected torque experienced by the satellite, the moment accumulation in the reaction wheels, and the fuel consumption to de-saturate the reaction wheels or perform any control maneuver.

8.2.1 De-tumbling

Tumbling is expected to occur either after separation or after escaping Mars' atmosphere. Falcon 9 provides accurate and stable payload separation, so no big rates are expected. Moreover, the aerobraking maneuver will get the satellite 150 km from the surface of Mars at least. As it will be seen in the Aerobraking section, torques experienced by the spacecraft are not very high, and they can be counteracted easily with the thrusters chosen in for the ADCS. NASA's paper on a study done to determine the Therefore, it is assumed that the maximum tumbling angular rate the spacecraft will experience is 1rad/s (equivalent to 57 deg/s) in all axes, at most. Using a simple PD controller done, the expected propellant expenditure per de-tumbling operation was estimated to be 2.7 kg. At nominal thrust, the attitude thrusters would be able to bring the satellite to stability (almost 0 deg/s in all axes) in less than 1000 seconds (or 16 minutes and 40 seconds), as it can be seen in Figure **8.2**, given an initial rate of [1, 1, 1] rad/s in the body frame.

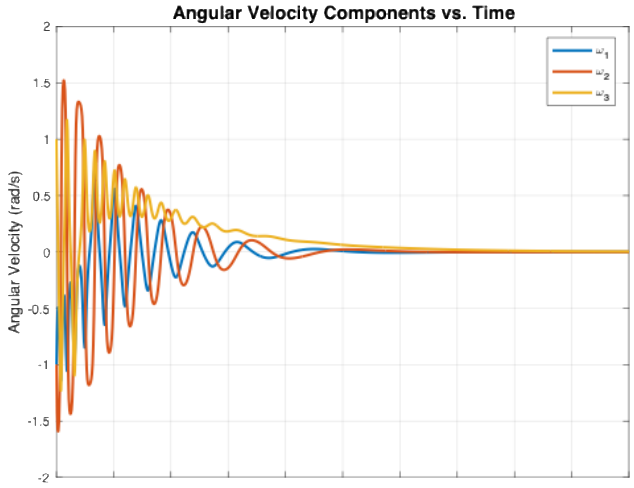

Figure 8.2 Principal Axes Frame Angular Rates of Satellite

8.2.2 Trajectory to Mars

During this phase, the satellite will have its negative body z-axis pointing towards the Sun to (1) protect the payload from extreme temperatures, and (2) to keep the solar panels pointing directly towards the Sun to generate the necessary power. Only two environmental disturbances have been considered: gravity gradient and SPR. During transit to Mars, the satellite will find itself in a heliocentric orbit with an eccentricity of 0.2074 and a semi-major axis of 1.888×10^{11}. The estimated duration of this phase is about 288 Earth days, with a total moment accumulation of 1.08×10^{-11} *Nms*. This value is well below the total *12 Nms* the chosen reaction wheels can accumulate. Therefore, ideally there will be no need to de-saturate the wheels during this stage.

8.2.3 Mars Approach and Aerobraking

After firing its main engines to put itself into orbit around Mars, the satellite will need to rotate to align its negative body z-axis with the x-axis of the LVLH frame. This is done to protect the payload from aerodynamic forces and to maximize drag forces. For this maneuver, it is assumed that the satellite will take 1 hour to complete, with an acceleration and deceleration period of 15 minutes each. The reaction wheels will need to generate 3.45×10^{-4} *Nm*, also well below the maximum torque the wheels can generate (0.2 Nm). On top of this, the satellite will also experience torques caused by aerodynamic forces and gravity gradient as its major contributors. To estimate the maximum torques experienced by the satellite, a MATLAB code was made using the atmospheric model taken from [56], and classical orbital equations to calculate the speed, altitude, and the vector going form the CoM of the satellite to the center of

Mars in the body frame for each time. was obtained which shows the accumulated momentum over one orbit. Since the accumulated momentum is greater than what the reaction wheels can store, the attitude thrusters would need to counteract those forces, using about 3.4 kg of propellant.

8.2.4 Science Orbit

During the science orbit, the main disturbances acting on the satellite will be gravity gradient, SPR, and torques related to the movement of the solar panels. The torques and the accumulated momentum in one orbit on the wheels are all summarized in the following table.

Table 8.3 Satellite Disturbances During the Science Orbit

Disturbance	Torque magnitude (Nm)	Accumulated momentum (Nms)
Gravity gradient	1.676×10^{-4}	1.16
SPR	1.724×10^{-4}	0.0222[18]
Solar panels movement	0.561[19]	2.24

The total amount of momentum accumulation 3.43 Nms. By adding a safety factor of 3, this comes out to 10.3 Nms. Since the maximum momentum storage of the reaction wheels is 12 Nms, it is concluded that the wheels will need to de-saturate every orbit. The ARES II satellite will orbit Mars 4,531 times around Mars every Earth year. Since the mission is 4 years long, the satellite will need to de-saturate 18,124 times. The ADCS thrusters have a capacity of 1,000,000 cycles, leaving plenty of margin for other maneuvers.

[18] This value comes from the yearly momentum accumulation due to solar radiation pressure, considering that the orientation of the solar panels changes over the course of one year. This method was done following [65] instead of just considering one orbit.
[19] Assuming the solar panels need to change their orientation 90 degrees during eclipse.

9 Electrical Power

The Electrical Power System (EPS) for ARES II is designed to ensure continuous, reliable power throughout all mission phases, including eclipses and peak load periods. The system uses dual articulated solar arrays with triple-junction GaAs cells to maximize generation efficiency in Mars orbit, supported by Ni-H_2 batteries sized for eclipse operations. Power is regulated through a peak power tracking system to accommodate variable loads, with full telemetry for system monitoring. These design choices balance performance, longevity, and reliability, and are further detailed in the following sections.

Table 9.1 below states the requirements for the power subsystem.

Table 9.1 Power Subsystem Requirements

Req. ID	Description
SYS-PWR-001	The power subsystem shall generate 1707 W of electrical power to meet all power demands.
SYS-PWR-002	The power subsystem shall support peak, operational, and eclipse power modes.
SYS-PWR-003	The solar arrays shall be articulated about one axis to actively track and remain pointed at the sun, ensuring optimal solar coverage.
SYS-PWR-004	The power subsystem shall consist of batteries with an energy capacity of 581 W-h to support the spacecraft during eclipse periods and/or during power disruptions.
SYS-PWR-005	The power system shall use a peak-power tracking system to accommodate varying voltage requirements for different subsystems.
SYS-PWR-006	The power system shall include telemetry sensors to monitor voltage, current, temperature, and other key metrics of the solar array and batteries.
SYS-PWR-007	The solar panels shall withstand extreme temperatures.
SYS-PWR-008	The power subsystem shall be designed to last for a minimum mission duration of 10 years with a margin for extended operations.

9.1 Power Budget and Operational Modes

As shown in Table **9.2** below, the total power budget encompasses all onboard subsystems and their individual components, outlining the allocated power for each element.

Table 9.2 Power Budget

Subsystem	Component	Power (W)
Payload	Metropolitan Altitude Sensor	40.2
	Metropolitan Imaging Device	20
	Radar	140
	Spectrometer	75
Propulsion	Attitude Thruster	140
	Major Thrusters	280
	Extra Components	15
Thermal	Heater	60
	Thermocouples	10
Communications	Gimbal Mechanism	30
	Ka-Band TWTA Transmitter	200
	X-Band Transponder	50
	Medium Gain Antenna	5
	UHF Relay Transceiver	20
ADCS	IMU	10
	Reaction Wheel	170
	Star Tracker	23.1
Structures	Motors and Actuators	40
Power	Telemetry Sensors + Losses	75
TOTAL	-	**1403 W**

The system operates under five distinct power modes that are tailored for specific mission requirements. There is a high demand peak mode, three operational modes (each with different payload configurations), and a low power eclipse mode. While the peak power mode is rarely used, the solar array is specifically designed to support this maximum power draw, guaranteeing enough power generation to support the spacecraft even under peak load. The breakdown of the different power modes are shown below.

Peak Power Mode (1063 W): all payload instruments, attitude thruster, thermocouples, communication system, ADCS system, motors, actuators, and telemetry sensors

Operational Mode A (903 W): altimeter, spectrometer, radar, thermocouples, communication system, ADCS system, motors, actuators, and telemetry sensors

Operational Mode B (848 W): altimeter, camera, radar, thermocouples, communication system, ADCS system, motors, actuators, and telemetry sensors

Operational Mode C (828 W): altimeter, radar, thermocouples, communication system, ADCS system, motors, actuators, and telemetry sensors

Eclipse Mode (523 W): altimeter, radar, heater, thermocouples, ADCS system, motors, actuators, telemetry sensors

9.2 Solar Array Configuration

The configuration of the solar array is a critical decision made when designing the spacecraft's power system. The primary options are body-mounted arrays, deployed and fixed arrays, and deployed and articulated arrays. Body-mounted arrays are integrated directly onto the spacecraft's structure and are limited by the surface area of the spacecraft. They are typically used for smaller spacecrafts that have minimal power requirements. For larger-sized spacecrafts, deployed arrays are most used as they can meet greater power requirements.

Regarding the ARES mission, the spacecraft will be in a sun-synchronous orbit at a 350 km altitude. Throughout the orbit, there will be periods of suboptimal solar orientation, causing a reduction in the power generation efficiency. To offset this, the deployed solar arrays will incorporate single-axis articulation, allowing them to actively track and maintain pointed towards the Sun. One axis articulation is enough for this mission, as in a 350 km sun-synchronous orbit around Mars, the estimated worst possible beta angle would be +/- 25 degrees. At this worst case, the arrays would still be operating at 90% efficiency [57].

The final design consideration for the solar array configuration involves the placement of the panels; either a single array on one side of the spacecraft or two smaller symmetrically positioned arrays on either side of the spacecraft. The single panel offers a simpler design, however as the length of the panel increases to meet power requirements, its contribution to the overall moment of inertia increases, which would require more torque from the attitude control system. However, by distributing the solar array area across two balanced panels on either side, the increase in the moment of inertia is substantially reduced.

9.3 Solar Array Cells

Solar photovoltaic (PV) cells were selected as the primary power source for this mission due to their reliability, high efficiency, and ability to provide continuous power in space. Three options were considered; silicon

solar cells, gallium Arsenide (GaAs) solar cells, and triple junction gallium arsenide solar cells. In Table **9.3** below, the performances of the three options are compared.

Table 9.3 Performance of Solar PV Cells

Parameter	Silicon	Gallium Arsenide	Triple Junction GaAs
Efficiency	22%	18.5%	30%
Ideal Output (W/m^2)	338	298	462
Lifetime (yrs)	10	33	33

Silicon cells are a cost-effective option that is commonly used in low-Earth orbits; however, they have a lower efficiency and have greater susceptibility to damage in high radiation environments. While both gallium arsenide options provide the necessary radiation resistance and increased lifetime for our mission, we opted for the triple junction. The deciding factor was its superior performance and notably higher efficiency (around 30%) compared to standard gallium arsenide, ensuring optimal power generation for our 10-year primary mission and any extended operations.

9.4 Solar Array Sizing and Specifications

With the selected solar cell and an understanding of the power requirements, the following equations were used to calculate the area and mass of the solar array.

$$P_{sa} = \frac{\left(P_e \cdot \frac{T_e}{X_e}\right) + \left(P_d \cdot \frac{T_d}{X_d}\right)}{T_d} \tag{9.1}$$

$$A_{sa} = \frac{P_{sa}}{P_{EOL}} \tag{9.2}$$

$$m_{sa} = 0.04 P_{sa} \tag{9.3}$$

It was calculated that the solar array of the ARES II will generate 1707.26 W of power with a surface area of 19.31 m^2 and a total mass of 68.29 kg.

9.5 Battery Selection

Given the mission's length being 10+ years with a margin for extension operations, using a secondary battery is essential. Unlike primary batteries, which are not rechargeable and ideal for shorter duration missions, secondary batteries can endure the numerous charging cycles this mission requires. Three secondary battery options were considered; nickel-cadmium batteries, nickel-hydrogen batteries, and lithium-ion batteries. In Table **9.4** below, the performances of the three options are compared.

Table 9.4 Performance Comparison for Secondary Batteries [57]

Parameter	Ni-Cd	Ni-H2	Li-Ion
Energy Density (W-hr/kg)	30	60	125
Energy Efficiency	72%	70%	98%
Temperature Range (°C)	0 to 40	-20 to 30	10 to 25

Lithium-Ion batteries offer significant volumetric and energy density advantages over both the Ni-Cd and Ni-H_2 batteries and have even been used on Mars Rovers with the use of warming boxes. However, due to its limited operating temperature range, its ability to perform in Martian orbiting conditions remains unproven. Both the Ni-Cd and Ni-H_2 batteries are very commonly used in space applications and are proven to work in Martian orbital conditions. Although the Ni-Cd batteries have slightly higher efficiency than the Ni-H_2 batteries, the superior energy density of the Ni-H_2 batteries gives a significant advantage for this mission. The higher energy density will allow for a more compact system, saving considerable amounts of space, and will potentially reduce the number of batteries required on the spacecraft.

Using the power demand for the established eclipse mode along with the selection of the battery, it was calculated that three 11-cell Ni-H_2 batteries with a total mass of 106.54 kg will be used, providing a battery capacity of 581.11 W-hr.

9.6 Battery Charging

Batteries can be charged individually or in parallel based on the needs of the mission. While a parallel charging configuration offers lower cost and is a simpler design, it is best suited for missions under five years as the batteries will eventually balance out, meaning faster degradation. Implementing individual linear charging will optimize the

battery use by charging all the batteries to their own limits. This will maximize both the energy storage potential as well as the longevity of the battery. Additionally, a charging efficiency of 80% will be implemented in each charging cycle to further increase battery longevity. This will keep the battery from charging above 80% and discharging below 20% [57].

9.7 Power Regulation and Control

The two main bus control techniques are a peak-power tracker (PPT) and a direct-energy-transfer (DET) system. A DET system directly transfers the power from the solar array to the bus, however, it can only produce power at its full capacity when the battery is fully charged, as the solar array is designed to never exceed the voltage at the peak power point. When the battery is at its minimum voltage, the solar array will be operating well below its peak. The PPT serves as a solution to this issue as it is a DC-DC converter operating in series with the solar array. By using a buck/boost converter to track the battery voltage, it will then adjust the duty cycle of the converter to bring the solar array voltage to the desired maximum power point [57]. The next consideration is to decide whether the system will be unregulated or fully regulated. Fully regulated subsystems are inefficient and are best suited for spacecrafts with low power requirements, making the ideal power regulation system for this mission an unregulated PPT system.

10 Structures and Mechanisms

The Structures and Mechanisms subsystem plays a critical role in the success of the ARES mission by serving as the primary structural framework that supports all other subsystems and payload instruments. Its core function is to maintain the mechanical integrity of the satellite throughout its mission, from launch to operation on orbit. This subsystem provides essential interfaces for integrating both the satellite's internal systems and the launch vehicle, while also incorporating mechanisms for deploying key components such as solar arrays and communication antennas. These deployment mechanisms are designed with built-in redundancies to mitigate the risk of single-point failures. The structural design must be capable of withstanding severe launch loads, dynamic vibrations, and aerobraking stresses, all while maintaining appropriate safety margins.

A summary of the subsystem's specific requirements is provided in Table **10.1**.

Table 10.1 Structures & Mechanisms Requirements

Requirement ID	Requirement Description
SYS-STR-001	All load bearing structure shall achieve a yield safety factor of 1, and an ultimate safety factor of 1.4, per NASA-STD-5001B [58].
SYS-STR-002	The satellite shall be designed to fit within the launch vehicle’s payload fairing envelop, including deployment mechanisms.
SYS-STR-003	The satellite mass shall not exceed the allowable mass capacity of the selected launch vehicle, including margins.
SYS-STR-004	The structural interface with the launch vehicle shall comply with the mechanical and dynamic environment requirements: 6g peak axial acceleration, and 2g peak lateral acceleration.
SYS-STR-005	Deployment mechanisms shall incorporate redundancy to prevent single-point failures.
SYS-STR-006	The structural material and coatings shall be selected to withstand thermal cycling and radiation exposure in Mars orbit.

10.1 Material Selection

Material selection for the satellite structure of ARES II was driven by a comparative trade study of various mechanical, thermal, and manufacturing properties, detailed in Table **10.2**. As a result of this study, Aluminum 6061-T6 was selected due to its combination of strength, weight, ease of fabrication, and extensive history of use in Aerospace applications.

Table 10.2 Material Trade Study

Candidate Material	Yield Strength (MPa)	Strength-to-Weight Ratio	Thermal Conductivity (W/m-K)	Weldability and Formability	Cost
Al 6061-T6 [59]	276	102	167	High	Low
Al 7075-T6 [60]	503	179	130	Med	Med
Ti-6Al-4V [61]	880	199	6.7	Low	High

10.2 Structural Design & Launch Vehicle Integration

The satellite's structural design is divided into two main sections: the primary structure, which bears the launch loads, and the secondary structure, which houses the payload instruments. Both structures are illustrated in Figure **10.1**. The primary structure consists of a cylindrical design, which was selected for its superior resistance to buckling under axial loads experienced during launch. Attached is the secondary structure, which is a modular box design that accommodates the scientific payload instruments. The location of payload instruments inside the secondary structure is displayed in Figure **10.2**. Separation of structural roles was important to ensure the load paths does not cross through the mounting interfaces of the delicate instruments.

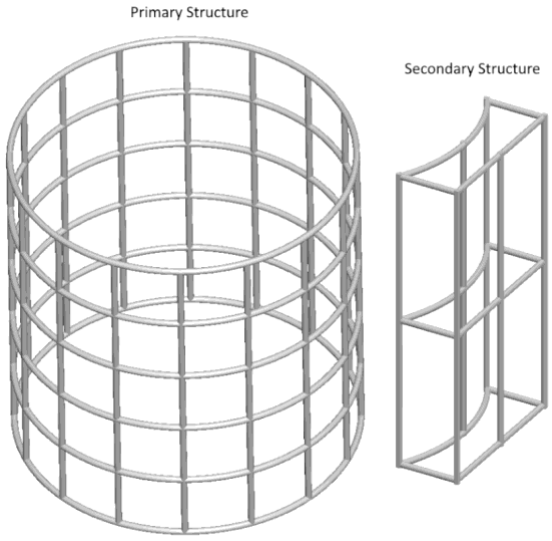

Figure 10.1 Skeleton of Primary and Secondary Structures

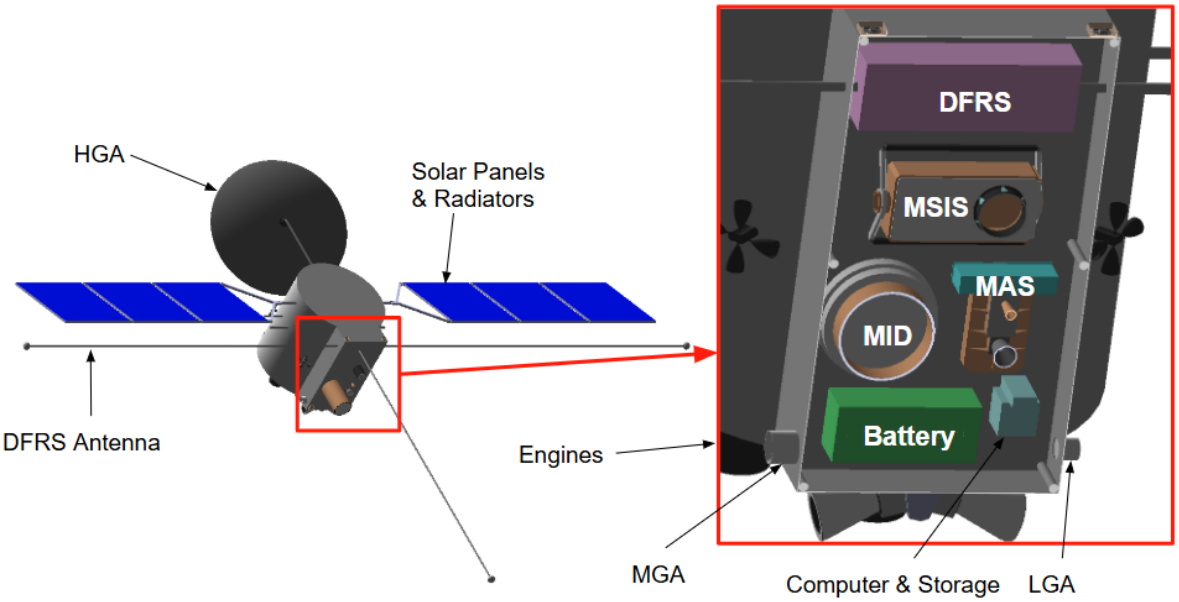

Figure 10.2 Placement of Payload Instruments in Secondary Structure

To prevent displacement of the fuel tanks due to launch vehicle oscillations, two concentric layers of support beams, shown in **Figure 10.3**, surround the tanks and are joined to an outer insulating sheet housing the fuel tanks. The beams are also fixed directly to the primary structure to stiffen the system and route transverse loads through the beams rather than the tanks.

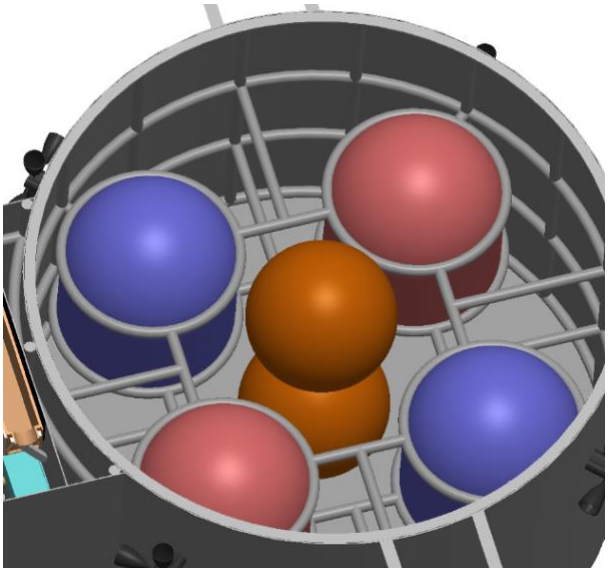

Figure 10.3 Fuel Tank Support Structure

The complete dimensions and assembly of ARES II in its operation and launch configurations are shown in **Figure 10.4** and **Figure 10.5**, respectively.

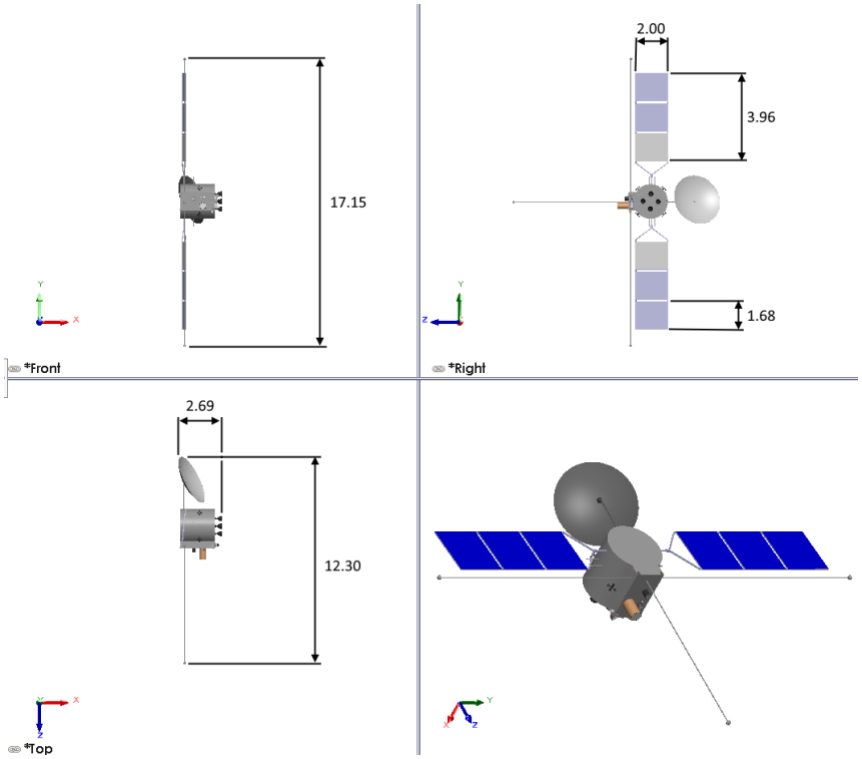

Figure 10.4 Operational Configuration of ARES II. Note: Dimension in meters.

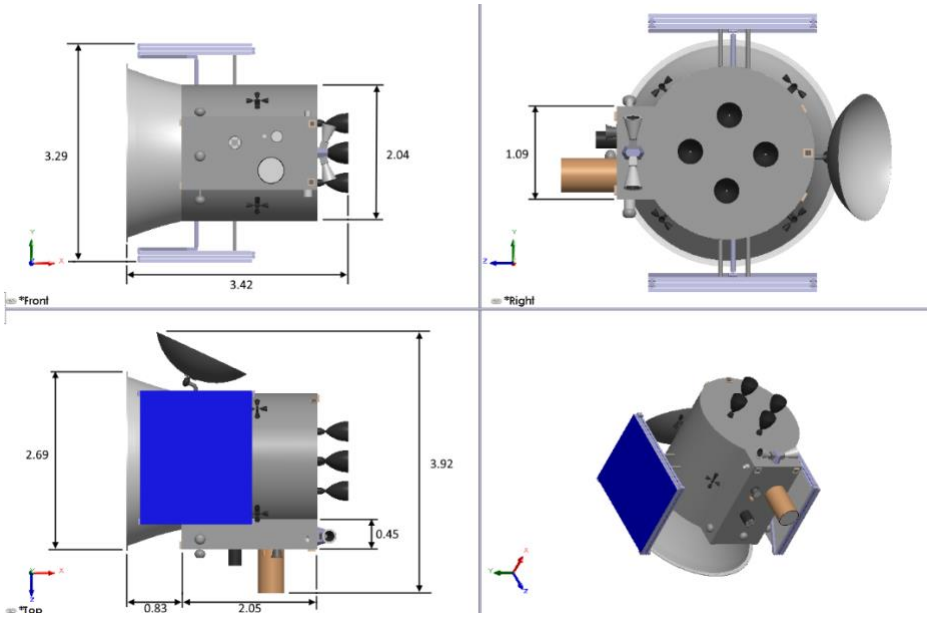

Figure 10.5 Launch Configuration of ARES II. Note: Dimension in meters

Integration of the launch configuration into the Falcon 9 fairing required an adapter to secure ARES II to SpaceX's standard 2624mm payload attachment fitting (PAF). This adapter is pictured in **Figure 10.6**.

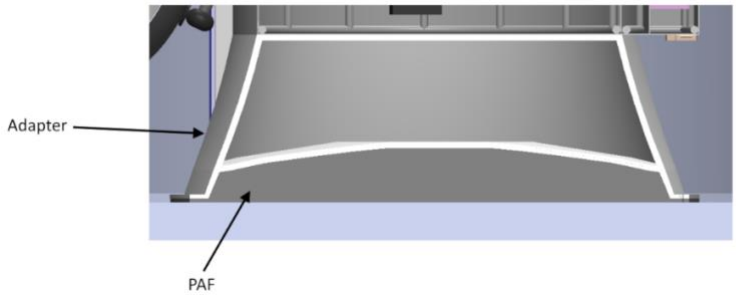

Figure 10.6 Payload Adapter for 2624mm PAF

The integrated satellite and launch vehicle assembly is shown in **Figure 10.7**. The successful integration of the satellite into the launch vehicle satisfies SYS-STR-002, with a minimum of 30 cm of radial clearance between the satellite and the internal fairing wall.

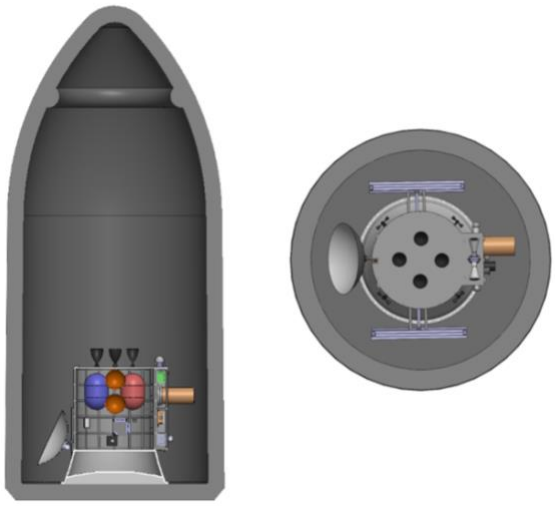

Figure 10.7 Front and Top Section Views of ARES II Launch Vehicle Integration

10.3 Structural Analysis

Structural analysis simulations were conducted on the primary structure to ascertain the structure's ability to sustain launch loads. **Figure 10.8** displays the design load factors for each direction for the Falcon 9 launch vehicle.

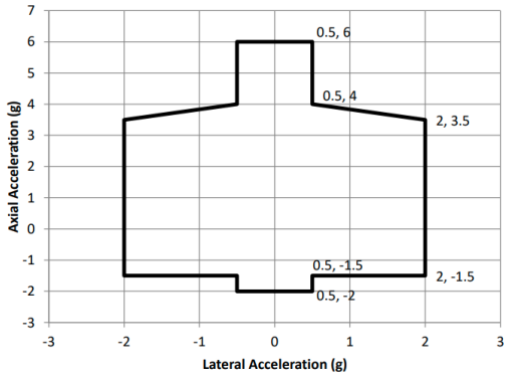

Figure 10.8 Falcon 9 Limit Load Factors. [27]

For this analysis, the combined worst-case combined axial and lateral loadings scenario were considered: 2g lateral, 6g axial. If the structure passed requirements under this load condition, it would 1be able to for any other combination of launch loads it may see. Analysis was run with the material properties for Al 6061-T6 shown in Table **10.3**.

Table 10.3 Material Properties of Al 6061-T6 for Structural Simulation [59]

Yield Strength (MPa)	Ultimate Strength (MPa)	Poisson Ratio
276	**313**	**0.33**

The result of the worst-case loading simulation is displayed in **Figure 10.9**. The peak von-Mises stress was 130 MPa, providing a yield safety factor of 2.1, and ultimate safety factor of 2.4 - satisfying requirements SYS-STR-001 and SYS-STR-004.

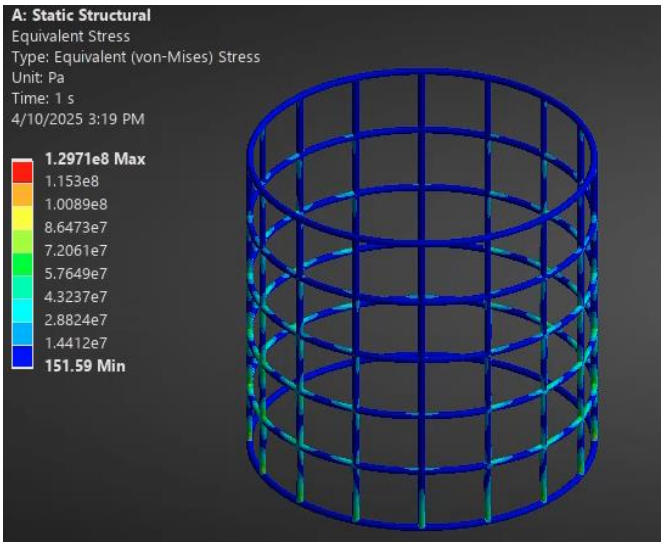

Figure 10.9 Results of Primary Structure von-Mises Stress Simulation

10.4 Modal Analysis

Modal simulations of the satellite structure and components were also performed to ensure there will no interaction with launch vehicle vibrations. The results of the analysis, summarized in Table **10.4**, shows that every component met the minimum required resonant frequency, excluding the retracted solar panels. This warranted further analysis to determine if the solar panel design was safe for the mission.

Table 10.4 Modal Analysis Simulation Results

	Frequency (Hz)			
	Lateral		**Axial**	
	Requirement [27]	**Result**	**Requirement** [27]	**Result**
Primary Structure	> 10	22	> 25	61
Secondary Structure	> 35	62	> 35	57
Attitude Thrusters	> Primary	100	> Primary	97
Main Engines	> Primary	70	> Primary	97
Solar Panels	> Primary	0.8	> Primary	1.5
MID	> Secondary	373	> Secondary	603
MSIS	> Secondary	757	> Secondary	1979
MAS	> Secondary	2532	> Secondary	1014
DFRS	> Secondary	218	> Secondary	704

It was necessary to determine that, if the solar panels interact with launch vibrations, then the deflection of the panels must not exceed the minimum clearance between the fairing walls and payload. It was found that the panels may experience a maximum of 5.3 cm, reducing the total clearance to 24.7 cm.

11 System Summary

This section summarizes the integrated spacecraft system and its subsystems. The system architecture diagram shows the main connections between subsystems. The most prominent connections are data and power with some propellant connections. The N2 diagram (interface matrix) captures inter-subsystem interactions. The mass and cost breakdown are also included.

11.1 System Architecture

The system architecture diagram, Figure **11.1**, shows the overall spacecraft layout with all the key subsystems. The command and data handling and electrical power subsystems play central roles providing data and power connections to the majority of the spacecraft's components.

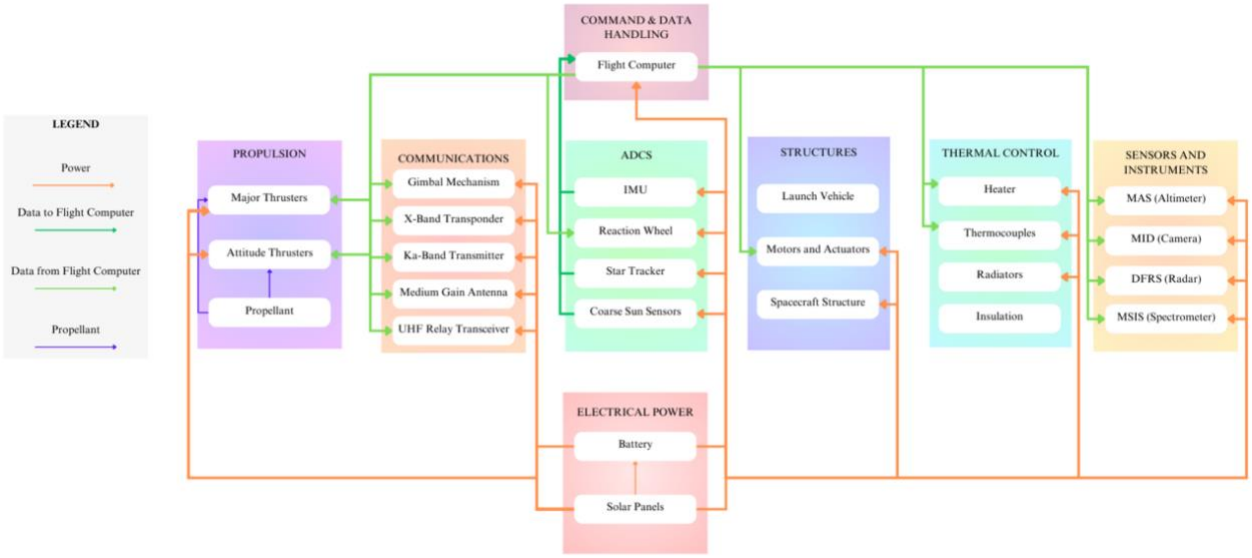

Figure 11.1 System Architecture Diagram

11.2 Mass & Cost Budgets

Table **11.1** breaks down the mass budget of the ARES II mission. The table is separated by payload instruments and subsystem components. Most of the satellite weight stems from the structure and propellant, leading to a total wet mass of 2452 kg.

Table **11.2** breaks down the ARES II mission cost. This budget plan was adapted from NASA's project cost estimating capability tool [62]. Accounting for allowances, the total predicted cost to conceptualize, research, design, manufacture, integrate, and get the satellite to Mars is $771 million. For the prescribed budget of $1 billion, there remains an additional $229 million to be spent on operational costs over the remaining duration of the mission.

Table 11.1 Mission Mass Breakdown

Description	Mass (kg)	Quantity	Total Wet Mass (kg)
ARES II Mission	**2,341.80**		**2,452.01**
Payload			
Instruments			
Camera	21.00	1	21.00
Radar	45.00	1	45.00
Spectrometer	80.00	1	80.00
Altimeter	9.60	1	9.60
Spacecraft			
Structure			
Round Bar & Paneling	666.60	1	666.60
Power			
Solar Panels+Radiator+Motors	105.00	1	105.00
Battery	78.00	1	78.00
ADCS			
Star Trackers	9.20	1	9.20
Coarse Sun Sensors	0.22	7	1.51
IMU	1.36	2	2.72
Attitude Thrusters	0.65	16	10.40
Reaction Wheel	5.00	4	20.00
Propulsion			
Propellant + Pressurant	1,080.34	1	1,080.34
Tanks	79.54	1	79.54
Engines/Main Thrusters	27.60	4	110.40
Extra Components	40.99	1	40.99
Thermal			
Multi Layer Insulation	12.00	1	12.00
Thermocouples	0.20	1	0.20
Electric Heaters	3.00	1	3.00
Heat Pipes	7.00	1	7.00
Communications			
Dual-Band High-Gain Antenna (HGA)	30.00	1	30.00
Ka-band TWTA Transmitter	10.00	1	10.00
Medium-Gain Antenna (MGA)	5.00	1	5.00
Low-Gain Antennas (LGAs)	4.00	1	4.00
UHF Relay Transceiver	3.00	1	3.00
Onboard Flight & Data Handling Computer	6.00	1	6.00
Onboard Data Storage (2 TB)	1.50	1	1.50
RF Front-End & Signal Processing Unit	5.00	1	5.00
Modulator/Demodulator (Modem)	2.00	1	2.00
TT&C System	3.00	1	3.00

Table 11.2 Mission Cost Breakdown

Description	Cost (USD)	Growth Allowance (%)	Predicted Cost (USD)
ARES II Mission	**602,747,396**		**771,007,827**
Payload			**178,100,000**
Instruments			178,100,000
Camera	25,000,000	30	32,500,000
Radar	40,000,000	30	52,000,000
Spectrometer	35,000,000	30	45,500,000
Altimeter	37,000,000	30	48,100,000
Spacecraft			30,182,827
Structures			**4,225,043**
Bar stock	3,245,487	30	4,219,133
Sheet	4,546	30	5,910
Power			**8,250,000**
Articulated Arrays	5,000,000	10	5,500,000
Battery	1,500,000	10	1,650,000
PPT System	1,000,000	10	1,100,000
ADCS			**969,235**
Star Trackers (x2)	280,000	15	322,000
Coarse Sun Sensors (x7)	10,500	7	11,235
IMU (x2)	120,000	10	132,000
Reaction Wheel (x4)	480,000	5	504,000
Propulsion			**5,227,049**
Propellant + Pressurant	324,863	10	357,349
Engines/Thrusters + Tanks	4,325,000	10	4,757,500
Extra Components	102,000	10	112,200
Thermal			**136,500**
Multi Layer Insulation	50,000	30	65,000
Thermocouples	4,000	30	5,200
Electric Heaters	6,000	30	7,800
Heat Pipes	45,000	30	58,500
Communications			**11,375,000**
Dual-Band High-Gain Antenna (HGA)	4,500,000	30	5,850,000
Ka-band TWTA Transmitter	500,000	30	650,000
Medium-Gain Antenna (MGA)	200,000	30	260,000
Low-Gain Antennas (LGAs)	100,000	30	130,000
UHF Relay Transceiver	150,000	30	195,000
Onboard Flight & Data Handling Computer	2,000,000	30	2,600,000
Onboard Data Storage (2 TB)	300,000	30	390,000
RF Front-End & Signal Processing Unit	500,000	30	650,000
Modulator/Demodulator (Modem)	200,000	30	260,000
TT&C System	300,000	30	390,000
Launch Vehicle Services	73,000,000	20	**87,600,000**
Project Development and Labor	350,000,000	30	455,000,000
System Integration, Assembly & Test	17,500,000	15	20,125,000
Remaining Budget for Operation Costs	397,252,604	-	228,992,173

11.3 Risk Matrix

The purpose of the risk matrix is to identify, assess, and mitigate potential risks. The risks are categorized by likelihood and impact. Mitigation strategies are in place to reduce overall risk. The risk categories are outlined in Table **11.3**.

Table 11.3 Risk Classification

Risk Classification	Category
A	ADCS
C	Communications
L	Launch
P	Propulsion
Pw	Power
S	Structural
SM	Science Mission
T	Thermal

Figure 11.2 Risk Classification Colour Chart

The likelihood and impact of the risks are colour coded according to Figure 11.2 above. Mitigation strategies must be ensured for risks that are red and dark red. Table **11.4** lists the potential risks, their classification, and mitigation strategies.

Table 11.4 Risk Mitigation Matrix

Index	Risk	Consequence	Risk Classification (likelihood, severity)	Mitigation
A1	ADCS failure	Spacecraft will not point in the proper direction limiting sun exposure to solar panels and accurate data collection from sensors.	Possible, moderate (3, 5)	No mitigation possible, satellite will go most likely become uncontrollable.
A2	Orbital drift	Payload is not able to acquire proper measurements.	Unlikely, moderate (2, 3)	Perform orbital correction maneuvers.
C1	Communications failure	Spacecraft will not be able to communicate and exchange data with	Unlikely, catastrophic	Implement dual-redundant subsystems

Index	Risk	Consequence	Risk Classification (likelihood, severity)	Mitigation
		Mission Control resulting in mission failure.	(2, 5)	with diversified HGA, MGA, and LGAs and deploy autonomous fault recovery algorithms
C2	Communications blackout	Spacecraft will not be able to communicate and exchange data with Mission Control temporarily.	Likely, moderate (4, 3)	Employ onboard data buffering and schedule non-critical operations during blackout intervals using multi-station DSN coverage
C3	Data corruption	Data will be inaccurate and unreliable resulting in mission failure.	Possible, catastrophic (3, 5)	Utilize advanced forward error correction alongside redundant telemetry verification
L1	Excessive launch vibrations	Damage will be incurred to spacecraft components due to vibrations.	Possible, critical (3, 4)	Modal analysis was conducted to ensure no interaction occurs. Dampers will be used in structures where necessary.
L2	Weather delay	The launch date will be delayed.	Likely, negligible (4, 1)	Monitor weather patterns to ensure good launch conditions
L3	Missed launch window	The mission will be cancelled or majorly delayed. The required data will not be collected in time.	Unlikely, catastrophic (2, 5)	Ensure the timeline Gantt Chart is closely followed
P1	TMI burn failure	The spacecraft will be off course.	Rare, catastrophic (1, 5)	Mid-course corrections will be executed.
P2	Orbital insertion burn failure	The spacecraft will not be in its intended orbit for data collection leading to inaccurate or no data collection.	Unlikely, catastrophic (2, 5)	Perform orbital corrections. If not successful, mission fail.
P3	Thruster failure	The spacecraft will not be on its intended course or orbit leading to inaccurate or no data collection.	Possible, critical (3, 4)	Perform orbital corrections. If not successful, mission fail.

Index	Risk	Consequence	Risk Classification (likelihood, severity)	Mitigation
Pw1	Solar panel deployment failure	The spacecraft will not be able to fully power all its subsystems.	Unlikely, critical (2, 4)	Will incorporate redundant deployment mechanisms that will be ground tested and approved.
Pw2	Battery failure	The spacecraft will not be able to be powered during eclipse periods resulting in thermal management failure.	Possible, critical (3, 4)	Multiple battery units on board that exceed the required capacity for redundancy.
S1	Damage to spacecraft during launch, TMI, orbit	The spacecraft will not function as intended depending on the damage.	Rare, catastrophic (1, 5)	Significant safety margin accounted for in structural design.
SM1	Data collection failure	No data will be collected or used for research.	Possible, moderate (3, 3)	Shut down data collection system and perform a restart.
SM2	Sensor malfunction	Data will be inaccurate or corrupted.	Likely, moderate (4, 3)	Shut down instrument and perform a restart and re-calibration.
T1	Electronics overheating	Equipment onboard will malfunction or break leading to internal spacecraft damage or data corruption.	Likely, critical (4, 4)	Radiators are sized for higher-than-expected capacities.

12 Conclusion

The ARES II mission and spacecraft design satisfies the main requirements outlined in Section 2.1.3, which are also repeated in the compliance matrix, Table **12.1**, below. This matrix lists the verification methods used to verify the requirements are complied with and the section of this paper in which more information can be found.

Table 12.1 Compliance Matrix

Index	Requirement	Verification Methods	Compliance	Section
MLR-001	The mission shall be able to identify slopes, elevation and small-scale hazards.	Analysis, Testing, Demonstration	YES	3
MLR-002	The mission shall characterize surface and subsurface resources, including hydrated minerals, water ice, and caves and lava tubes.	Analysis, demonstration	YES	3
MLR-003	The mission shall complete the primary data collection activities, covering 75% of Mars surface by December 31, 2033.	Analysis, demonstration	YES	3
MLR-004	The mission shall support extended operations, with the payload continuing to gather data until at least 2039.	Analysis, demonstration	YES	6
MLR-005	The project shall remain within a total program cost of $1 Billion (FY24), including design, manufacturing, testing, integration, launch, and primary operations, and incorporating a contingency reserve of ≥15%.	Analysis, inspection	YES	11
MLR-006	The spacecraft shall be designed to operate reliably in the deep-space environment, including exposure to radiation, thermal extremes, launch vehicle and aerobraking loads.	Analysis, testing, demonstration	YES	7, 10

Testing refers to measures of performance (MOPs) being tested via hardware testing or simulations. Analysis refers to MOPs being proven through calculations, models, or simulations. Demonstration refers to MOPs being shown through operation in a relevant environment. Inspection refers to MOPs being verified by visual or document-based review.

In conclusion, the overall mission objective to be completed by ARES II is to conduct detailed geographic and resource mapping of Mars in support of future human exploration. The spacecraft is a single orbiter equipped with an altimeter, camera, radar and spectrometer. The design was selected through rigorous trade studies and system level

analysis. Payload selection was based on science traceability matrix alignment and performance versus cost trade-offs. The spacecraft is designed to launch from Earth using Space X's Falcon 9 launch vehicle. The final scientific orbit around Mars in which the primary and secondary data will be collected has an orbital altitude of 350 km, is circular, sun-synchronous, and near-polar. This orbit allows the spacecraft to collect continuous data at a constant altitude and lighting conditions and will cover 76.12% of the Martian surface in four years, satisfying the 75% coverage requirement by 2033 outlined in the RFP. The primary operations are completed by the end of 2033 and then the secondary data collection period will begin to enhance data accuracy and observe Mars' changing environment. The entire mission costs less than 1 billion USD (FY24) satisfying this constraint detailed in the RFP, with a total of 771 million USD (FY24). The high-level mission requirements were all satisfied which can be seen by the compliance matrix. At this point, the system design is ready for prototyping, testing, and final integration. The mission schedule, which is depicted in the form of a Gantt Chart, allows for an Earth departure and Mars arrival date of November 29th, 2028, and September 13th, 2029, respectively. The ARES II mission is technically sound, scientifically valuable, and aligns with the goals of future human exploration of Mars.

Bibliography

[1] R. (. Davis, L. Cho, H. McDonald, J. O'Brien and M. Parks, "Red Planet Dispatch," NASA, 13 December 2022. [Online]. Available: https://blogs.nasa.gov/redplanetdispatch/2022/12/13/criteria-for-landing-site-selection/. [Accessed 17 02 2025].

[2] NASA/JPL, "Mars Topography," NASA, 17 January 2001. [Online]. Available: https://www.jpl.nasa.gov/images/pia02820-mars-topography/. [Accessed 23 February 2024].

[3] M. K. Barker, E. Mazarico, G. A. Neumann, M. T. Zuber, J. Haruyama and D. Smith, "A new lunar digital elevation model from the Lunar Orbiter Laser Altimeter and SELENE Terrain Camera," *Icarus,* vol. 273, pp. 346-355, 2016.

[4] O. Aharonson, M. T. Zuber and D. H. Rothman, "Statistics of Mars' topography from the Mars Orbiter Laser Altimeter' Slopes, correlations, and physical Models," *JOURNAL OF GEOPHYSICAL RESEARCH,,* vol. 106, no. E10, pp. 23723-23735, 2001.

[5] S. A. Striepe, C. D. Epp and E. A. Robertson, "Autonomous Precision Landing and Hazard Avoidance Technology (ALHAT) Project Status as of May 2010," NASA, Barcelona, 2010.

[6] F. S. Anderson, A. F. C. Haldemann, N. T. Bridges, M. P. Golombek, T. J. Parker and G. Neumann, "Analysis of MOLA data for the Mars Exploration Rover landing sites," *Journal of Geophysical Research,* vol. 108, no. E12, pp. ROV 25 1-27, 2003.

[7] K. S. Deal, E. E. Arvidson and G. A. Neumann, "The Surface Roughness of Terrains on Mars," Goddard Space Flight Center: LPI, 2003.

[8] E. Pardo-Igúzquiza and P. Dowd, "The roughness of martian topography: A metre-scale fractal analysis of six selected areas," *Icarus,* vol. 101, no. 1, p. 115109, 15 September 2022.

[9] B. A. Campbell, N. E. Putzig, L. M. Carter, G. A. Morgan, R. J. Phillips and J. J. Plaut, "Roughness and near-surface density of Mars from SHARAD radar echoes," *Journal of geophysical research,* vol. 118, no. 3, pp. 436-450, 2013.

[10] R. D. Lorenz, G. M. Martínez, A. Spiga, A. Vicente-Retortillo, C. E. Newman, N. Murdoch, F. Forget, E. Millour and T. Pierron, "Lander and rover histories of dust accumulation on and removal from solar arrays on Mars," *Planetary and Space Science,* vol. 207, 2021.

[11] L. &. M. J. &. S. J. &. P. P. Bandeira, "Automated Detection of Sand Dunes on Mars. Lecture Notes in Computer Science," *ResearchGate,* 2010.

[12] "Ripple Movement on Sand Dune in Nili Patera, Mars," NASA, 9 May 2012. [Online]. Available: https://science.nasa.gov/resource/ripple-movement-on-sand-dune-in-nili-patera-mars/. [Accessed 2 February 2025].

[13] M. C. Malin, J. F. Bell III, B. A. Cantor, M. A. Caplinger, W. M. Calvin, R. T. Clancy, K. S. Edgett, L. Edwards, R. M. Haberle, P. B. James, S. W. Lee, M. A. Ravine and P. C. Thomas, "Context Camera Investigation on board the Mars Reconnaissance Orbiter," *Journal of Geophysical Research. E. Planets,* vol. 112 (E5), 2007.

[14] S. Do, G. Morgan and T. Putzig, "Subsurface Water-Ice Mapping Project Briefing," Human Landing Sites Study HLS2 (Exploration Zones), 2019.

[15] G. A. Morgan, N. E. Putzig, D. M. H. Baker, A. Pathare, C. M. Dundas, M. B. Russell, M. R. Perry, M. Chojnacki, H. G. Sizemore, A. M. Bramson, E. I. Petersen, S. Nerozzi, R. H. Hoover and Z. Bain, "Refined Mapping of Subsurface Water Ice on Mars to Support Future Missions," *The Planetary Science Journal,* vol. 6, no. 2, pp. 1-19, 2025.

[16] M. D. West and J. D. Clarke, "Potential martian mineral resources: Mechanisms and terrestrial analogues," *Planetary and Space Science,* vol. 58, no. 4, pp. 574-582, 2010.

[17] J. Liu, H. Li, L. Sun, Z. Guo, J. Harvey, Q. Tang, H. Lu and M. Jia, "In-situ resources for infrastructure construction on Mars: A review," *International Journal of Transportation Science and Technology,* vol. 11, no. 1, pp. 1-16, 2022.

[18] L. Carrer, D. Castelletti, R. Pozzobon, F. Sauro and L. Bruzzone, "A Novel Method for Hidden Natural Caves Characterization and Accessibility Assessment From Spaceborne VHR SAR Images," *IEEE Trasnactions on Geoscience and Remote Sensing,* vol. 61, pp. 1-11, 2023.

[19] J. Blamont, "A roadmap to cave dwelling on the Moon and Mars," *Advances in Space Research ,* vol. 54, no. 10, pp. 2140-2149, 2014.

[20] R. J. P. S. Liberatore, "NASA's $2.2bn Perseverance LANDS on Mars: Rover survives 'seven minutes of terror' to embark on 2-year mission to search for extra terrestrial life in crater that was once a lake," 2021. [Online]. Available: https://planets.ucla.edu/?p=13329.

[21] "Mars Global Coverage by Context Camera on MRO," [Online]. Available: https://science.nasa.gov/resource/mars-global-coverage-by-context-camera-on-mro/.

[22] K. Sergieieva, "Satellite Constellations: Existing And Emerging Swarms," [Online]. Available: https://eos.com/blog/satellite-constellation/ .

[23] J. M. Logsdon, "Mars Global Surveyor," [Online]. Available: https://www.britannica.com/topic/Mars-Global-Surveyor.

[24] R. W. Z. a. S. E. Smrekar, "An overview of the Mars Reconnaissance Orbiter (MRO)," *Journal of Geophysical Research: Planets,* 2007.

[25] "First results from the ExoMars Trace Gas Orbiter," [Online]. Available: https://www.esa.int/Science_Exploration/Human_and_Robotic_Exploration/Exploration/ExoMar.

[26] R. D. F. a. M. L. M. L. M. Burke, "Interplanetary Mission Design Handbook: Earth-to-Mars Mission Opportunities 2026 to 2045," 2010. [Online]. Available: https://ntrs.nasa.gov/api/citations/20100037210/downloads/20100037210 .pdf.

[27] SpaceX, "Falcon User's Guide," Space Exploration Technologies, 2021.

[28] Arianespace, "Ariane 6 User's Manual," Arianespace SA, 2021.

[29] ULA, "Vulcan Launch Systems User's Guide," United Launch Alliance, 2023.

[30] D. D. E. Smith, "Mars Orbiter Laser Altimeter (MOLA)," 1996. [Online]. Available: https://nssdc.gsfc.nasa.gov/nmc/experiment/display.action?id=1996-062A-03.

[31] "Lunar Orbiter Laser Altimeter (LOLA)," 2024. [Online]. Available: https://science.nasa.gov/mission/lro/lola/.

[32] D. E. Smith, M. T. Zuber, G. B. Jackson, J. F. Cavanaugh, G. A. Neumann, H. Riris, X. Sun, R. S. Zellar, C. Coltharp, J. Connelly, R. B. Katz, I. Kleyner, P. Liiva, A. Matuszeski and E. Mazarico, "The Lunar Orbiter Laser Altimeter investigation on the Lunar," *NASA Technical Reports Server,* 2019.

[33] A. W. Yu, A. M. Novo-Gradac, G. B. Shaw, G. Unger, L. A. Ramos-Izquierdo and A. Lukemire, "The Lunar Orbiter Laser Altimeter (LOLA) laser transmitter," *NASA.*

[34] NASA, "Lunar Orbiter Laser Altimeter," 1 August 2020. [Online]. Available: https://science.nasa.gov/mission/lro/lola/.

[35] J. R. Bruzzi, K. Strohbehn, B. G. Boone, S. Kerem, R. S. Layman and M. W. Noble, "Laser Altimetry on the Lunar Reconnaissance Orbiter," *Johns Hopkins APL Technical Digest,* vol. 30, no. 4, pp. 331-345, 2012.

[36] A. W. Yu, G. B. Shaw, A. M. Novo-Gradac, S. X. Li and J. Cavanaugh, "The lunar orbiter laser altimeter (LOLA) laser transmitter," *SPIE,* vol. 6871, no. 1, pp. 68710D 1-4, 2008.

[37] N. E. Putzig, "Science results from sixteen years of MRO SHARAD operations," 1 September 2024. [Online]. Available: https://doi.org/10.1016/j.icarus.2023.115715.

[38] "Mars Express," ESA, 2005. [Online]. Available: https://sci.esa.int/web/mars-express/-/37917-insight-into-marsis-radar-data-analysis. [Accessed 6 February 2025].

[39] S. Murchie, R. Arvidson, P. Bedini, K. Beisser, J.-P. Bibring, J. Bishop, J. Boldt, P. Cavender, T. Choo, R. T. Clancy, E. H. Darlington, D. Des Marais, R. Espiritu, D. Fort, R. Green, E. Guinness, J. Hayes and C. Hash, "Compact Reconnaissance Imaging Spectrometer for Mars (CRISM) on Mars Reconnaissance Orbiter (MRO)," *Journal of Geophysical Research,* vol. 112, no. E5, pp. 1-57, 2007.

[40] G. Bonello, J.-P. Bibring, F. Poulet, A. Gendrin, B. Gondet, Y. Langevin and S. Fonti, "Visible and infrared spectroscopy of minerals and mixtures with the OMEGA/MARS-EXPRESS instrument," *Planetary and space science,* vol. 52, no. 1, pp. 133-140, 2004.

[41] eoPortal, "PRISMA (Hyperspectral)," eoPortal, 31 July 2023. [Online]. Available: https://www.eoportal.org/satellite-missions/prisma-hyperspectral. [Accessed 12 March 2025].

[42] Teledyne Brown Engineering, "DESIS Instrument," 2025. [Online]. Available: https://www.tbe.com/what-we-do/markets/space/geospatial-solutions/desis/instrument. [Accessed 2 March 2025].

[43] J.-P. Bibring, Y. Langevin, F. Altieri, R. Arvidson, G. Bellucci, M. Berthe, S. Douté, P. Drossart, T. Encrenaz, F. Forget, T. Fouchet, A. Gendrin, B. Gondet, N. Mangold, L. V. Moroz and J. F. Mustard, "The OMEGA instrument summary results," *ESA Special Publication,* vol. The Mars Express Results, pp. 1-27, 2009.

[44] eoPortal, "PRISMA2GEN," eoPortal, 9 May 2024. [Online]. Available: https://www.eoportal.org/satellite-missions/prisma2gen. [Accessed 2 March 2024].

[45] G. A. Center, "DESIS - Hyperspectral Images - Global," German Aerospace Center, [Online]. Available: https://geoservice.dlr.de/data-assets/hxom21uqeo90.html. [Accessed 2 March 2025].

[46] S.-E. Qian, Hyperspectral Satellites And System Design, Boca Raton: CRC Press, 2020.

[47] A. A. Siddiqi, Beyond Earth, National Aeronautis & Space Administration, 2018.

[48] A. Rocketdyne, "Aerojet Rocketdyne," 4 Aug 2020. [Online]. Available: https://satcatalog.s3.amazonaws.com/components/845/SatCatalog_-_Aerojet_Rocketdyne_-_MR-106L_22N_-_Datasheet.pdf?lastmod=20210710010020.

[49] H. P. Trinh, "High-Performance Bipropellant Engine," 1 April 1999. [Online]. Available: https://ntrs.nasa.gov/citations/20050187014.

[50] ArianeGroup, "ArianeGroup_Chemical_Bipropellant_Thruster_Family," 1 September 2024. [Online]. Available: https://ariane.group/app/uploads/2024/09/ArianeGroup_Chemical_Bipropellant_Thruster_Family.pdf.

[51] A. Majumdar, "NUMERICAL MODELING OF PRESSURIZATION OF A PROPELLANT TANK," 1999. [Online]. Available: https://ntrs.nasa.gov/api/citations/20000025232/downloads/20000025232.pdf.

[52] V. Deniz, "Thermal stability of Butyl/EPDM/Neoprene based rubber compounds," *Applied Polymer Science,* 2007.

[53] MatWeb, "MatWeb Material Property Data," [Online]. Available: https://www.matweb.com/. [Accessed 17 Feburary 2025].

[54] J. F. G. a. R. M. A. John A. Dec, "Thermal Modeling of the Mars Reconnaissance Orbiter's Solar," NASA Langley Research Center.

[55] A. B. Sonja Caldwell, "State-of-the-Art of Small Spacecraft Technology," 14 Febuary 2025. [Online]. Available: https://www.nasa.gov/smallsat-institute/sst-soa/thermal-control/. [Accessed 4 Apirl 2025].

[56] Z.-F. Luo and F. Topputo, "Mars orbit insertion via ballistic capture and aerobraking," *Astrodynamics,* vol. 5, no. 2, pp. 167-181, 2021.

[57] D. F. E. J. J. P. James R. Wertz, Space Mission Engineering: The New SMAD, Hawthorne, CA: Microcosm Press, 2015.

[58] NASA, "STRUCTURAL DESIGN AND TEST FACTORS OF SAFETY," National Aeronautics and Space, 2022.

[59] ASM, "Aluminum 6061-T6," Aerospace Specification Metals, [Online]. Available: https://asm.matweb.com/search/specificmaterial.asp?bassnum=ma6061t6. [Accessed 10 04 2025].

[60] ASM, "Aluminum 7075-T6," Aerospace Specification Metals, [Online]. Available: https://asm.matweb.com/search/specificmaterial.asp?bassnum=ma7075t6. [Accessed 10 04 2025].

[61] ASM, "Titanium Ti-6Al-4V (Grade 5)," Aerospace Specification Metals, [Online]. Available: https://asm.matweb.com/search/specificmaterial.asp?bassnum=mtp641. [Accessed 10 04 2025].

[62] NASA, "PCEC - Project Cost Estimating Capability," 22 110 2024. [Online]. Available: https://www.nasa.gov/ocfo/ppc-corner/pcec-project-cost-estimating-capability.

[63] J. Redfearn, "Europe goes to Mars," July 2001. [Online]. Available: https://www.esa.int/esapub/br/br174/br174.pdf. [Accessed 2 March 2025].

[64] T. N. Service, *Italian Space Agency's PRISMA Satellite Successfully Launched,* Washington, D.C: Targeted News Service , 2019.

[65] H. B. Hablani, "Momentum accumulation due to solar radiation torque, and reaction wheel sizing, with configuration optimization," NASA. Goddard Space Flight Center, Flight Mechanics, Seal Beach, 1993.

[66] ESA, "Ariane 6 Joint Update Report, 16 September 2024," European Space Agency, 2024.

[67] R. Speed, "Vulcan Centaur Avoids FAA Scrutiny After Losing Solid Rocket Booster Nozzle," 2024.

[68] J. F. G. a. R. M. A. John A. Dec, "Thermal Modeling of the Mars Reconnaissance Orbiter's Solar," NASA Langley Research Center.